



UNIVERSITÀ DEGLI STUDI DI MILANO  
FACOLTÀ DI MEDICINA VETERINARIA

PhD Course in Veterinary and Animal Science  
Class XIX

**Biodistribution and toxicity of metallic nanoparticles:  
*in vivo* studies in mice**

PhD Candidate: Dr. Marcella De Maglie  
R10588

Tutor: Prof. Eugenio Scanziani

Academic year 2015/2016

## Table of contents

1. INTRODUCTION	4
1.1 NMs applications	5
1.2 Types of NMs	7
1.3 Metallic NPs	8
1.4 General mechanisms of metallic NPs toxicity and routes of exposure	18
2. AIMS	25
3. MATERIAL AND METHODS	26
3.1 Physicochemical characterization of NPs	26
3.2. Dissolution study for AgNPs	29
3.3. <i>In vivo</i> Studies	30
3.4. Determination of silver in the organs (inductively coupled plasma mass spectrometry: ICP-MS)	32
3.5. Histopathological examination	33
3.6. Special histological stains	34
3.7. Immunohistochemistry and immunofluorescence	34
3.8. Digital Image Analysis (DIA)	35
3.9. TEM	36
3.10. Statistical analysis	36
4. RESULTS	37
4.1. BIODISTRIBUTION AND TOXICITY OF AgNPs	37
4.2. BIODISTRIBUTION AND TOXICITY OF IRON OXIDE NPs (IONP)	80
5. DISCUSSION	88
6. ACKNOWLEDGEMENT	93
7. REFERENCES	94
Appendix A: ADDITIONAL DATA	102
Appendix B: PUBLISHED PAPER	111

## Abstract

In the last decade, nanotechnology has emerged as one of the fastest growing area of science. This is a highly promising field for the generation of new engineering applications, consumer products, medical healthcare and medicine. However, the increasing development of nanomaterials (NMs) is not supported by *in vivo* studies taking systematically into consideration nanoparticles (NPs) types, doses and period of treatment that would allow to forecast possible adverse outcomes that might occur upon human exposure.

In our studies, fully characterized silver nanoparticles (AgNPs) and iron oxide nanoparticles (IONP), designed for cancer treatment, were used to assess biodistribution and potential toxic effects after single intravenous and repeated oral administration in mice.

Unexpected histopathological findings, strictly related to the physicochemical properties, i.e. size and vehicle used for the NPs synthesis, were observed after intravenous administration. This confirms that a complete characterization of NPs is of the most importance for the identification of *in vivo* outcomes. NPs mainly localized in organs containing large number of specialized tissue-resident macrophages belonging to the mononuclear phagocyte system. The retention of NPs in these tissues raises concerns about the potential toxicity.

The 28 days repeated oral administration of AgNPs demonstrated that the brain is the organ where Ag accumulation takes place. In fact, Ag it is still detected in brain after the recovery period because of its low clearance. Morphological changes observed in the blood brain barrier (BBB), and the involvement of glial cells in response to AgNPs administration, suggested a perturbation of brain homeostasis that should be taken into consideration and further investigated.

## Sintesi

Negli ultimi anni lo sviluppo delle nanotecnologie ha subito un crescente e rapido sviluppo. Le peculiari caratteristiche e potenzialità dei nanomateriali hanno permesso la loro applicazione in diversi settori, quali l'ingegneria (dispositivi elettronici e meccanici), il campo medico e sanitario (come nanovettori per il veicolo di farmaci, come sonde nella diagnostica per immagini, come componenti di strumenti chirurgici) e sono inoltre applicati in molti prodotti di largo consumo (cosmetici, indumenti, supplementi alimentari, contenitori per alimenti).

Con l'aumento dell'utilizzo dei nanomateriali, anche il rischio di esposizione umana cresce e con esso l'impatto che i nanomateriali hanno sull'organismo. Ad oggi, non sono del tutto chiari e identificati gli effetti che i nanomateriali inducono *in vivo*, questo perché gli studi sperimentali condotti sono molto eterogenei in termini di tipo di nanomateriali usati, non comparabili per le loro caratteristiche chimico fisiche (dimensione, coating, etc) e per la loro sintesi, ed in termini di dosi somministrate e periodi di trattamento considerati. Queste variabili non hanno permesso ad oggi l'identificazione e la valutazione del rischio associato all'uso accidentale o intenzionale di nanomateriali.

Data la rilevanza delle caratteristiche chimico-fisiche dei nanomateriali nel conferire le peculiari proprietà che li rendono differenti dal materiale di dimensione convenzionale, lo scopo degli studi proposti in questa tesi è di valutare l'effetto di queste caratteristiche sulla biodistribuzione e sugli eventuali effetti tossici a seguito della somministrazione intravenosa o orale di nanoparticelle metalliche. Nello specifico sono state utilizzate due tipi di nanoparticelle, nanoparticelle di argento (AgNPs), disponibili commercialmente e nanoparticelle di ossido di ferro (IONP) sintetizzate per essere applicate nel trattamento di tumori.

Dopo la somministrazione intravenosa, le nanoparticelle si distribuiscono negli organi contenenti un elevato numero di cellule appartenenti al sistema fagocitico-mononucleato, in maniera dipendente dalla dimensione (le più piccole si distribuiscono e si accumulano maggiormente negli organi rispetto a quelle di dimensioni maggiori). Anche le lesioni istologiche osservate, non comparabili con quelle descritte negli altri studi in letteratura, sono dipendenti dalla dimensione delle nanoparticelle e dal veicolo utilizzato per la loro sintesi, caso quest'ultimo delle IONP.

La somministrazione ripetuta orale di AgNPs di piccole dimensioni ha permesso di stabilire che esse si accumulano nel cervello, seppure in quantità molto bassa rispetto alla dose iniziale somministrata. A causa della bassa capacità di clearance di quest'organo, anche dopo il periodo di recovery è possibile quantificare una residua dose di argento. I cambiamenti morfologici ultrastrutturali osservati a livello della barriera emato-encefalica e le modifiche a carico delle cellule gliali (astrociti e microglia) suggeriscono che probabilmente la somministrazione orale di AgNPs agisce sull'omeostasi cerebrale. I risultati preliminari ottenuti aggiungono nuove informazioni sul potenziale rischio in seguito ad esposizione ripetuta di AgNPs e suggeriscono ulteriori approfondimenti per meglio caratterizzare gli effetti osservati.

## 1. INTRODUCTION

Nano-objects or nanomaterials (NMs) are defined by the European Union as “a natural, incidental or manufactured material containing particles, in an unbound state or to an aggregate or an agglomerate and where, for 50% or more of the particles in the number size distribution, one or more external dimensions is in the size range 1–100nm” [1].

At the same time it is specified that “In specific cases and where warranted by concerns for the environment, health, safety or competitiveness, the number size distribution threshold of 50 % may be replaced by a threshold between 1 and 50 %”, indicating that the legislation aimed to ensure a high level of health, safety and environmental protection as far as it should permit access to innovative products and promote innovation and competitiveness [1].

The number of NMs have increased during the past years, and the total annual quantity of NMs on the market at the global level is estimated at around 11 million tons, with a market value of roughly 20bn €[2], [3]. The increase in applications of NMs is related to their properties which vary according to their size and shape as well as their chemical environment. The structure and properties of NMs differ significantly from those of atoms as well as of those of the bulk materials. Compared to their bulk material counterparts, the distinct physicochemical properties of the NMs, such as size, surface properties, shape, composition, molecular weight, identity, purity, stability and solubility, might prove attractive in various industrial applications and are critically relevant to particular physiological interactions [4], [5].

The small size and corresponding large specific surface area of solid NMs confer specific properties to them, for example, making them desirable as catalysts for chemical reactions. The importance of surface area becomes evident when considering that surface atoms or molecules play a dominant role in determining bulk properties; the ratio of surface to total atoms or molecules increases exponentially with decreasing particle size. The increase on the volume to surface ratio increase in the particle surface energy and may render NPs more biological reactive [6].

These unique physicochemical properties suggest that they can interact with organs and cells in unpredictable ways and this raises concern about their potential toxicity. However, the lack of high

quality exposure and dosimetry data both for humans and the environment does not allow to single out, quantify and manage the potential risks that might be involved in NMs uses, especially the long-term ones and does not allow an adequate risk assessment. Because nanotechnology is so novel the challenge for future years will be centered around the knowledge on essential questions such as characterization, hazards, exposure, risk assessment and the risk management of NMs[7].

### **1.1. NMs applications**

The properties of NMs make possible to employ them in several applications, such as:

- Electronics. Remarkable technological progress has come from reductions in the size of transistors, thereby increasing the number of transistors possible per chip. It is already generating ultrafast semiconductors and microprocessors, low voltage and high brightness displays [8], [9] [[http://ec.europa.eu/research/industrial\\_technologies/nanotechnology-fields\\_en.html](http://ec.europa.eu/research/industrial_technologies/nanotechnology-fields_en.html)].
- Environment. Nanotechnology's great sustainability promise is to bring about the much needed power shift in renewable energy: a new generation of highly efficient photovoltaics, nanocomposites for stronger and lighter wind energy rotor blades, but also a new class of nanomembranes for carbon capture at fossil fuel power plants, and for the removal of finest contaminants of water supplies and mitigation of pollutants in the environment[10][[http://ec.europa.eu/research/industrial\\_technologies/nanotechnology-fields\\_en.html](http://ec.europa.eu/research/industrial_technologies/nanotechnology-fields_en.html)].
- Consumer and healthcare products. A significant portion of products utilize NMs to confer antimicrobial protection, to provide protective coatings and for environmental treatment (to protect products against environmental damage or to treat air and water in the home). Goods containing NMs are clothing, cosmetics, sporting equipment, food packaging, dietary supplements. Personal care products includes such products as a hair growth–stimulating shampoo, tooth pastes and sunscreens that use NMs because they effectively block ultraviolet light [11], [12].
- Medicine. Nanomedicine is an emerging field that combines nanotechnology with pharmaceutical and biomedical sciences, with the goal of developing drugs and imaging agents

with higher efficacy and improved safety and toxicological profiles. It has been defined as the monitoring, repair, construction and control of human biological system at molecular level, using engineered nanodevices and nanostructures. Current applications of nanotechnology in medicine involve engineered molecules to develop drugs, drug delivery techniques, diagnostics, medical devices and tissue engineering procedures [9], [11], [13]. Nanotechnology contributes in the development of novel drugs especially in cancer therapy. In most cases, the nanoparticle/drug conjugates achieve their effect through passive targeting, which relies on non-specific accumulation in diseased tissue (usually tumors). This approach has been used to target solid tumors, since the increased permeability of blood vessels in combination with poor lymphatic drainage or transport (the so-called enhanced permeability and retention (EPR) effect) leads to accumulation of nanomedicines within the tumor microenvironment [14].

Nanomaterial research has also focused on creating mechanisms to more effectively deliver drugs. The most basic drug delivery systems based on nanotechnology enhance the effectiveness of drugs by targeting specific cells that over-express certain cell-surface receptors; it can also be achieved by immobilizing ligands (e.g. proteins, antibodies, small molecules) to the surface of the nanoparticle, leading to active targeting which results in accumulation followed by specific uptake of the nanomedicine into the tissue of interest (e.g. tumors) [13], [14]. Another means of drug delivery is to stabilize drug with nanoparticles like albumin as natural carrier and for safe administration of high drug doses. Example of that is the FDA approved nanoparticle albumin-bound paclitaxel (Abraxane™) resulting in significant antitumor activity in patient with metastatic breast cancer [15].

Many approaches have been developed to use nanoparticles in biomedical imaging and drug delivery. Applications for these systems will provide materials for controlled drug delivery by directing carriers to a specific location with magnetic fields or fluorescence biological markers. The carrier will then be activated on demand in a limited region. The predictable and extended duration of action help to reduce inconvenience of frequent re-dosing, improve patient compliance and avoid the side effects that so often result from potent medicines [15], [16].

In the field of *in vivo* imaging and diagnostic the most promising investigated area aims to increase the efficiency and accuracy of diagnosis from samples of body fluids. Researchers are attempting to develop microchips that use electrodes to identify the dielectric properties of



cancerous cells, viruses, and bacteria in body fluids. Furthermore, nanomedicine could result in non-invasive devices that can enter the body to determine glucose levels, distinguish between normal and cancerous tissue, and provide genetic screening for multiple diseases. It is the case of nanoscale needles that can probe cells for carcinogenic chemicals [13].

## **1.2. Types of NMs**

NMs exist in a variety of forms, including nanoparticles (NPs), nanofibres, nanotubes and nanostructured surfaces and may be tailored for individual properties or uses (Fig. 1) [17].

NMs cover a heterogeneous range of materials. In terms of market volume, the main categories on the market are:

- inorganic non-metallic NMs (e.g. synthetic amorphous silica, aluminium oxide, titanium dioxide),
- carbon based NMs (e.g. carbon black, carbon nanotubes),
- organic, macromolecular or polymeric particulate materials (e.g. dendrimers),
- metal nanoparticles (e.g. nanosilver) [18].

Inorganic non-metallic NMs are already in a wide-spread use in the non-medical fields as additive to chemical polishing, cosmetics, food, and recently as vehicle for drug delivery (silica NMs), sunscreen and cosmetics (titanium dioxide NMs) [19], [20].

Carbon nanotubes can be used to deliver a variety of therapeutic agents, including biomolecules, to the target disease sites. In addition, their unparalleled optical and electrical properties make them excellent candidates for bioimaging and other biomedical applications [21].

An increasing number of studies focus on the uses of organic NMs with organic structure for regeneration of bone, cartilage, skin or dental tissues [22]. Among these NMs, dendrimers are characterized by individual features that make them hopeful candidates for a lot of applications. The dendritic polymers are analogous to protein, enzymes, and viruses, and are easily

functionalized. The most promising potential of dendrimers is in their possibility to perform controlled and specified drug delivery and as a sensor in bioimaging [23].

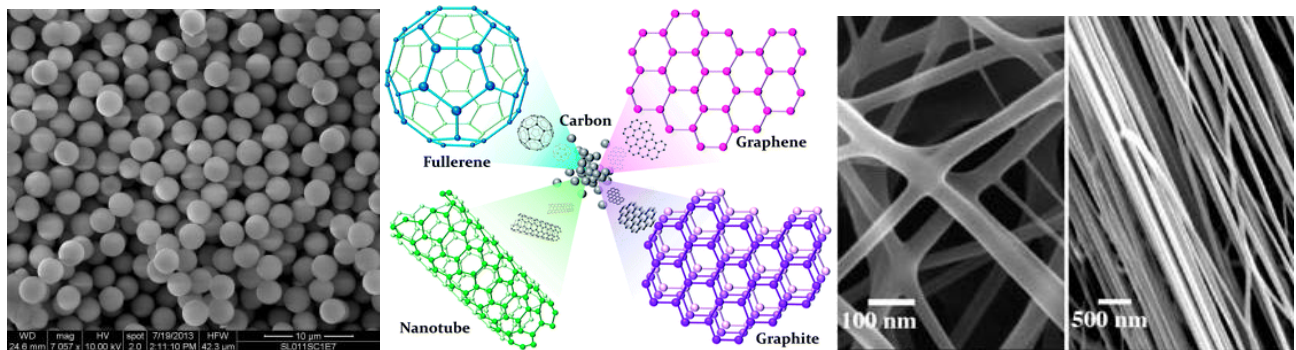


**Fig.1.** Example of different NMs: silica nanoparticles (left, SEM image), carbon based NMs (central), chitosan-based nanofibres (right, SEM image).

### 1.3. Metallic NPs

Gold, silver and iron are three most widely used materials that are considered inert to biological systems because they are biocompatible and not toxic [24].

In fact, NPs are based on small, well defined aggregates of the metals in the zero valent state.

Two approaches are used in the preparation of ultrafine particles. The first is the breakdown (top-down) method by which an external force is applied to a solid that leads to its break-up into smaller particles. The second is the build-up (bottom-up) method that produces NPs starting from atoms of gas or liquids based on atomic transformations or molecular condensations [4].

The preparation of metal NPs is generally based on a wet chemical reduction of a suitable metal salt in the presence of a capping or stabilizing agent to prevent both aggregation and oxidation away from the reduced state. The size and more importantly the shape of the NPs can be controlled by the reducing agent, the capping agent and the reaction conditions used in the preparation. While spherical forms are most commonly prepared, rod-like shapes, cubes, hexagonal and even hollow forms are known [25].

Numerous techniques have been developed to synthesize metal NPs, including both chemical methods (e.g., chemical reduction, photochemical reduction, coprecipitation, thermal decomposition, hydrolysis, etc.) and physical methods (e.g., vapor deposition, laser ablation, grinding, etc.). Biological methods based on microorganisms (bacteria, fungi and yeast) have been also developed for the synthesis of silver NPs. The ultimate goal is to obtain NPs with a high level of homogeneity and provide fine control over size, shape and surface properties [25], [26].

The introduction of capping agents, such as proteins, enzymes, oligonucleotides, allows the introduction of molecular recognition properties to the surface of the metal NPs, responsible of their applications in specific fields of the biomedical research (diagnostic, drug delivery, etc.) [25].

### **1.3.1. Properties of metallic NPs**

The remarkable optical properties of metal NPs, are due to their unique interaction with light which causes the collective coherent oscillation of their free conduction band electrons, termed localized surface plasmon resonance. Oscillation of the free electron results in either radioactive decay with a strong visible scattering of light or nonradioactive decay, which causes the conversion of photon energy into thermal energy. These two decay mechanisms have been readily utilized in biodiagnostic and imaging and therapeutic applications. The plasmonic resonance of metallic NPs depends on several parameters, such as size, shape, the physical properties in which the NPs are dispersed and the nature of metallic NPs (Fig. 2) [25]–[27].

Metal NPs possess also electrical properties that are similar to those of the corresponding bulk metals. The electronic properties of metallic NPs have been used for many applications, such as electrical sensors using metal NPs, as a tag for recognizing a specific target molecule, and the development of new electronic chips [25].

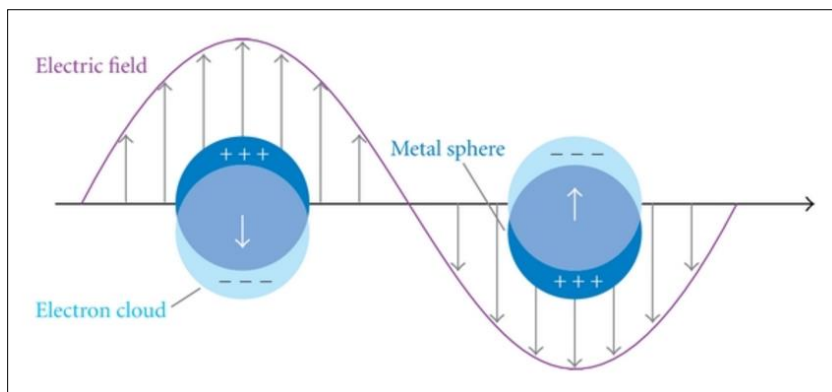


**Fig.2.** Scheme representing the plasmonic effect induced by white light on the absorbance of a silver nanoparticle. The plasmon is represented by the oscillation of an electron cloud along the surface of the nanoparticle[25].

### 1.3.2. Silver NPs (AgNPs)

Silver (Ag) is a metallic element that is known to be used by humans since ancient times in a broad range of applications, including jewelry, utensils, monetary currency, dental alloy, photography and explosives. Nowadays, the main field of application is in the electronic industry, however Ag is better known as an effective antimicrobial agent in various products. In fact, Ag was perhaps the most important antimicrobial compound before the introduction of antibiotics in the 1940s and is still used today in a wide range of medical applications because of its antibacterial effects and low toxicity to human cells (Fig 3) [28].

Nano-silver particles (AgNPs) are generally smaller than 100 nm and contain 20–15,000 silver atoms and have unusual and enhanced physical, chemical and biological properties compared to their bulk parent materials[29]. AgNPs have been shown to be effective biocides against bacteria (such as *Escherichia coli*, *Staphylococcus aureus*, *Staphylococcus epidermis*, *Leuconostoc mesenteroides*, *Bacillus subtilis*, *Klebsiella mobilis*, and *Klebsiella pneumonia*), fungi and yeasts (such as *Aspergillus niger*, *Candida albicans*, *Saccharomyces cerevisiae*, and *Penicillium citrinum*) and viruses (such as Hepatitis B, HIV-1, respiratory syncytial virus)[30].

Because of the reported antimicrobial activity, there is a widespread use of AgNPs in many consumer products (in bedding, washing machine, water purification, toothpaste, clothes, shoes,

detergents, fabrics, nursing bottle, deodorants, filters and humidifiers) including food packing materials, but also in food itself and dietary supplements [31]–[33].

Furthermore, the use of AgNPs is already established for some medical applications, including wound dressing (the antibacterial, antiviral and antifungal properties of AgNPs can facilitate healing), with many new potential application currently being investigated at preclinical level, including the applications as antiviral agents, photosensitizers and/or radiosensitizer, anticancer therapeutic agents in leukemia, breast cancer, hepatocellular carcinoma, lung carcinoma [26], [34]. Implantable medical devices, such as neurosurgical and venous catheters, have greatly benefited from the broad antibacterial activity of AgNPs by reducing patient infection and dependence on the antibiotic use [35].

Additionally AgNPs prevent the occurrence of resistance to microorganisms, so they are considered as a potential additive to animal feed or alternatives to growth-promoting antibiotics in animal agriculture [36], [37].

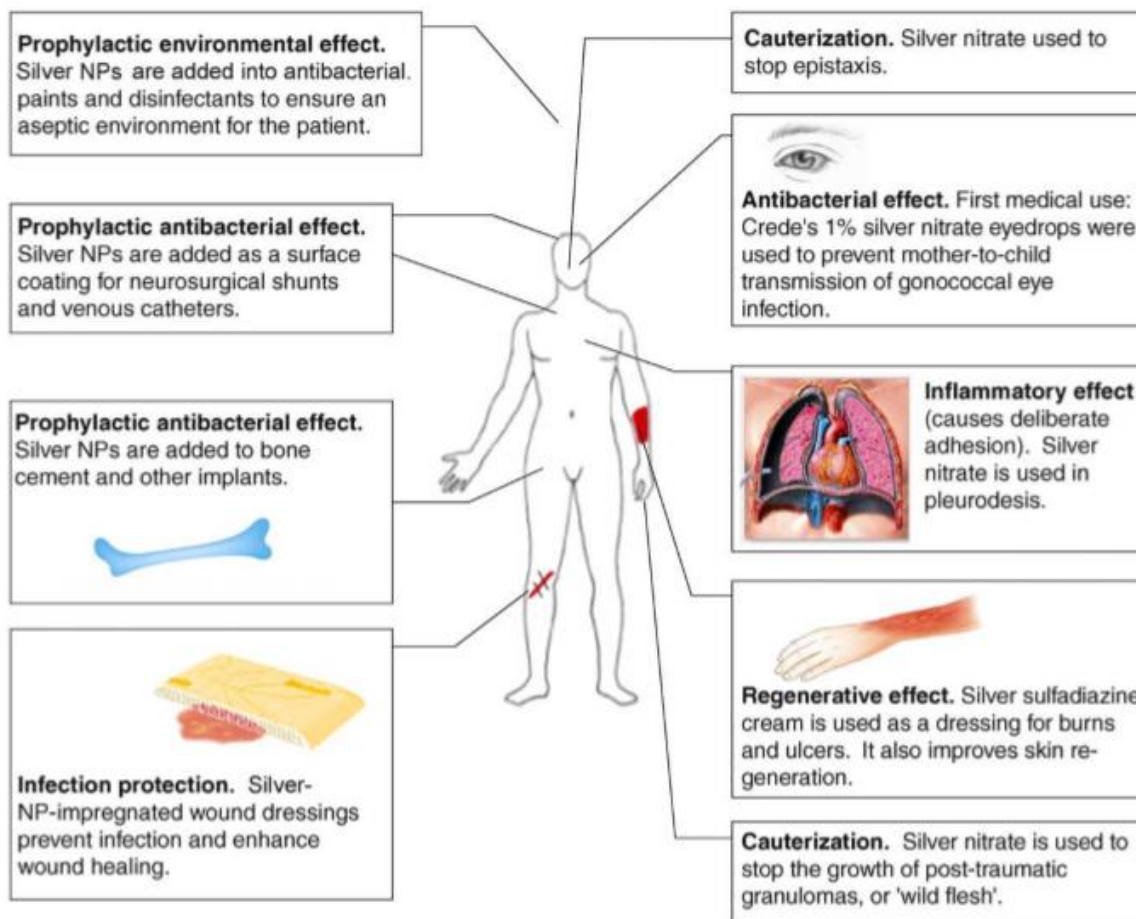


**Fig.3.** Uses of silver (right-hand side) and silver NPs (left-hand side) in medicine. Traditionally, silver nitrate is used in a number of clinical contexts: to stem the flow of blood from nosebleeds, to induce the pleurodesis when closing chest tube wounds and cauterization of granulomas. AgNPs is emerging as a next-generation antibacterial agent, augmenting antibiotics and disinfectants for coating of medical devices. AgNPs-based wound dressings are already commercially available (e.g. Acticoat™) and in current clinical use. NS is used as an antibacterial additive or coating in a range of catheters and in bone cement. NS can also be used in hand gels and paints as a prolonged antibacterial disinfectant[35].

### *Mechanism of AgNPs antimicrobial activity*

Although the mechanisms behind the activity of nano-scaled silver on bacteria are not yet fully elucidated, the three most common mechanisms of toxicity proposed to date are: (1) uptake of free silver ions followed by disruption of ATP production and DNA replication, (2) silver nanoparticles and silver ions generation of ROS, and (3) silver nanoparticles direct damage to cell membranes (Fig. 4)[30], [38].

The detailed mechanism by which silver nanoparticles interact with cytoplasmic membranes and are able to penetrate inside the cells is not fully clarified. One hypothesis is that the interaction between nanoparticles and bacterial cells are due to electrostatic attraction between negatively charged cell membranes and positively charged nanoparticles[30]. Morphological changes become evident upon such interaction and can be characterized by shrinkage of the cytoplasm and membrane detachment finally leading to rupture of the cell wall. Besides electrostatic attraction, the interaction of AgNPs with the sulfur-containing proteins present in the cell wall causes changes in the cell wall structure that result in its disruption. This, in turn, affects the integrity of the lipid bilayer and of the permeability of the cell membrane [38]. After adhesion to the cell membrane, the AgNPs may also penetrate inside the cells and affect their vital cellular functions, in fact, Ag (+) ions can affect the functionality of the respiratory electron transport chain by uncoupling it from oxidative phosphorylation through the inhibition of the respiratory chain enzymes[39]. The excessive amount of generated free radical directly damages the mitochondrial membrane through the hyperoxidation of lipids, proteins and DNA [38], [40].

Several studies suggest that the toxicity of AgNPs is affected by their size, which is responsible for their specific physiochemical characteristics[41]–[43]. The smaller the nanoparticles are, the larger the surface available for interaction is, resulting in a higher specific activity. In addition, compared to larger AgNPs, small AgNPs release more Ag ions and consequently exhibit stronger antimicrobial activities[28]. Moreover the bactericidal properties of the AgNPs are strongly influenced by their shape and concentration. AgNPs interacts with bacteria, fungi and viruses in a shape-dependent manner. As compared to the spherical or rod-shaped AgNPs, truncated triangular shaped AgNPs demonstrate enhanced antibacterial action. AgNPs with the same surface areas, but, different

shapes show differential bactericidal activity, which can be attributed to the variations in the effective surface areas and active facets of AgNPs[38]. The antibacterial effect is also concentration-dependent. Interestingly, the Gram-positive bacteria, such as *S. aureus*, are less susceptible than Gram-negative bacteria, such as *E. coli* and *Salmonella typhi*; however, both classes of bacteria display complete growth inhibition at higher AgNPs concentrations[44].

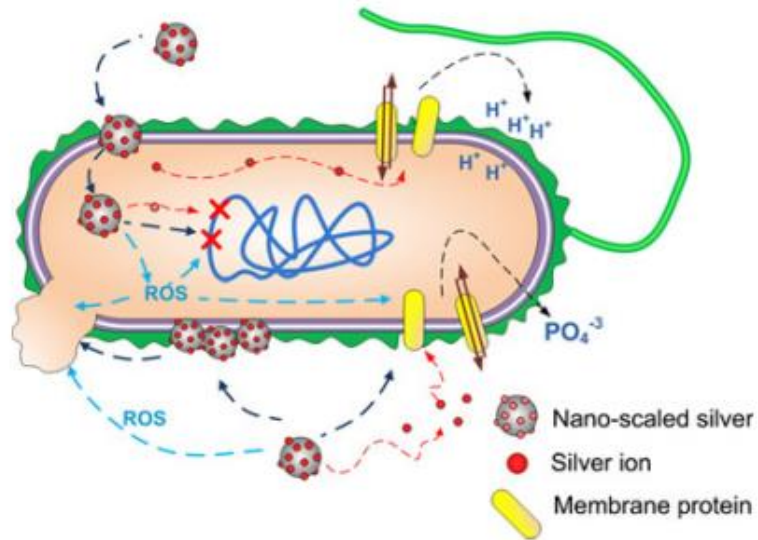


**Fig.4.** Nano-scaled silver may (1) release silver ions and generate ROS; (2) interact with membrane proteins affecting their correct function; (3) accumulate in the cell membrane affecting membrane permeability; and (4) enter into the cell where it can generate ROS, release silver ions, and affect DNA. [30].



### 1.3.3. Iron oxide NPs

Iron is the most current transition metal that chemically combines with oxygen to form iron oxides compounds, such as magnetite ( $\text{Fe}_3\text{O}_4$ ), maghemite ( $\gamma\text{-Fe}_2\text{O}_3$ ), and hematite ( $\alpha\text{-Fe}_2\text{O}_3$ ) as the most common. Iron oxides are prevalent, widely used as they are inexpensive, and play an imperative role in many biological processes. They are also extensively used by humans, in catalysts, durable pigments (coatings, paints, and colored concretes) [45].

Iron oxide NPs (IONP) are a specific type of metallic NPs that exhibit magnetic properties and are becoming the popular magnetic core composite for metallic NPs due to their excellent relaxivity and biocompatibility [46].

Iron oxide magnetic NPs with appropriate surface chemistry are prepared by various methods, such as wet chemical, dry processes, or microbiological techniques and several synthesis routes to achieve shape, size, crystallinity, dispersity, and magnetic behavior have been developed [47]. Once synthesized, the iron oxide core is coated with a biocompatible coating, such as a carbohydrate or polymer. Biocompatible coatings are imperative for stability of NPs in a biological environment, to protect the NPs from biodegradation. The choice of the coating material to be utilized makes a substantial difference in cellular response material and applications [46].

Due to their super-paramagnetic properties IONP have attracted much attention and are especially interesting in biomedical applications for protein immobilization, such as diagnostic magnetic resonance imaging (MRI), thermal therapy, and drug delivery. The ability of IONP to bind with a range of substances like antibodies, dyes, chemotherapeutic agents, and nucleic acid, enables them to have multiple functions (Fig. 5) [48].

As therapeutic applications, the majority of IONP FDA-approved materials are indicated as iron replacement therapies. There are several approved compounds (Venofer<sup>®</sup>, Ferrlecit<sup>®</sup>, INFed<sup>®</sup>, Dexferrum<sup>®</sup> and Feraheme<sup>®</sup>), which are employed to treat anemia related to chronic kidney disease (CKD). Each of these are composed of an iron oxide core, coated with hydrophilic polymers (e.g. dextran, sucrose), which provide slow dissolution of the iron following intravenous injection.

This allows rapid administration of large doses without increasing free iron in the blood to a level which causes toxicity [14].

In the area of cancer therapy, the aminosilane-coated super-paramagnetic IONP designed for tumor therapy (glioblastoma) by using local tissue hyperthermia (Nanotherm™), was approved by European regulatory. Here, the magnetic fluid is injected directly into the tumor, and an alternating magnetic field applicator is used to selectively heat the particles, resulting in local heating of the tumor environment (temperatures reach 40–45°C), leading to programmed (apoptosis) and not programmed (necrosis) cell death. In a recent clinical trial, the treatment of 59 patients with recurrent glioblastoma with thermotherapy using magnetic iron-oxide nanoparticles in conjunction with fractionated stereotactic radiotherapy, was associated with a remarkable increase in overall patient survival, comparing to the median survival for patients treated with chemotherapy following glioblastoma recurrence [14], [49].

IONP is applied for their used in enhancing MRI contrast and parameters such as surface coating, shape and composition are all factors in determining the magnetic and biological behavior of IONP. Coating is important to prevent opsonization and rapid blood clearance while size is important in MR signal-enhancing effect [50], [51]. As example, ferumoxytol (Feraheme®) is under investigation as an imaging agent [52].

Moreover, the outer coating on the metal-based core ensures that the NPs can be utilized in diagnostic procedures. In a multifunctional system, metallic NPs may be further incorporated with therapeutic payloads (chemotherapeutics or biotherapeutics), serving as both an imaging agent and a therapeutic carrier, and the ability of cellular tracking in MRI can be improved by linking antibodies or gene expressing cells to the NPs' surfaces [46].

However, despite the increasing production of new tools based on metallic NPs for potential applications in therapeutic and diagnostic area, to date only few of them have reached the clinics. Yet, some formulations based on gold and iron oxide NPs have already been approved or are in phase 3 of clinical trials. One of the most challenging technical difficulties that NMs are facing in biomedicine, is to successfully cross biological barriers and specifically recognize their targets while

they circulate through the body. Moreover, the use of NMs may pose unknown risks to patients, until now poorly investigated [53].

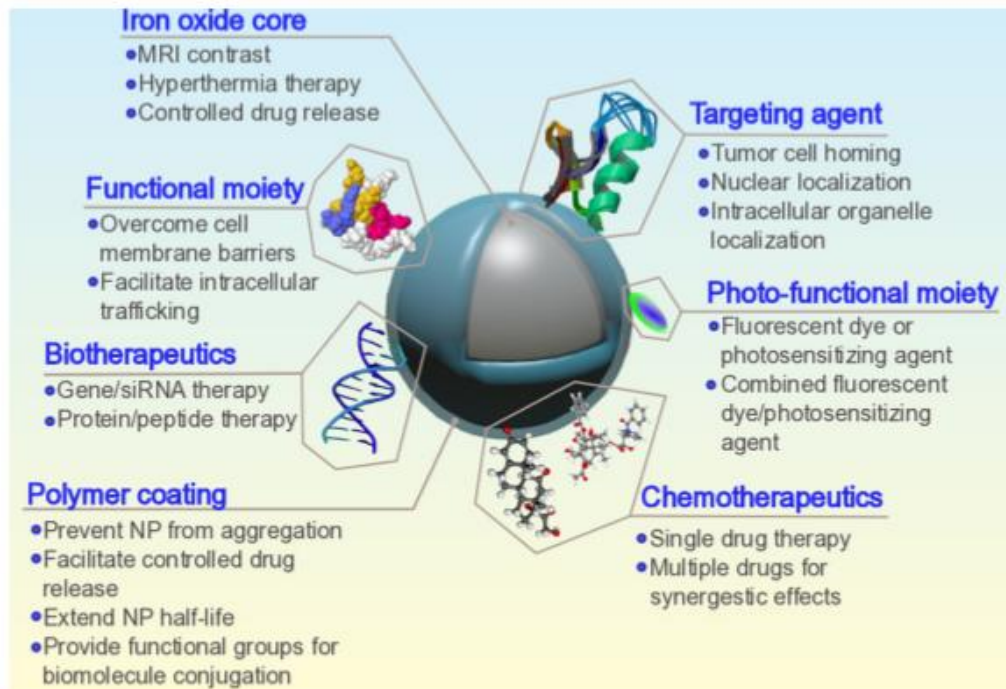


**Fig.5.** Schematic illustration of a full-suite theranostic NP. The magnetic core serve as a MRI contrast agent and heat source for magnetic hyperthermia, and a polymer coating increases biocompatibility, mitigates mononuclear phagocytes system uptake, and allows for facile functionalization with chemotherapeutic and targeting moieties [50].

#### 1.4. General mechanisms of metallic NPs toxicity and routes of exposure

The widespread applications of NPs raise concerns about the potentially unpredictable and adverse consequences of human exposure. In this context, nanotoxicology refers to the study of interactions of NPs with biological systems with an emphasis on elucidating the relationship between the physical and chemical properties with induction of toxic biological responses[54]. The unusual properties of NMs (which are due to their small particle sizes, large surface to volume ratios, and material differences) could lead to a modified distribution model and different biokinetic behavior, thereby producing different, unexpected effects [55]. Even though it became clear that cellular responses were strongly dependent on specific NM physicochemical properties, the elucidation of these unique correlations has presented a major challenge. The need for advanced assessment tools which are accurate at lower concentrations and in a physiologically relevant fluid, and the complete characterization of manufactured NM (as it produced by a manufacturer, as it actual used in products, as to which consumers may be exposed) are two main aspects to be fulfilled in order to obtain comparable results not affected by NM behavioral patterns (e.g. insoluble nature, ability to agglomerate, particle sedimentation) [7], [56].

The assessment of NPs toxicity has largely been determined *in vitro*. Typical end points measured include mortality, growth, respiration, oxidative stress, and gene expression. Generation of reactive oxygen species (ROS) and free radicals causes oxidative stress (activation or inhibition of the antioxidant defense system), lipid peroxidation, and DNA damage are recognized as some of mechanisms by which NPs might induce toxicity [57]–[60].

*In vitro* tests do not consider the complexity of *in vivo* interactions. Factors that might influence *in vivo* NPs toxicity include particle-related properties, the administered dose, the route of administration and extent of tissue distribution. Additionally, the toxicity of these materials depends on their persistence or clearance from the different organs due to the immune response of the host [16], [61], [62]. For these reasons, *in vivo* studies are important in elucidating potential health hazards associated with NMs exposure in a physiological environment.

The diverse routes of human exposure include inhalation, dermal uptake, ingestion, and injection (for drug delivery system).

Inhalation is the most common route of exposure to NPs in the workplaces. Once inhaled, these materials are carried by electrostatic force of the air from the upper to the lower respiratory tract. The NPs are absorbed across the lung epithelium and enter the blood and lymph depending on the nanomaterial size. When the NPs are deposited in the alveolar, they are usually attacked by the process of phagocytosis. This also leads to chemotactic activities which trigger the inflammatory cell response [61].

Oral is another route whereby NPs may enter the body. NPs can reach the gastrointestinal tract through the food, water, cosmetics, drugs, and drug delivery devices. Furthermore, exposure can occur during handling of the materials that contain the NPs. NPs administered orally are usually absorbed, through the epithelial cells of the Peyer's patches in the gut-associated lymphoid tissue (GALT) and also through the gut enterocytes and can translocate to other organs [54], [61]. However most of the effects observed after oral dosing in experimental animals are low and most of the NPs are excreted [63].

The intravenous administration of NPs is a very important route for the conduction of toxicological assessment in experimental animals. After i.v. injections, NPs have a rapid systemic distribution and most substances are subject to first-pass metabolism within the liver where they may accumulate or distribute via the vasculature to end organs including the brain. The blood—brain-barrier (BBB) protects the brain from external chemical insults, but the potential for nanoparticulate matter to pass through tight junctions makes the brain vulnerable to particle-mediated toxicity [16].

Upon inhalation, ingestion, or injection of pristine NPs, they encounter various complex physiological environments, leading to the covering of NPs with various biomolecules. Of particular importance is the adsorption of proteins on the nanoparticle surface. The formation of nanoparticle-protein complexes is commonly referred to as the nanoparticle-protein corona (NP-PC). Upon the formation of such a corona of biomolecules, the *in vivo* transformation of pristine NPs is rapidly initiated [53]. Serum/plasma and cellular proteins represent complex biological system that may cause the NP to undergo a complex sequence of modifications, so far not fully understood. Even within one environment the NP-protein interactions are constantly changing. For

example, when exposed to blood plasma, the nano-bio interface has been reported to change with time due to constant adsorption and desorption of proteins. NPs uptake could be influenced by protein adsorption, physical characteristics of the NPs, and the their properties to interact with cells [64], [65].

#### **1.4.1. AgNPs *in vivo* toxicity**

Biodistribution and toxicity of AgNPs were assessed in rodents by inhalation, intravenous, or oral exposure. An update of studies performed were revised by the Scientific Committee on Emerging and Newly Identified Health Risks (SCENHIR) and concluded that data on absorption and internal systemic exposure of nanomaterials is limited and may vary depending on physicochemical properties of the individual particles and the local barriers present in different organs[66].

The most common route of pulmonary exposure to AgNPs is via the occupational inhalation of airborne particles during manufacturing. Some studies have demonstrated in a rat model that inhaled NPs can translocate from their original site of deposition (e.g. lungs) to other tissues[67]. In the acute setting, no significant body weight changes or clinical changes were observed. Furthermore, lung function tests did not reveal any statistical differences between exposed and control groups. The subchronic inhalation induced a time- and dose-dependent inflammatory response in the alveoli and granulomatous changes as well as decreased lung function[68], [69].

In most AgNPs studies in rodents, the liver has been described as the primary organ for Ag distribution, followed by the spleen, kidneys, lung and brain. The results of i.v. injection suggested that tissue distribution of AgNPs was size-dependent and further suggest the potential size-dependent toxicity and health risks[70]. Adverse effects were generally recognized through changes in the blood biochemical parameters of liver function (such as ALT, AST, ALP, and cholesterol), while only occasionally mild histopathological changes were reported, such as biliary hyperplasia, fibrosis, hepatocellular vacuolar degeneration, and rarely necrosis [69], [71], [72].

Orally administered ionic and nanoparticulate silver have been described to be deposited in a wide range of organs. Some studies mainly performed in rats using different doses of AgNPs and different particle size, found the majority of the silver in the stomach and intestine followed by liver, spleen, testis, kidneys, brain and lungs [73], [74].

Adverse effects reported in AgNPs oral dosing studies were mild and only evident at doses of 125 mg/kg and above. In a range of oral investigations, no effects on body weight were reported [31], [73], [75], [76]. At that dose, an elevated cholesterol and cholestatic enzymes (alkaline phosphatase)

was observed and was accompanied by biliary hyperplasia [77]. This suggests that the biliary system may be a target for Ag accumulation [63]. Only one study evaluated adverse effects at a lower, more physiologically relevant dose [31]. In mice was found mild, dose-dependent increases in both serum pro-inflammatory (IL-1, IL-6, IL-12) and anti-inflammatory (IL-10, TGF $\beta$ ) cytokines. Among the different studies performed, no evidence of genotoxicity was detected [31], [78].

In the gastrointestinal tract some pathological findings were reported. AgNPs(5–20 nm) damaged the epithelial cell microvilli and intestinal glands [79]with an increased number of goblet cells [77].

In the brain, it was shown that exposure to AgNPs induces destruction of the BBB[80], astrocyte swelling, and causes neuronal degeneration [81]. Orally administered AgNPs affected also neurotransmitters (5-HT and dopamine) concentration in rat brain [82]. AgNP-treated rats, further subjected to heat stress, showed greater BBB disruption leading to edema formation, impairment of cognitive and motor functions and brain damage [83]. Moreover both AgNPs and Ag ions induced considerable synaptic damage, mainly in the hippocampus and to a lesser extent in the cerebral cortex of exposed rats [84].

Overall, data suggest that both tissue distribution and bioavailability of ingested AgNP are low and there is indirect evidence that AgNP may have lower bioavailability than ionic Ag. Moreover, evidence suggests that the likelihood for adverse effects on host tissues caused by acute or subchronic oral administration of AgNP is low [63].

Released of Ag ions from NPs surface is considered to be an important font for nanosilver toxicity. However studies are controversial, it was concluded that the toxicity of AgNPs is due to both the particulate form and the ionic silver released. In specific environmental conditions silver can be oxidized and dissolved to silver ions, which are the main active and reactive species of silver. Due to the limited specific surface area of bulk silver the amount of ionic species available is usually quite limited. As the particle size decreases towards nanoscale this situation is reversed, with a much higher proportion of the atoms being at the surface and consequently greater propensity for dissolution, or reaction [85]. Due to the ion release, the comparison of silver in nano and ionic form seems to be important in assessing AgNPs biodistribution and toxicity.



The best-described adverse effects in humans of chronic exposure to silver are a permanent bluish-gray discoloration (argyria/argyrosis) of the skin or eyes. Inhalation of soluble silver compounds has been reported to cause both upper (nose and throat) and lower (lungs) respiratory tract irritation, although irritation is most likely caused by the corrosive effect of nitrate in some silver compounds rather than by silver itself. Silver ions possess a high affinity for the thiol groups in the liver and have been shown to bind to reduced glutathione and be transported into the bile, thus depleting the amount of reduced glutathione available for biochemical pathways. Reduced glutathione plays an important role in maintaining proper structure and function of red blood cells, as well as eliminating organic peroxides [86].

#### **1.4.2. IONP toxicity**

Iron is considered one of the most inert materials used in nanotechnology. Overall the IONP do not seem to induce oxidative stress mediated toxicological effects, nor altered physiological process or behavior changes or visible pathological lesions.

Size of IONP may not be of much significance except for its magnetic characteristics that are usually found to be safe. Coating is the parameters that may pose different toxicity issues, and results clearly revealed dependence of toxicity on surface ligation. It was established that the surface of IONP could be manipulated to alter the endocytosis of nanoparticles and their subsequent toxicity. Similarly, coating of IONP nanoparticles with three very closely related carbohydrates i.e. glucose, lactose and maltose resulted in very different behavior in human cell line suggesting that the effect of surface coating will markedly affect nanoparticles fate *in vivo*. In vitro studies gave insight into the relationship between NP-coating material and cell viability. It was discovered that positively charged coatings induced a decrease in cell viability, due to DNA damage. Also, it is critical to understand the mechanism and interactions in which the NPs are involved in the body, to alleviate any possible side effects. It was found that, at high concentrations (above 400ppm), cell viability decreased. From this observation, so it was proposed that iron concentration is the critical factor for cell viability [46].

The cytotoxicity assays (WST-8, DCF, and LDH) performed by Hong et al., tested increasing concentrations of each modified SPION for cell viability, oxidative stress, and cell membrane

integrity. When considering IONP for clinical application, we should also consider the factor of iron overload, the metal may dissolve inside the body and lead to hemosiderosis i.e. accumulation of iron in various body organs, especially in the liver [87].

The main important conclusion about NPs toxicity is that because of the wide differences in properties among NMs, each of these types of NPs can elicit its own unique biological responses. As a result, different types of NPs must be categorized, characterized, and studied separately, although certain concepts of nanotoxicology based on the small size and coating, could likely be applied to all NMs [67].

## 2. AIMS

The constant increase in the applications of NPs in multiple fields, and the consequent concern for the human exposure, impel for an in-depth investigation of their potential toxic effects. A definitive conclusion on toxicological properties of NPs cannot be drawn so far due to high variability of tested NPs in terms of source of NPs (generated in the laboratory vs commercially available materials products), size, coating, route of exposure, dose administered, and the length of treatment during the conduction of the in-vivo experiments.

Moreover, since the physicochemical properties strongly affect the behavior of different NPs, a comprehensive physicochemical characterization of tested NPs is required. The lack of sufficient characterization of the nanoparticles used in the various experiments makes any correlation unlikely and hinders the comparison between different experiments.

The *in vivo* studies undertaken during my PhD were aimed at investigating two main aspects related to the exposure to nanoparticles:

- The role of physicochemical properties, in particular the size and coating, in the biodistribution (and potential toxicity) of fully characterized NPs. To this purpose, AgNPs and newly synthesized IONP were selected and administered by intravenous route.
- The *in vivo* effects following repeated oral exposure to low doses of AgNPs, in the attempt of investigating the potential effects that may arise in humans after repeated ingestion of very low doses of AgNPs that represents the most likely route of human exposure to these NPs.

### 3. MATERIAL AND METHODS

#### 3.1. Physicochemical characterization of NPs

##### 3.1.1. AgNPs

In order to reduce variability in term of source of silver nanoparticles (AgNPs), commercially available AgNPs were used (NanoComposix, San Diego, USA). All the suspensions were supplied at a concentration of about 1.0 mg/ml. BioPure™ AgNPs were chosen because they were guaranteed to be sterile and with an endotoxin level lower or equal to 2.5 EU/ml. The suspending solvents of CT- and PVP-coated AgNPs were 2.0 mM sodium citrate and Milli-Q water (Millipore), respectively.

Since NPs toxicity is related to the corresponding physicochemical properties, a rigorous approach is essential to have a reliable characterization of NPs [5]. For this reason, before the administration, a quality control was performed to ensure manufacture's physicochemical properties; particularly to describe the size of the primary particles and to assess the presence of agglomerates and/or aggregates.

AgNPs were characterized by using three different techniques, namely Dynamic Light Scattering (DLS), UV-visible (UV-Vis) spectroscopy, and Transmission Electron Microscopy (TEM). The following parameters were reported:

- The hydrodynamic diameter of the particles and their possible aggregation when suspended in the testing medium were evaluated by DLS.
- UV-Vis spectroscopy measurements were performed to further investigate the intrinsic features of the putative aggregates detected in 10 nm AgNPs. AgNPs exhibit a characteristic absorbance maximum in the visible range due to the surface plasmon resonance (SPR) effect [37]. Notably, optical properties of AgNPs are closely related to their morphology, therefore UV-Vis spectroscopy can detect any change in size/shape as well as the presence of aggregates.
- Additionally, TEM analysis was performed to assess the shape and primary size distribution of tested AgNPs.

### **Dynamic Light Scattering (DLS)**

The actual size of AgNPs in dispersion was measured by DLS. Measurements were performed with a Malvern Zetasizer Nano ZS90 instrument operating with a light source wavelength of 532 nm and a fixed scattering angle of 90°. All the nanoparticles were diluted 1:100 except for 10 nm-sized AgNPs. Indeed, due to their small size, the 10 nm AgNPs presented increased absorption and lower scattering intensity compared to 40 nm and 100 nm AgNPs. Accordingly, the 10 nm AgNPs were diluted 1:50. All measurements were run at room temperature for at least three times.

### **UV-Visible (UV-Vis) Spectrophotometry**

The UV-Vis spectra were acquired in the 300–800 nm range using a DU730 Beckman Coulter Spectrophotometer. All the nanoparticles were diluted 1:100 except for 10 nm AgNPs, which were diluted 1:200 because of their increased UV-Vis absorbance with respect to larger nanoparticles. All measurements were run at room temperature for at least three times.

### **Transmission Electron Microscopy (TEM)**

Formvar coated copper TEM grids (cod. PE1GC300, Pelco) were pre-treated with 20 µl of poly-L-lysine 0.01 % (w/v) (Sigma Aldrich) for 15 min. After washing twice with MilliQ water, 3 µl of AgNPs suspensions were deposited onto the grid for 5 min and then rinsed with 3 µl of 2-propanol (Sigma Aldrich). According to the manufacturer's advice, 100 nm and 40 nm AgNPs were used at the concentration of 1.0 mg/ml, while 10 nm AgNPs were diluted up to 0.1 mg/ml before use. The grids dried overnight at room temperature in a covered crystallizing dish. TEM (FEI Tecnai G2, Eindhoven) images were analyzed with the ImageJ software ([http:// imagej.nih.gov/ij/](http://imagej.nih.gov/ij/)) to obtain the nanoparticles dimensional distribution. Small objects due to background and overlapping nanoparticles were omitted by using proper cut-off filters and Feret diameter (intended as the larger diameter of the NP projection) was used to evaluate the size of the particles. For each sample, a minimum of about 250 nanoparticles were considered.

### 3.1.2. IONP

The synthesis of an NP-enzyme system for cancer therapy was performed according to the paper of Cappellini et al (Appendix B). The NP-enzyme system was based on iron oxide magnetic NPs (IONP) conjugated to the ROS producing enzyme D-amino acid oxidase from *Rhodotorula gracilis* (Fe<sub>3</sub>O<sub>4</sub>-APTES-DAAO).

IONP were characterized by using Dynamic Light Scattering (DLS) and infra-red (IR) spectroscopy.

IR spectroscopy allows the detection of functional groups and adsorbed molecules at the surface of NPs, as well as monitoring changes of the surface chemistry.

#### **Dynamic Light Scattering (DLS)**

Fe<sub>3</sub>O<sub>4</sub>-APTES-DAAO NPs were analyzed at concentrations of 250, 25 and 2.5 µg/ ml in water. Samples dilutions were done in order to analyze the effect of concentration on NP aggregation. Each measurement was preceded by an equilibration time of 90 s. Analyses were performed with Zetasizer Nano ZS90 (Malvern, UK) instrument. Measures were reported as scattering intensity in function to diameter.

#### **Infra-red (IR) spectroscopy**

Fe<sub>3</sub>O<sub>4</sub>NP-APTES-DAAO NPs were characterized by IR analysis in different conditions. Samples (disks of 2 cm<sup>2</sup> area) were placed in a quartz cell equipped with KBr windows. A movable quartz sample holder allows to adjust the pellet in the infrared beam for spectra recording and to displace it into a furnace at the top of the cell for thermal treatment. The cell was connected to a vacuum line for evacuation (Presidual = ~10<sup>-6</sup> torr) and for the introduction of gases into the infrared cell. Spectra were recorded at room temperature. The addition of well-known doses of gas in the cell was possible via a pressure gauge for the control of the gas pressure. A Nicolet Nexus spectrometer equipped with a Mercury Cadmium Telluride (MCT) cryodetector and an extended KBr beam splitter was used for the acquisition of spectra in the 600–5500 cm<sup>-1</sup> range. IR spectra are absorption spectra and the notation used is a.u. for absorption units. The resolution of the spectra was 4 cm<sup>-1</sup>, and 256 scans were accumulated for each spectrum. Three different experiments were

performed: first the samples have been dispersed in the KBr, then on the surface of a silica pellet; finally on a silicon disk. In details: a wafer containing 98 mg of KBr has been pressed at 4 tons/cm<sup>2</sup>, together with ~2 mg of the targeted sample; a wafer of 20 mg silica has been casted mixing in its center ~6–7 mg of sample, then pressed to 2 tons /cm<sup>2</sup> and ~2 mg of powder was dispersed on the surface of a 2 cm<sup>2</sup> silicon disk by the help of a spot of ethanol.

### 3.2. Dissolution study for AgNPs

CT-coated particles were selected for this investigation given the higher stability and lower dissolution generally showed by PVP-coated AgNPs [88]. Dissolution of CT-coated AgNPs of 10, 40 and 100 nm was ascertained by ultrafiltration, using a PES spin filter membrane (Vivaspin 500, 3 kDa MWCO, Sartorius, Göttingen, Germany) and centrifugation at 15000 g for 20 min, followed by quantification of silver in the filtrates. The concentration of ionic silver was measured both in the AgNPs stock suspensions and in conditions simulating AgNPs interaction with biological fluids. For the latter purpose, each stock suspension was spiked to mouse serum (Euroclone, Milan, Italy) to provide the mass concentration of AgNPs of a single dose of 10 mg/ kg bw, which approximately corresponded to a 1:5 dilution (v/v) of the original AgNPs suspension. Spiked samples and serum blank were prepared in triplicate and incubated at 37 °C under agitation for 5, 10, 60 min and 24 h. Ionic silver was assessed for each time point. For ICP-MS determination of ionic silver, filtrates (prepared in triplicate) were vigorously shaken before further dilution and analysis as described in the section “Determination of silver”. In addition to ionic silver, each stock suspension of CT-coated AgNPs was characterized in terms of total silver concentration and the results for ionic silver were expressed as percentages of total silver (AgNPs+Ag<sup>+</sup>). Samples for total silver determinations were prepared in triplicate by dilution with acidified (HNO<sub>3</sub>) water as necessary. In order to establish possible sources of bias from the filtration membrane, procedural blanks were run in parallel and the recovery of ionic silver (10 µg/L) from the filtration unit was assessed. No silver was detected in the procedural blanks and the average recovery of ionic silver was found to be 102.6± 3.8 %, showing absence of silver release/adsorption during filtration.

### **3.3. *In vivo* Studies**

The following studies were described in this thesis:

- Single intravenous administration of AgNPs: effect of size and coating on biodistribution and toxicity.
- Single intravenous administration of AgNPs: batch dependent toxicity.
- 5 days repeated oral administration of AgNPs: effect of coating on biodistribution
- 28 days repeated oral administration of AgNPs: effect of repeated administration of low doses on accumulation and toxicity
- Single intravenous administration of IONPs: effect of dose and vehicle on distribution and toxicity

The detailed experimental designs are reported for each study in chapter 4, while common material and methods applied are described in the following sections.

#### **3.3.1. Animals**

Male CD-1(ICR) mice of 4–5 weeks were purchased from Charles River (Calco, Italy). They were acclimated to the environment for a week prior to the initiation of the study, with free access to water and a standard pellet diet ad libitum. The environmental conditions were set at a temperature of  $22\pm 2$  °C, relative humidity of  $55\pm 10$  % and a 12 h light/dark cycle. Animals were euthanized by carbon dioxide inhalation.

All the experiments were approved by an independent Ethical Committee on Animal Experimentation (Ethical Committee of the University of Milan, Opinion no. 81/14 and 5/15) and were performed in accordance with the Italian Laws (D.L.vo 116/92 or D.L.vo 26/2014), which enforce EU 86/609 or 2010/63 Directive.

#### **3.3.2. Irwin test**

The Irwin observation test is commonly used to evaluate the effects of a new substance on behavior and physiological function. The Irwin test can also be used in a safety approach for



detecting untoward effects of a new compound on general behavior and for evaluating its acute neurotoxicity.

Behavioral modifications, physiological and neurotoxicity symptoms are recorded according to a standardized observation grid. Irwin's rating scale for the mouse consists of three major categories with which the behavioral, neurological and autonomic profiles are graded. All the measurable effects are scored on an arbitrary scale from 0 to 9. Four is assigned to a characteristic which is usually present under normal circumstances. The degree to which this characteristic is altered is scored from 4 to 8, if it is increased and 4 to 0 if it is decreased. Observations are performed 15, 30, 60, 120 and 180 minutes after administration of the test substance and 24 and 48 hours later.

### **3.3.3. Body and organ weight**

The body weight of each mouse was measured before the treatment and the sacrifice. In the 28 days repeated oral administration study, body weight was measured each day, immediately before treatment. During the recovery period mice were weighted two days a week.

The organ weight was measured after the sacrifice and relative organ weights (%) were calculated as wet organ weight/total body weight.

### **3.3.4. Sampling**

At the end of the studies mice were euthanized by carbon dioxide inhalation and mice underwent complete necropsy. Blood and tissues were sampled for different analyses (total silver determination, histology, special stains, immunohistochemistry, immunofluorescence, TEM) as detailed in this and following chapters.

### **3.3.5. Hematology and clinical chemistry**

Blood was counted on a laser based counter (Sysmex-XT 2000iV) with species-specific software. A blood smear was prepared, samples were centrifuged, and plasma (300 to 750  $\mu$ Ls) was transferred in another tube and frozen at  $-20^{\circ}$ . WBC differential, cell morphology, and platelet estimate were determined on May Grünwald-Giemsa stained smears. Clinical chemistry was

performed on thawed plasma with an automated spectrophotometer (ILAB-300, Instrumentation Lab).

#### **3.4. Determination of silver in the organs (inductively coupled plasma mass spectrometry: ICP-MS)**

Total silver content was determined in organs and in the whole blood by means of a triple quadrupole inductively coupled plasma mass spectrometer (ICP-MS) at the Department of Food Safety and Veterinary Public Health, National Health Institute-Roma. A 8800 ICPQQ spectrometer (Agilent Technologies, Japan, Tokio) equipped with an autosampler, a peristaltic pump, a Micro-Mist glass concentric nebuliser, and operated at a RF power of 1550 W, was used. All sample manipulations were carried out in clean room conditions under a laminar flow box. Before ICP-MS measurements, whole organs and blood were placed in Falcon tubes and pre-digested for 5 h at room temperature with 2–4 ml HNO<sub>3</sub>, depending on the organ weight. After adding 1 ml H<sub>2</sub>O<sub>2</sub>, samples were digested in a microwave system at 90 °C for 8 h, maximum power 800 W. After cooling, the digests were diluted by adding HCl (final concentration 3.0 M) to promote the formation of soluble silver complexes and prevent the precipitation of insoluble Ag<sup>+</sup> salts. Prior to analysis the digests were highly diluted with 0.1 % HNO<sub>3</sub> and the appropriate amount of HCl to maintain silver in complexed form. Measurements were carried out on 107Ag and 103Rh, as internal standard, by the method of external calibration. The method detection limit ranged from 0.4 to 0.7 µg/kg, depending on the tissue, and was 0.09 µg/l for blood. Truthfulness of ICP-MS measurements was assessed by analyzing the certified reference material SRM 1577c Bovine Liver (NIST, Gaithersburg, MD, USA), with a certified value for silver of 5.9 ± 1.6 µg/kg and the control material Seronorm™ Trace Elements Whole Blood L-1 (SERO AS, Billingstad, Norway) with an indicative value for silver of 185 ± 10 ng/l, both included in every analytical batch. The average determined silver concentrations were 6.0 ± 0.5 µg/kg (n = 6) and 179 ± 2 ng/l (n = 6) for the liver-based and the blood-based materials, respectively, in good agreement with the reference values. The truthfulness of determinations was also assessed through spikes of known amounts of silver in tissues and blood before sample dissolution, giving recoveries within the range of 90-100 % with no appreciable differences between sample types.

### 3.5. Histopathological examination

For histological examination organs were fixed in formalin solution, 10% neutral-buffered (pH 7.2, Bio-optica, Milan) for at least 48h at room temperature, routinely processed for paraffin embedding by using an automated tissue processor (Leica Microsystems). Formalin fixed paraffin embedded (FFPE) tissues were sectioned at 4  $\mu$ m thickness, stained with hematoxylin-eosin according to standardized protocol ([http://www.ihcworld.com/\\_protocols/special\\_stains/HE\\_Mayer.htm](http://www.ihcworld.com/_protocols/special_stains/HE_Mayer.htm)), and blindly evaluated under a light microscope.

The trimming procedures for sampled organs are here reported:

Liver: median lobe including the gall bladder, spleen: apical portion, kidney: half of the right kidney, lung: the left lobe, brain: half brain, for intravenous administration studies; after oral repeated administration, transversal sections were obtained after the fixation by using a brain matrix (Adult Mouse Brain Slicer Matrix BSMAS005-1, Zivic Instruments, USA), heart, small intestine (proximal and distal), colon and caecum.

Grading of histopathological lesions in the examined organs was performed as follows: 0 = absence of lesions; 1 = minimal lesions; 2 = mild lesions; 3 = moderate lesions; 4 = severe lesions.

### 3.6. Special histological stains

To visualize silver and iron in tissue sections, the following special stains were applied:

#### Autometallography (AMG)

According to Danscher [113], this method visualizes trace amounts of silver in paraffin sections from biological tissue. After exposure to light, which ensures reduction of silver ions that are not bound to sulphide, histological sections from animals treated with silver compounds are exposed to a photographic developer containing silver ions.

After AMG staining, sections were counterstained with safranin O and evaluated under a light microscope for the identification of tissue and cellular localization of silver, visible as black granular pigment.

#### Perls' iron stain

The stain aims to visualize iron deposits within tissues. The technique is based on the conversion of ferrocyanide to insoluble crystals of Prussian blue in the presence of  $Fe^{3+}$  under acidic conditions. Protocol applied according to Prophet et al. [114].

### 3.7. Immunohistochemistry and immunofluorescence

Four  $\mu m$  sections of FFPE tissues were simultaneously deparaffinized and heat induced epitope retrieval (HIER) was performed by immersion in a Buffer H solution according to the datasheet procedure (Dewax and HIER Buffer H, Thermo Scientific). Then the following primary antibodies were applied:

Antibody	Clonality	Marker of
GFAP (Glial Fibrillary Acidic Protein)	Rabbit polyclonal	Astrocyte
IBA1 (Ionized calcium binding adaptor molecule 1)	Rabbit polyclonal	Pan-macrophage/histiocyte and microglia
Albumin	Rabbit polyclonal	Blood Brain Barrier damage
Cleaved-caspase 3	Rabbit polyclonal	Apoptotic cells

Sections were then incubated with biotinylated secondary antibody, labelled by the avidin-biotin-peroxidase procedure. The immunoreaction was visualized with 3,3'-diaminobenzidine substrate and sections were counterstained with Mayer's haematoxylin. Known positive control sections were included in each immunolabeling assay.

For immunofluorescence (IF), following secondary antibody was applied: AlexaFluor555 F(ab')<sub>2</sub> Fragment of Goat Anti-Rabbit IgG (H + L) (Molecular Probes, Life Technologies Europe BV, Monza, Italy). Immunofluorescent labeled sections were acquired with the Leica TCS SP5 confocal microscope (Leica Microsystems). The fluorophore was excited with the 532 nm laser line and the emitted fluorescence acquired in sequential scan mode with ACS APO 63x/1.15 Oil CS objective. Nuclei were visualized by DAPI staining (405nm laser line excitation). Silver aggregates were visualized by reflection of light at 561 nm.

### **3.8. Digital Image Analysis (DIA)**

Images were acquired using a 20x or 40x objective and analyzed using the ImageJ analysis program (<http://rsb.info.nih.gov/ij/>).

#### **DIA for Perls stain**

Three 200x microscopic fields in liver, spleen, lung, kidney, brain, heart were randomly acquired and the area of Perls staining was measured in each field. The percentage of Perls positive area per field was then calculated.

#### **DIA for IBA1 and GFAP IHC**

Area of Iba1 and GFAP immunostaining was measured in three 400x/microscopic fields randomly selected in the hippocampus (CA1- CA2 and CA3 regions). The percentage of immunostained positive area per field was then calculated. Additionally, the number of IBA1 positive cells per 400x field was then counted.

### 3.9. TEM

Hippocampus and small intestine samples were reduced and fixed with 4% paraformaldehyde (PFA) and 2% glutaraldehyde in phosphate buffer 0.12 mol/l pH 7.4 for 6 hours, followed by incubation at room temperature for 2 h in 1% OsO<sub>4</sub>. After dehydration in a graded series of ethanol preparations, tissue samples were cleared in propylene oxide, embedded in epoxy medium (Epoxy Embedding Medium kit; Sigma-Aldrich, St. Louis, MO 63103 USA) and polymerized at 60°C for 72 h. From each sample, one semi-thin (1 µm) section was cut with a Leica EM UC6 ultramicrotome (Leica Microsystems, Vienna, Austria), stained with Toluidine Blue and mounted on glass slides to identify the areas of interest. Ultra-thin (60 nm thick) sections were then obtained, counterstained with uranyl acetate and lead citrate, and examined with an energy filter transmission electron microscope (Libra120, Carl Zeiss NTS GmbH, Oberkochen, Germany) equipped with a yttrium aluminum garnet (YAG) scintillator slow-scan charge-coupled device (CCD) camera (Sharp eye, TRS, Moorenweis, Germany).

### 3.10. Statistical analysis

Data were analyzed using Graph Pad Prism version 5.0 (GraphPad Software, San Diego, CA). Since the numbers of data obtained from *in vivo* experiments and from digital image analyses do not assume normal distribution, nonparametric tests (Kruskal-Wallis and Mann-Whitney U test) were used to compare the different groups of treatment.

#### List of abbreviation:

DLS: Dynamic Light Scattering

TEM: transmission Electron Microscopy

AgNPs: Silver Nanoparticles

IONP: Iron Oxide Nanoparticles

AgAc: Silver Acetate

H&E: Haematoxylin and Eosin

AMG: Autometallography

IHC: Immunohistochemistry

IF: Immunofluorescence

DIA: Digital Image Analysis

## 4. RESULTS

### 4.1. BIODISTRIBUTION AND TOXICITY OF AgNPs

#### 4.1.1. Single intravenous administration: effect of size and coating on biodistribution and toxicity

(published paper: Recordati-De Maglie et al, 2016)

In order to assess the impact of the physicochemical properties of AgNPs on the mice behavior *in vivo*, a preliminary study was conducted to investigate the effect of the size and coating of AgNP on tissue distribution and toxicity after single intravenous administration. The results obtained were compared with those obtained after administration of silver ions. In comparison to the studies selected from the literature, lower doses were administered.

#### Physicochemical characterization

AgNPs of 10, 40 and 100 nm in size, coated either with citrate(CT) or polyvinylpyrrolidone (PVP) were checked according to methods described in chapter 3 (3.1). Following methods was applied:

- DLS
- UV-vis spectroscopy
- TEM

A dissolution study was performed in mouse serum in conditions simulating AgNPs interaction with biological fluids.

#### Study design

Mice were randomly assigned to 8 groups of treatments (n=3 per group) (Tab.1). Mice were intravenously injected with AgNPs of different size (10 nm, 40 nm and 100 nm), either CT or PVP-coated, at a single dose of 10 mg/kg, and with AgAc (silver acetate) at a single dose of 15.5 mg/kg, corresponding to 10 mg Ag/kg bw (n=3 animals per group). The dosing volume was 10 ml/kg bw. Animals belonging to the control group were treated with deionized water. Immediately after the treatment and the following hours, the general health and behavior of mice was monitored (Irwin

test). The body weight of each mouse was measured before treatment and at sacrifice which occurred 24 hours after the treatment.

Tab. 1. Experimental Groups:

Treatment	Dose	Time of sacrifice
CTR (vehicle)	10 ml/kg	T +24h
CT-AgNPs 10nm	10 mg/kg	
CT-AgNPs 40nm	10 mg/kg	
CT-AgNPs 100nm	10 mg/kg	
PVP-AgNPs 10nm	10 mg/kg	
PVP-AgNPs40nm	10 mg/kg	
PVP-AgNPs 100nm	10 mg/kg	
AgAc	15.5 mg/kg	

According to the procedures described in chapter 3, organs (liver, spleen, kidney, lung, brain, heart) were sampled and the following determinations were done:

- Determination of silver content in tissues: ICP-MS;
- Visualization of silver in tissues: AMG
- Identification of cells containing silver aggregates: immunofluorescence for IBA1.
- Histopathological examination.



## Results and discussion

(Additional details in the published paper Recordati.De Maglie et al 2016, Annex B and additional data in Annex A)

### Physicochemical characterization

The particles were thoroughly characterized before the investigation of their toxicological effects *in vivo* and their accordance to manufacturer's specifications assessed.

- DLS

The hydrodynamic diameter of the particles and their possible aggregation when suspended in the testing medium were evaluated by DLS. The results are summarized in Table 2. Monomodal distributions were observed for 40 nm and 100 nm AgNPs, coated with both CT and PVP. The 10 nm AgNP-CT and 10 nm AgNP-PVP suspensions showed multimodal distributions. The peaks at 18.1 and 19.6 nm were indicative of isolated nanoparticles in 10 nm AgNP-CT and 10 nm AgNP-PVP, respectively, while larger peaks in both samples suggested the possible presence of aggregates with variable dimensions. However, these large peaks were still detected by DLS even after filtration (0.22  $\mu\text{m}$  pore size), thus indicating their dynamic nature.

- UV-vis spectroscopy

To further investigate the intrinsic features of the putative aggregates detected in 10 nm AgNPs, UV-Vis. spectroscopy measurements were performed. AgNPs exhibit a characteristic absorbance maximum in the visible range due to the surface plasmon resonance (SPR) effect [89]. Notably, optical properties of AgNPs are closely related to their morphology, therefore UV-Vis spectroscopy can detect any change in size/shape as well as the presence of aggregates. The UV-Vis results are shown in Table 2. The correspondence between the optical properties given by the manufacturer and those measured in our laboratory appeared satisfactory. In particular, we did not observe any decrease in the maximum absorbance value ( $H_{\text{max}}$ ), indicating absence of aggregates. Then, full absorbance spectra of all samples were considered (Fig. 6). In 10 nm AgNP-CT and 10 nm AgNP-PVP the optical density in the 600–800 nm range, which is typical for aggregate absorption, was

not detected, further demonstrating that the presence of stable aggregates in these samples could be excluded.

**Tab. 2.** Physicochemical characterization of tested AgNPs.

Biopure™ Silver NPs	DLS			UV-Vis		TEM
	Mean hydrodynamic diameter (nm)	Max intensity peaks	pdl	$\lambda$ max (nm)	Hmax (a.u.)	Diameter (mean $\pm$ SD, nm)
10 nm AgNP-CT	np	18-4646	0,258	392	163,5	8,4 $\pm$ 1,5
10 nm AgNP-PVP	np	19,6-11-4292	0,343	389	163,6	10,8 $\pm$ 2,6
40 nm AgNP-CT	40,1	49,8	0,213	412	125,6	39,3 $\pm$ 4,8
40 nm AgNP-PVP	51,8	97,6	0,251	410	145,7	40,3 $\pm$ 5,6
100 nm AgNP-PVP	87,6	102,9	0,148	490	45,1	107,7 $\pm$ 5,6
100 nm AgNP-PVP	104,1	119,4	0,124	491	46,8	105,5 $\pm$ 10,9

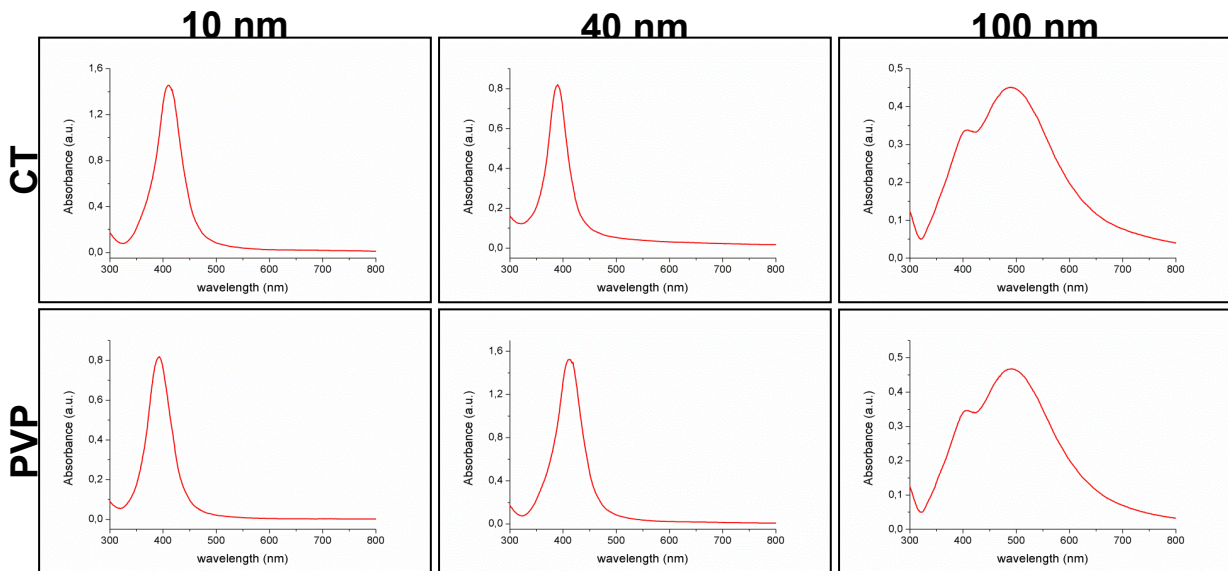


**Fig.6.** Particle characterization by UV–Vis spectroscopy: full absorbance spectra of the tested silver nanoparticles. The optical density in the 600–800 nm range, which is typical for aggregate absorption, was not detected in any of tested AgNPs, indicating the absence of stable aggregates in these samples.

- TEM

Eventually, TEM analysis was performed to assess the shape and primary size distribution of tested AgNPs. All the tested AgNPs were spherical in shape (Fig.7), and their Feret diameter distributions were in good accordance with data reported by the manufacturer ( $p > 0.05$  in all cases).

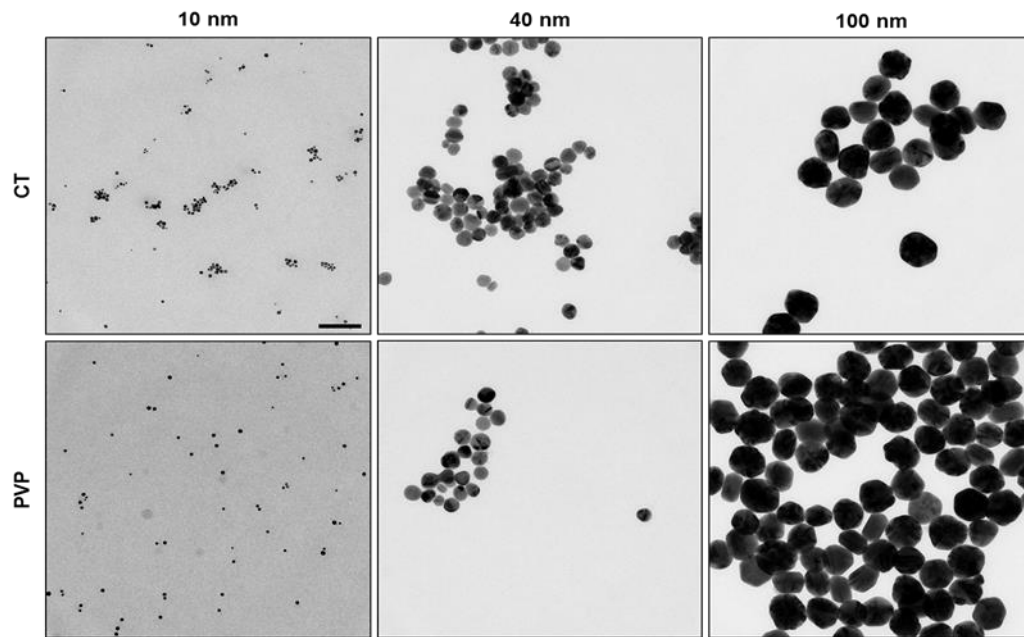


**Fig. 7.** TEM of tested silver nanoparticles. Representative transmission electron micrographs of 10, 40, and 100 nm AgNPs, CT- and PVP-coated. All purchased particles were spherical in shape, and no stable aggregates were visible (scale bar = 100 nm).

## Dissolution study

The presence of ionic silver in the stock suspensions of CT-coated AgNPs as well as AgNPs dissolution upon interaction with mouse serum was investigated by filtration on membranes with a pore size allowing discrimination of ionic silver from AgNPs. The percentage of ionic silver in the original stock suspensions was found to be negligible (0.002 %, 0.001 %, 0.001 % of total silver for 10, 40 and 100 nm AgNPs, respectively). Time dependent dissolution of AgNPs in simulated biological conditions is shown in Table 3. As expected, the dissolution was greater for smaller particles and increased with time; however even for 10 nm-sized particles at 24 h, the percentage of ionic silver was found to be exceedingly low (0.005 %). The low dissolution of AgNPs when incubated in mouse serum is in accordance with other studies, which suggest that when AgNP are introduced in a physiological environment, their ability to release Ag<sup>+</sup> is inhibited. This could be probably due to the formation of the protein corona [39]. Interaction of protein thiol groups with the charged surface of AgNPs in a medium with a high ionic strength is at the basis of the sulfidation process that leads to an extensive decrease of the dissolution rate *in vitro*, causing also the formation of nanobridges between particles, and has the potential to stabilize them *in vivo*. The formation of the protein corona decreases the extracellular dissolution of AgNPs. This leads to the cellular uptake of particles, which may lose the corona after the internalization resulting in an exacerbated release of Ag ions and toxicity [39]. Dissolved silver ions likely react with chlorine in serum to form AgCl [90]. On the other hand, it cannot be ruled out that a minor part of the released silver ions might have been complexed with high affinity S-containing proteins and thus has been excluded by the membrane used, leading to a possible underestimation of the level of Ag<sup>+</sup> released [91]. However, even if the method used for the study of particles dissolution may have not provided an entirely accurate measure of ionic silver formation in physiological conditions – all available methods have some limitations in this respect [92] – it clearly shows that the extracellular dissolution of the AgNPs used in this study is very limited, and animals dosed with AgNPs were internally exposed to particulate and not ionic silver.

**Tab. 3.** Time dependent dissolution of AgNPs in simulated biological conditions. Results for ionic silver are expressed as percentage of total silver measured in the stock suspensions

Biopure™ Silver NPs	5 min	10 min	60 min	24 h
10 nm AgNP-CT	0,377*10 <sup>-3</sup>	0,510*10 <sup>-3</sup>	0,937*10 <sup>-3</sup>	5,010*10 <sup>-3</sup>
40 nm AgNP-CT	0,049*10 <sup>-3</sup>	0,075*10 <sup>-3</sup>	0,176*10 <sup>-3</sup>	1,235*10 <sup>-3</sup>
100 nm AgNP-PVP	0,005*10 <sup>-3</sup>	0,016*10 <sup>-3</sup>	0,038*10 <sup>-3</sup>	0,366*10 <sup>-3</sup>

### Clinical signs

Immediately after the administration of AgNPs and AgAc, and during the following hours, all mice appeared healthy and no abnormal behavior was observed (see Irwin test for 10 nm AgNPs, Appendix A). However, 24 h after the treatment, two mice (one mouse treated with 10 nm AgNP-CT and another one treated with 10 nm AgNP-PVP) were found dead. Complications related to the injection procedure or formation of large aggregates after administration were reasonably ruled out given the delayed onset of mortality and the results of the subsequent histopathological evaluation (i.e. absence of thromboembolic lesions associated with silver aggregates). At sacrifice, no significant differences in bodyweight gain and organ weights were recorded between CT- and PVP-coated AgNPs of the same size. In mice treated with 10 nm AgNPs, a significant difference in weight loss and relative spleen to body weight were observed when compared to controls, and 40 and 100 nm AgNP-treated mice (Tables 4-5). No other significant differences were observed in the relative organ weights between treated and control mice.

**Tab. 4.** Mean of body weight and body weight gain in all groups of treatment.

Treatment	Weight (gr)		Weight gain	
	pre-treatment	sacrifice	(g)	weight (%)
CTR				
mean	28,73	27,82	-0,91	-3,31
SD	1,34	2,67	1,35	4,95
CT-coated Ag-NPs 10 nm				
mean	27,82	24,34	-4,25	-14,84
SD	1,47	0,56	0,37	0,83
CT-coated Ag-NPs 40 nm				
mean	27,66	27,65	-0,01	0,04
SD	1,82	1,42	0,84	2,98
CT-coated Ag-NPs 100 nm				
mean	28,50	28,08	-0,42	-1,39
SD	1,86	1,38	0,48	1,57
PVP-coated Ag-NPs 10 nm				
mean	28,31	24,73	-2,48	-9,32
SD	2,30	3,34	1,53	6,23
PVP-coated Ag-NPs 40 nm				
mean	27,56	26,84	-0,72	-2,61
SD	1,61	1,64	0,62	2,28
PVP-coated Ag-NPs 100 nm				
mean	27,73	28,06	0,33	1,21
SD	0,56	2,06	2,07	7,49
AgAc				
mean	28,2	26,4	-1,8	-6,3
SD	2,6	2,5	0,9	3,3

**Tab. 5.**Total and Relative organ weights.

	TOTAL WEIGHT					RELATIVE WEIGHT				
	spleen	liver	kidney	Brain	lung	spleen	liver	kidney	Brain	lung
CTR										
mean	0,13	1,84	0,50	0,49	0,18	0,45	6,61	1,80	1,77	0,66
SD	0,05	0,32	0,09	0,01	0,03	0,14	0,75	0,16	0,14	0,05
CT-coated Ag-NPs 10 nm										
mean	0,15	1,85	0,41	0,45	0,17	0,64	7,26	1,68	1,75	0,62
SD	0,01	0,16	0,05	0,04	0,05	0,04	0,31	0,25	0,01	0,10
CT-coated Ag-NPs 40 nm										
mean	0,12	1,81	0,45	0,48	0,18	0,43	6,53	1,64	1,73	0,65
SD	0,03	0,24	0,07	0,01	0,05	0,10	0,58	0,24	0,11	0,16
CT-coated Ag-NPs 100 nm										
mean	0,11	1,97	0,52	0,47	0,17	0,39	7,01	1,86	1,66	0,61
SD	0,01	0,05	0,07	0,02	0,02	0,03	0,29	0,15	0,11	0,09
PVP-coated Ag-NPs 10 nm										
mean	0,17	1,70	0,44	0,44	0,13	0,65	6,18	1,64	1,81	0,76
SD	0,03	0,32	0,07	0,02	0,10	0,03	0,49	0,08	0,16	0,07
PVP-coated Ag-NPs 40 nm										
mean	0,12	1,93	0,52	0,49	0,18	0,45	7,21	1,95	1,83	0,66
SD	0,02	0,17	0,05	0,02	0,01	0,08	0,61	0,27	0,14	0,04
PVP-coated Ag-NPs 100 nm										
mean	0,11	1,94	0,49	0,46	0,18	0,40	6,92	1,73	1,64	0,65
SD	0,03	0,17	0,04	0,03	0,02	0,09	0,20	0,03	0,15	0,03
AgAc										
media	0,12	1,85	0,51		0,21	0,47	6,99	1,92	0,00	0,80
SD	0,02	0,31	0,07		0,01	0,03	0,49	0,22	0,00	0,08

### Biodistribution (ICP-MS, AMG, IF)

Distribution and localization of silver in the different organs 24 hours after IV administration of the different AgNPs were evaluated using two distinct, but complementary approaches: ICP-MS and autometallography (AMG) staining. ICP-MS was used to quantitatively measure the silver concentration in blood, spleen, liver, lung, kidney, and brain; while AMG was used to qualitatively assess its localization within the sampled organs. After 24 hours, the silver concentration in blood was severely reduced in all groups.

For all particle sizes, regardless their coating, the highest silver concentration was found in the spleen and liver, followed by lung, kidney and brain. These results are in line with previous studies that investigated tissue distribution of AgNPs 24 h after IV administration [72], [93]. When considering the percentage of the administered silver dose recovered after administration, for all tested AgNPs, approximately 40 % of the administered dose was found in the liver, which resulted to be the main target organ of silver distribution, followed by spleen, lung, kidney, and brain. Most of the silver that reaches the blood is filtered by the liver and excreted into the bile [50], while the remaining circulating particles are distributed to organs containing a large number of phagocytic cells. Concentrations of silver in the lung, kidney, and brain were higher in mice treated with 10 nm-AgNPs (CT- and PVP-coated) than in mice treated with larger particles (40 nm and 100 nm). In addition, silver concentration in the brain of mice treated with 10 nm-AgNPs was higher than in mice treated with larger particles. Regarding the effect of coating on tissue distribution of AgNPs, coating of AgNPs did not have any relevant effect on biodistribution, in line with previous studies [73](Fig. 6).

The tissue localization of silver was further evaluated after AMG staining that allows enhancing the silver present within the tissues, thus providing a rapid and more sensitive histochemical approach for the detection of the distribution of silver within the organs. Tissues from control mice were negative for the specific staining. In the liver of AgNPs treated mice, most of silver was found within Kupffer cells. Also sinusoidal endothelial cells and hepatocytes were occasionally stained. In the spleen, regardless the size and coating, silver was localized within the cytoplasm of macrophages in the marginal zone of the white pulp and in the red pulp, and occasionally within



splenic endothelial cells. In the lung, scattered silver containing cells were found in the alveolar septa, either within the capillaries or the interstitium. AMG is not able to identify particles and thus to assess localization of silver in the brain and kidney (Fig.7). In AgAc treated mice, silver was found in renal tubule (Fig. 8).

Immunostaining of sections with IBA1 (a pan-macrophage marker) confirmed that the majority of the silver-containing particle aggregates were accumulated within the cytoplasm of Kupffer cells in the liver in all the examined groups(Fig. 9).The amount and size of silver containing aggregates within macrophages decreased with the reduction in size of AgNPs. In 10 nm AgNPs treated mice, only scattered and very small aggregates were found throughout the liver, while no visible silver-containing aggregates were found in the liver of AgAc treated mice.

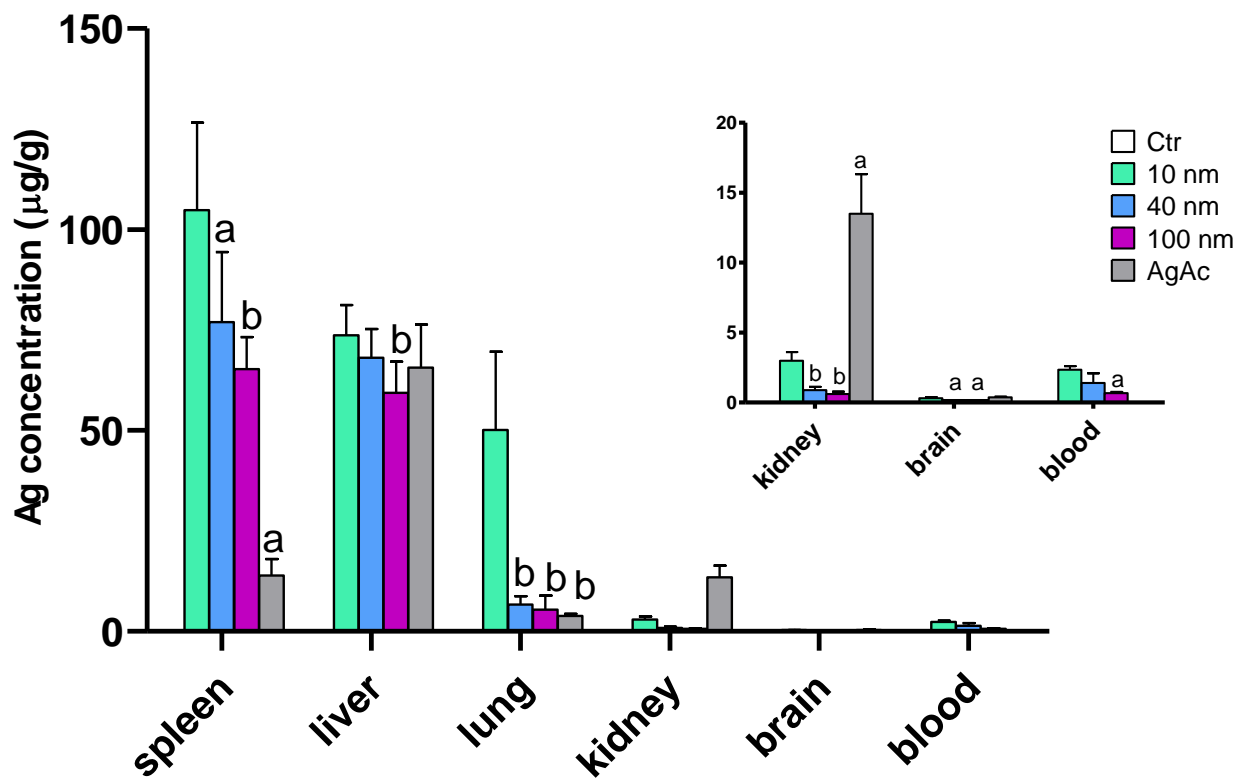


**Fig. 6.** Silver tissue concentration after IV administration of AgNPs (Ct and PVP-coated) and AgAc in mice. Data are expressed as means±SD. Statistical significance: a=p<0.05; b=p<0.01vs10nm.

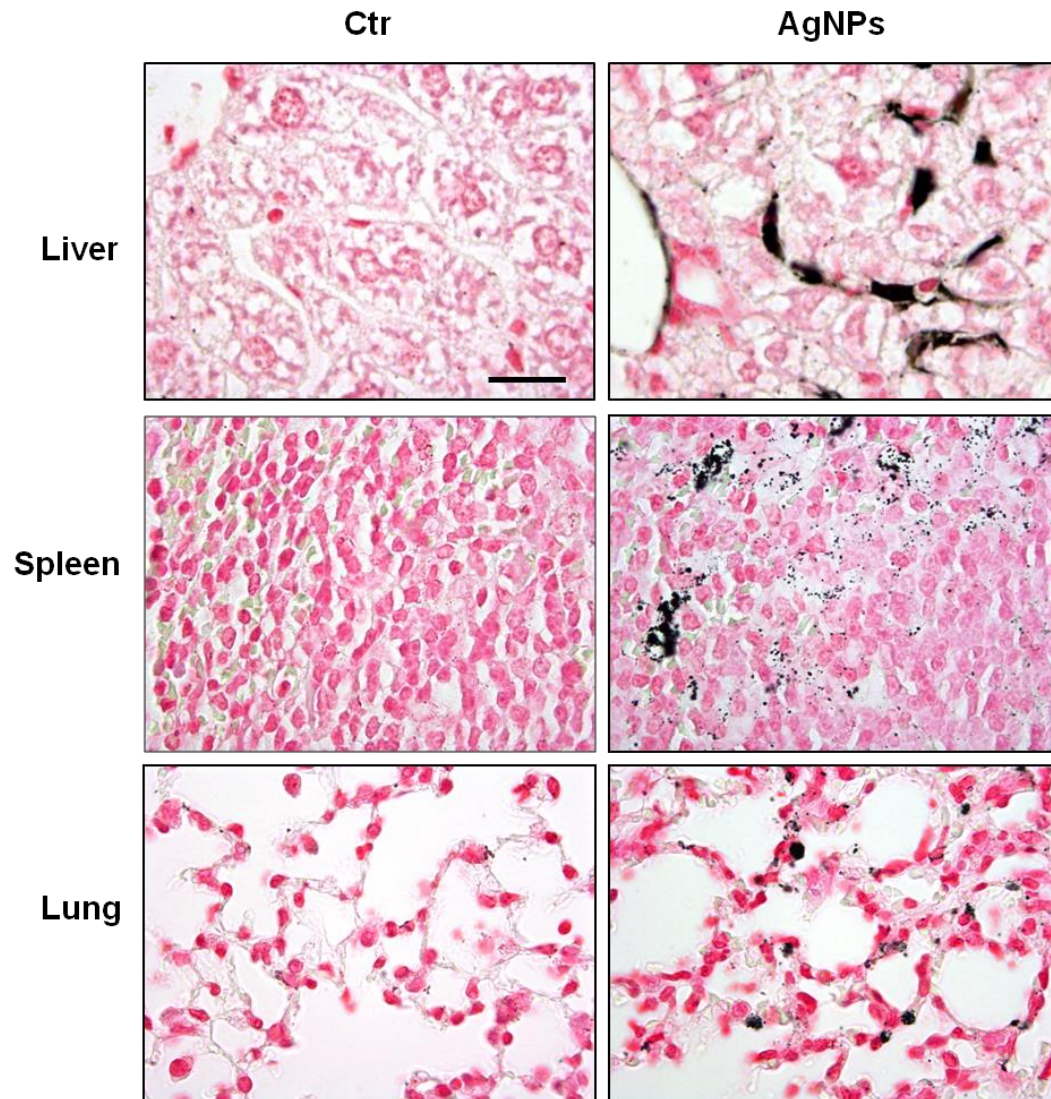


**Fig.7.** AMG staining, 1000x (scale bar 20  $\mu$ m). Treated animals: Silver localized in liver Kupffer cells, marginal zone macrophages in the spleen and in the alveolar septa in the lungs. No silver was detected in tissues of control group (left panel).

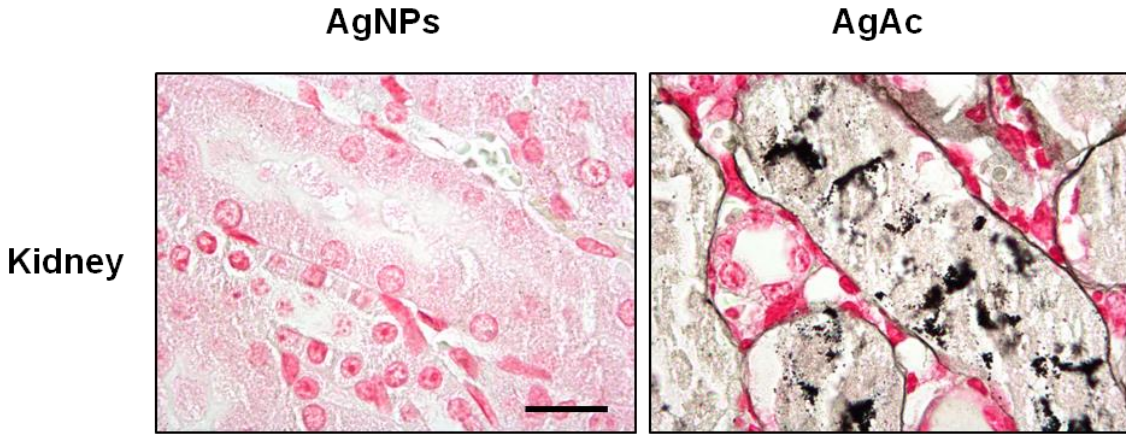


**Fig.8. AMG staining.** 1000x (scale bar 20  $\mu$ m). In AgAc treated mice, silver was found in renal tubules (left panel). Silver accumulation was not observed in AgNPs treated amice.

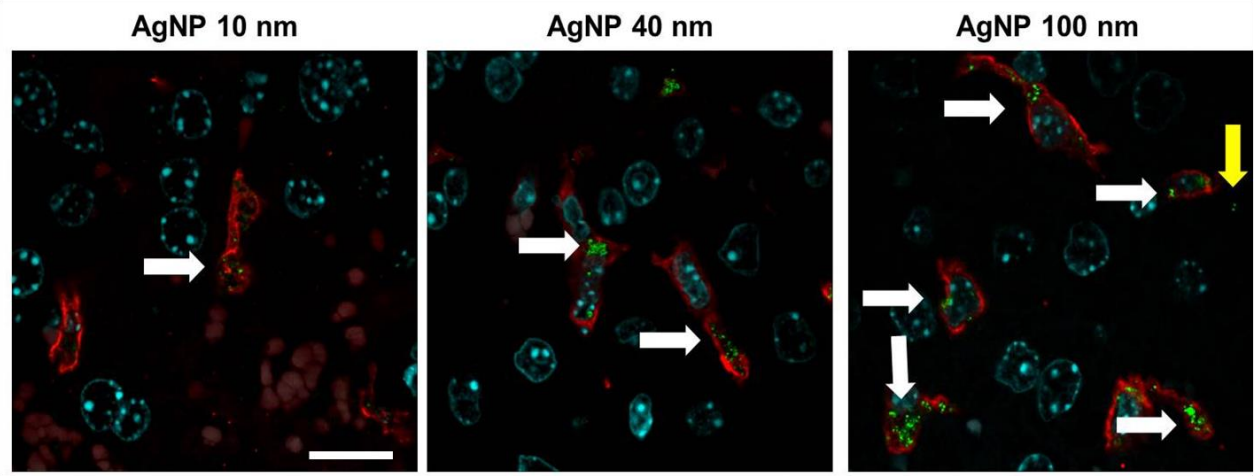


**Fig.9. Immunofluorescence** for Iba1 (red) and co-localization with AgNPs (green) in the liver (magnification, 400x, scale bar 20  $\mu$ m).

### Histopathological examination

Histological AgNP-related lesions were observed in the spleen, liver, and gall bladder of AgNP-treated mice. No relevant differences were found between CT- and PVP-coated particles of the same size. Overall, the prevalence and severity of lesions (in particular those involving liver and gall bladder) were size-dependent, and most frequently observed in mice treated with 10 nm AgNPs, that are more severely affected compared to 40 nm and 100 nm AgNP-treated mice, that respectively show milder or negligible lesions (Table 7). Splenic hyperemia was present in all mice treated with AgNPs, but it was particularly pronounced only in mice treated with 10 nm-sized particles. They might be responsible for the splenomegaly observed, as well as the increased relative spleen weight measured in this group. Mice treated with 10 nm AgNPs were affected by diffuse and severe midzonal hepatocellular necrosis and hemorrhage, multifocal peribiliary microhemorrhages, occasional portal vein endothelial damage (i.e. endothelial sloughing, subendothelial hemorrhages, intraluminal fibrin thrombi), and diffuse mural and intraluminal hemorrhage of the gall bladder. Among mice treated with 40 nm AgNPs, only one out of six had early peri-portal coagulative necrosis, scattered hepatic single cell necrosis, and gall bladder severe mural and intraluminal gall bladder hemorrhage. In the other mice treated with 40 nm AgNPs, the hepatic lesions were not observed and gall bladder lesions were milder, usually consistent with mural hyperemia and/or edema. Mice treated with 100 nm AgNPs had only occasional and mild gall bladder mural hyperemia and/or edema. No relevant pathological changes were observed in the lung, kidneys, and brain of AgNP-treated mice, and in all the examined organs of control mice (Fig. 10). A completely different pathological scenario was observed after administration of AgAc. Hepatobiliary lesions were not observed, whereas a marked acute renal tubular necrosis and apoptosis with intraluminal accumulation of hyaline casts was found in all treated mice. Presence of renal lesions, associated with the identification of silver in the affected renal tubules and relevant silver concentrations in the kidney of AgAc-treated mice indicates that, dissolved silver ions resulted in an increased renal silver distribution compared to AgNPs, and that renal lesions were linked to the renal excretion of silver (Fig. 11).

**Tab. 7.** Prevalence of histopathological lesions in mice following IV exposure to 10 mg/kg of AgNPs. Data are expressed as number of mice with lesions/total number of examined mice per group (%).

Group	Spleen	Liver	Gall bladder	Lung	Kidneys	Brain
Control	1/3 (33%)	0/3 (0%)	0/3 (0%)	0/3 (0%)	0/3 (0%)	0/3 (0%)
10 nm AgNP-CT	3/3 (100%)	3/3 (100%)	3/3 (100%)	0/3 (0%)	0/3 (0%)	0/3 (0%)
10 nm AgNP-PVP	3/3 (100%)	3/3 (100%)	3/3 (100%)	0/3 (0%)	0/3 (0%)	0/3 (0%)
40 nm AgNP-CT	3/3 (100%)	1/3 (33%)	2/3 (67%)	1/3 (33%)	0/3 (0%)	0/3 (0%)
40 nm AgNP-PVP	2/3 (67%)	0/3 (0%)	1/3 (33%)	1/3 (33%)	0/3 (0%)	0/3 (0%)
100 nm AgNP-CT	1/3 (33%)	0/3 (0%)	2/3 (67%)	0/3 (0%)	0/3 (0%)	0/3 (0%)
100 nm AgNP-PVP	1/3 (33%)	0/3 (0%)	0/3 (0%)	0/3 (0%)	0/3 (0%)	0/3 (0%)
AgAc	0/3 (0%)	0/3 (0%)	0/3 (0%)	0/3 (0%)	3/3 (100%)	0/3 (0%)

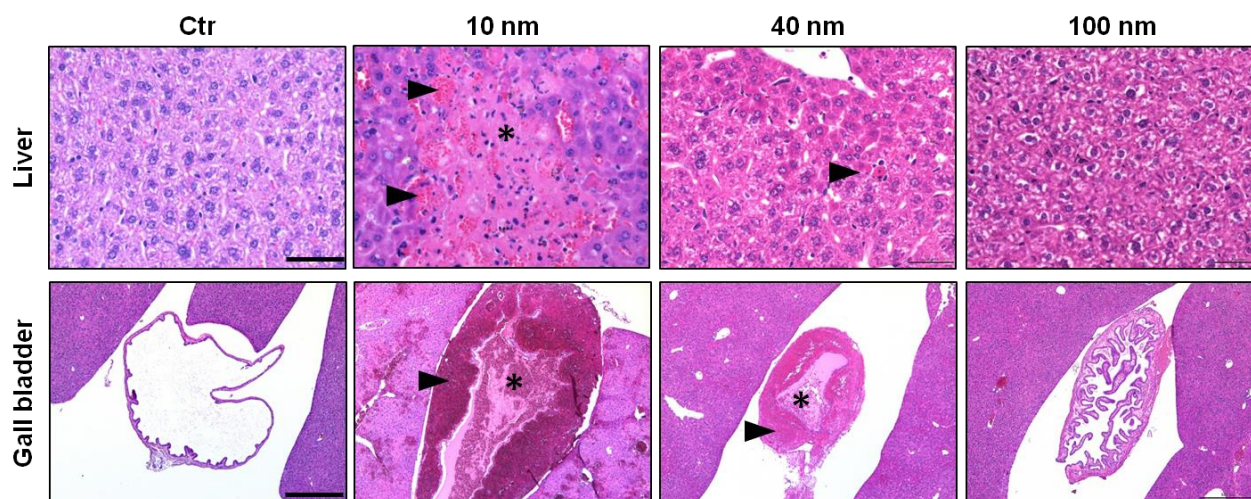


**Fig. 10.** Hematoxylin&Eosin. Liver, 200x (scale bar 50  $\mu$ m): in 10 nm AgNP, treated mice showed a marked midzonal hepatocellular necrosis (\*) and hemorrhage (arrow), while in 40 nm treated mice only occasional single cell necrosis (arrow) was occasionally found. Gall bladder, 100x (scale bar 500  $\mu$ m): intraluminal (\*) and mural (arrow) hemorrhage in 10 nm and 40 nm AgNPs treated mice.

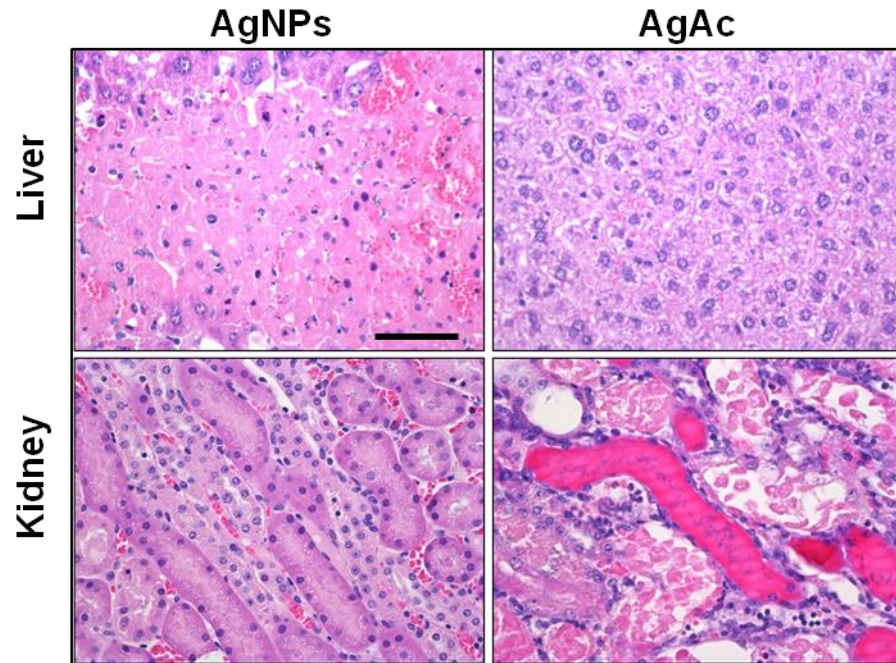


**Fig. 11.** Hematoxylin&eosin, 400x (scale bar 50  $\mu$ m). Midzonal hepatocellular necrosis (upper panel) was found in liver of mice treated with AgNPs, while renal tubular necrosis with intraluminal accumulation of hyaline casts was observed in mice treated with AgAc.

## Conclusions

- The physicochemical characterization ensured that the AgNPs used in the experimental conditions were suitable for *in vivo* studies and no stable aggregates were detected.
- The dissolution study of AgNPs performed in mouse serum indicated that the tested AgNPs underwent a very low dissolution and animals dosed with AgNPs were thus internally exposed to particulate and not ionic silver.
- After IV administration, we concluded that the organs most affected by Ag accumulation were the spleen and the liver, followed by the lungs. These results are in line with other *in vivo* studies conducted in rodents [71], [72], [93]. Some authors suggested that tissues with a fenestrated or incomplete endothelial lining, such as liver and spleen, respectively, contribute to a significant uptake of nanoparticles[93]. The accumulation occurred in tissues containing large numbers of phagocytic cells involved in clearing foreign body particles and xenobiotic NPs from the blood stream.

In the liver, those cells residing within the portal tract region exhibit increased levels of scavenger receptors, phagocytosis and lysosomal enzyme activity compared to centrally located cells, which have increased cytokine activities. Splenic macrophages that reside within the red pulp, white lymphatic pulp and marginal regions significantly differ in the levels of endocytosis, with marginal zone macrophages exhibiting significant increases in MARCO (macrophage receptor with collagenous structure) receptors. These receptors were also used by the alveolar macrophages for the uptake and processing of NPs [94].

- The biodistribution of Ag was size dependent, confirming the results of other studies [93] which demonstrated that particles smaller than the pore size of liver fenestrae (~100 nm) undergo to an enhanced liver uptake.
- The toxicity of AgNP was size dependent. The smallest AgNPs induce the more severe effects. This might be due to their greater surface area; a much higher proportion of the atoms being at the surface and consequently greater propensity for dissolution, or reaction [85].
- Concerning the observed histopathological changes, the hepatocellular midzonal necrosis is the least common histopathological pattern of hepatocellular necrosis following exposure to hepatotoxicants. The gall bladder mural hemorrhage, as well as the portal peribiliary



hemorrhages, could result from the endothelial damage consequent to the massive elimination of AgNPs in the bile, which is considered the main route of silver excretion following IV administration of AgNPs [95].

- The toxicity was different between AgNPs and Ag ions, and this is because of the different excretion routes. Dissolved silver ions resulted in an increased renal silver distribution compared to AgNPs, and renal changes were likely consequent to the renal excretion of silver.
- The different coating of AgNPs did not have any relevant effect on toxicity, likely because of the protein corona formation after injection.
- Due to the severe toxicity and the higher distribution showed by the smallest AgNPs, the 10 nm were selected to conduct oral studies.

#### 4.1.3. Single intravenous administration of AgNPs: batch dependent biodistribution and toxicity

To confirm the lesions occurred after administration of 10 nm AgNPs, additional three different batches of AgNPs of the same size were tested. Eventually, to assess the hypothesis that very small NPs determine the most severe toxic effects, 5 nm AgNPs was administered.

##### Physicochemical characterization

Three batches of 10 nm AgNPs, CT coated, were checked according to the methods described in chapter 3 (3.1). Specifically the following methods were applied:

- DLS
- UV-vis spectroscopy
- TEM

##### Study design

Mice were randomly assigned to 7 groups of treatments (n=3 per group). Mice were intravenously injected with 10 nm AgNPs from three different batches (A, used in study 4.1.1, B, C) at two different doses (5 mg/kg and 10 mg/kg). Additionally a group of mice (n=3) was treated with 5 nm AgNPs at a single dose of 10 mg/kg. The dosing volume was 10 ml/kg bw. Immediately after the treatment and the following hours up to 24 hours, the general health and behavior of mice were monitored. The body weight of each mouse was measured before treatment and at sacrifice, which occurred 24 hours after the treatment.

Tab. 8. Experimental Groups:

Treatment	Dose	Time of sacrifice
CTR (vehicle)	10 ml/kg	T +24h
AgNPs 10nm Batch A	5- 10 mg/kg	
AgNPs 10nm Batch B	5- 10 mg/kg	
AgNPs 10nm Batch C	5- 10 mg/kg	
AgNPs 5nm	10 mg/kg	

According to procedure described in chapter 3, organs (liver,spleen, kidney, lung, brain, heart) were sampled and the histopathological examination was done.

## Results

### Physicochemical characterization

- DLS

Monomodal distributions were observed for tested batches indicating the absence of aggregates, as showed in table 9.

- UV-vis spectroscopy

The correspondence between the optical properties given by the manufacturer and those measured in our laboratory appeared satisfactory; in particular, it is worth to point out, that it was not observed any decrease in the maximum absorbance value (Hmax), indicating the absence of aggregates (Tab. 9). Then, full absorbance spectra of all samples were analyzed (Fig. 12). The optical density in the 600–800 nm range, which is typical for aggregates absorption, was not detected in 10 nm AgNP-CT and 10 nm AgNP-PVP, further demonstrating that the presence of stable aggregates in these samples could be excluded.

**Tab. 9.** Physicochemical characterization of tested AgNPs.

Biopure™ Silver NPs	DLS			UV-Vis	
	Mean hydrodynamic diameter (nm)	Max intensity peaks	pdl	$\lambda$ max (nm)	Hmax (a.u.)
Batch A	np	18-4646	0,258	392	1635
Batch B	np	18,17 – 122,4	0,680	392	145,5
Batch C	16,31	16,53 – 569,4	0,253	392	169,5

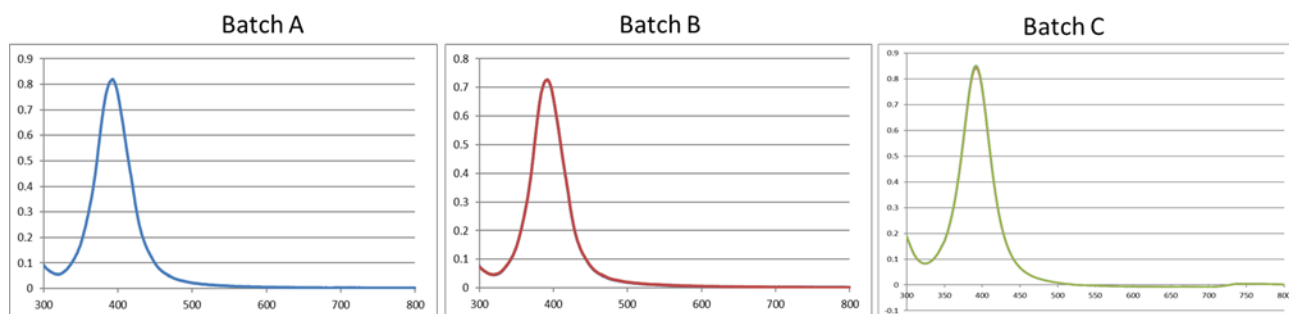


**Fig.11.** Particle characterization by UV–Vis spectroscopy: full absorbance spectra of the tested silver nanoparticles. The optical density in the 600–800 nm range, which is typical for aggregates absorption, was not detected in any of tested AgNPs, indicating the absence of stable aggregates in these samples

- TEM

All the tested AgNPs were spherical in shape, as represented in TEM images (Fig. 13).

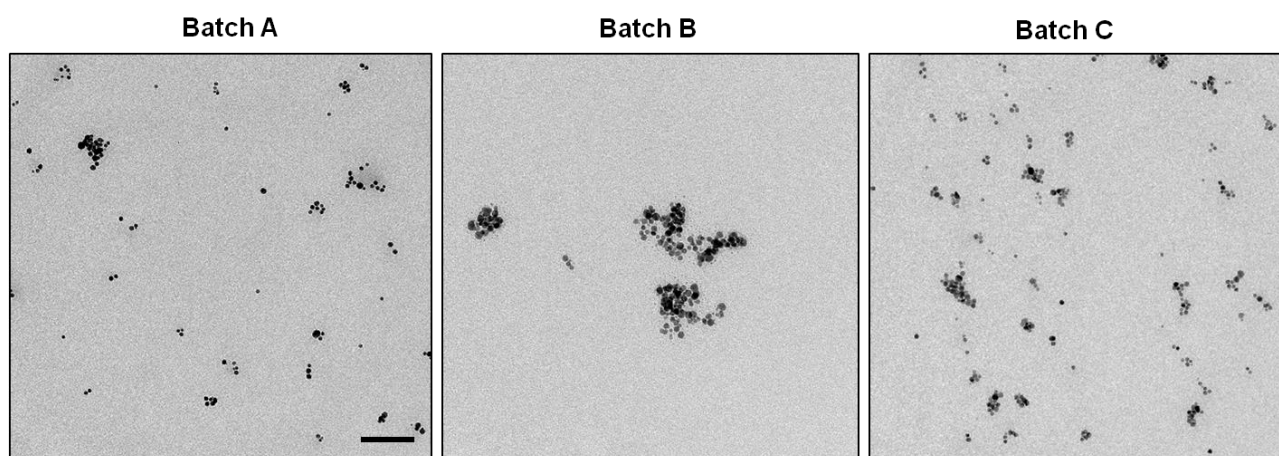


**Fig. 13.** TEM of tested silver nanoparticles. All purchased particles were spherical in shape, and no stable aggregates were visible (scale bar = 100 nm).

### Histopathological examination

All batches induced liver changes and hemorrhages in the gall bladder, confirming the effects observed in the previous study. As demonstrated in table 9, the severity of the lesions was dose and batch dependent, with batch A inducing the most severe effects (Fig. 14). Some in vitro studies reported that the toxicity of AgNP suspensions varied between batches, and hypothesized to be related to some differences occurring in the physicochemical properties [96].

Comparing the particle size distribution of tested batches (as reported in the datasheet) we noted that there was a difference in the percentage of very small AgNPs. The percentage of AgNPs<8nm was about 30%, 23% and 17% in batch A, B, and C, respectively, suggesting that at least part of the observed changes (in particular the hemorrhages) could be related to the very small AgNPs (Fig. 15).

In order to test this hypothesis, a single dose (10 mg/Kg) of 5 nm AgNPs was administered i.v., resulting in moderate to severe hepatobiliary lesions. Gall bladder hemorrhages were particularly severe in this group, as compared to those observed after administration of 10 nm AgNPs. This could be due to a more specific endothelial damage induced by very small AgNPs consequent to their massive elimination in the bile, as discussed in previous study.

AgNPs Batch n.	AgNPs size	Dose	Histopathological grading (median scores)		
			Hepatocellular necrosis/hemorrhage	Gall bladder hemorrhage	Total score
A	10 nm	5 mg/kg	1	2.5	3.5
		10 mg/kg	4	2	6
B	10 nm	5 mg/kg	1	1	2
		10 mg/kg	2	2	4
C	10 nm	5 mg/kg	2	0	2
		10 mg/kg	4	0.5	4.5
	5 nm	10 mg/kg	3	4	7

**Tab.9.** Histopathological grading. Mice treated with 10nm CT-coated AgNPs at different doses and with 3 different AgNPs batches (score: 0 = absence of lesions; 1 = minimal lesions; 2 = mild lesions; 3 = moderate lesions; 4 = severe lesions).

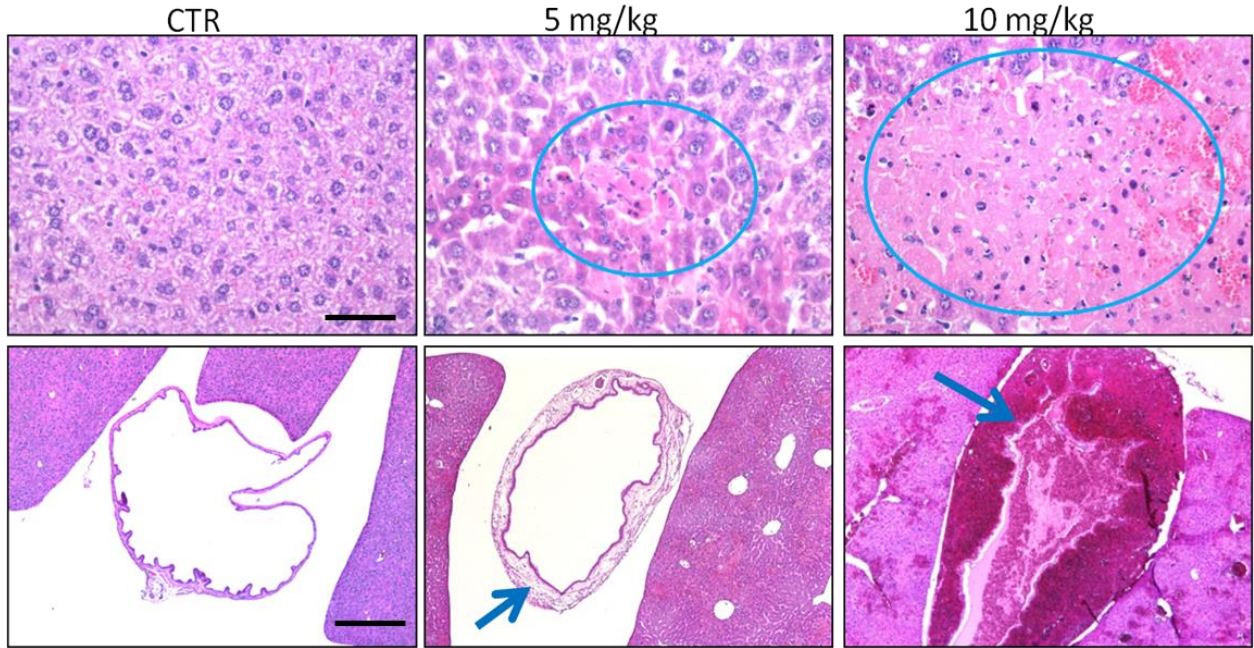


**Fig. 14.** Hematoxylin&Eosin, Upper panel, Liver, 400x (scale bar 50  $\mu\text{m}$ ). Lower panel: gall bladder, 50x (scale bar 500  $\mu\text{m}$ ). Mild to severe hepatocellular necrosis and gall bladder hemorrhages in mice treated with two different doses (Batch A).

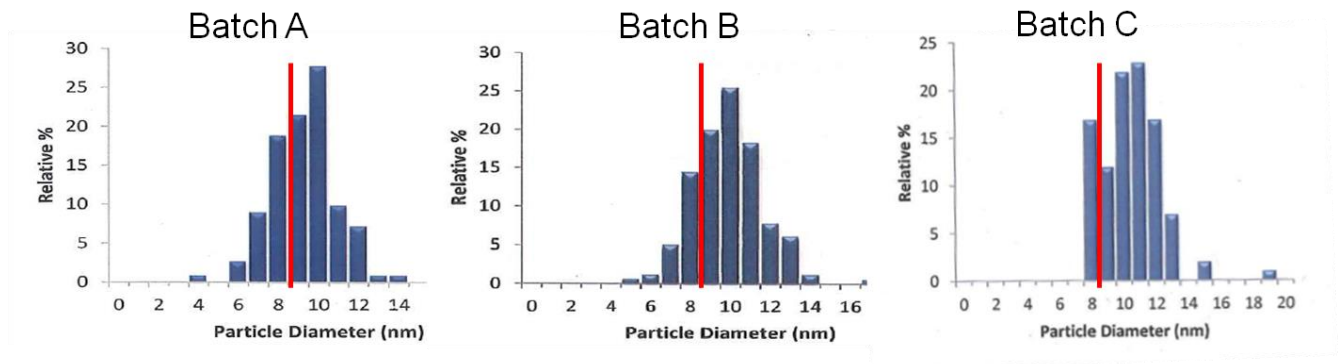


**Fig.15.** Size distribution of the three analyzed batches (datasheets of the manufacture). Variable presence of very small particles (less than 10 nm in diameter) in batches A and B that could have affected the toxicity observed.

## Conclusions

- The toxicity of 10 nm AgNPs observed in the study 4.1.1 was confirmed after testing 2 additional batches of 10 nm AgNPs.
- The toxicity of 10 nm AgNPs was dose-dependent.
- The very small AgNPs (5nm) induced the most severe hepatobiliary lesions.
- Among the AgNPs with same size, it seems that the size distribution is relevant to predict the *in vivo* outcomes.



#### **4.1.3. 5 days repeated oral administration of AgNPs: effect of coating on biodistribution after oral exposure**

The aim of this study was to compare the effect of two different coating (Ct or PVP) on the biodistribution of silver after oral administration of 10 nm AgNPs in order to select the coating for the 28 days repeated oral administration study.

##### **Physicochemical characterization**

10 nm AgNPs coated with either citrate (CT) or polyvinylpyrrolidone (PVP) from the same batches used in the study 4.1 were tested according to methods described in chapter 3 (3.1).

##### **Study design**

Three groups of mice received AgNPs 10 nm CT-coated, AgNPs 10 nm PVP-coated and an aqueous solution of deionized water (vehicle control) respectively by oral gavage once a day for 5 days at a dose of 5 mg/kg bw (n=3 per group). The dosing volume was 10 ml/kg bw. The body weight of each mouse was measured before treatment and at sacrifice which occurred 24 hours after the treatment.

According to the procedure described in chapter 3, organs (liver, spleen, kidney, lung, brain, heart, small intestine) were collected and the following determinations were done:

- Determination of silver content in tissues (liver, spleen, small intestine): ICP-MS;
- Visualization of silver in tissues: AMG
- Histopathological examination.

## Results and discussion

### Physicochemical characterization

See results of the study 4.1.1

### Biodistribution (ICP-MS, AMG)

Administration of the CT coated AgNPs resulted in a higher accumulation of Ag in spleen and liver compared to PVP-coated ones. In the liver silver concentration detected after CT coated AgNPs administration was twofold higher than that observed after administration of PVP-coated AgNPs (Fig. 16). Although there was no significant difference in Ag content in the intestine, the Ag concentration was slightly higher after administration of PVP-coated AgNPs.

Silver aggregates were not detected by AMG staining in any of the analyzed organs (intestine, liver, spleen).

### Histopathological examination

No treatment related histopathological changes were observed in any of the treated groups.

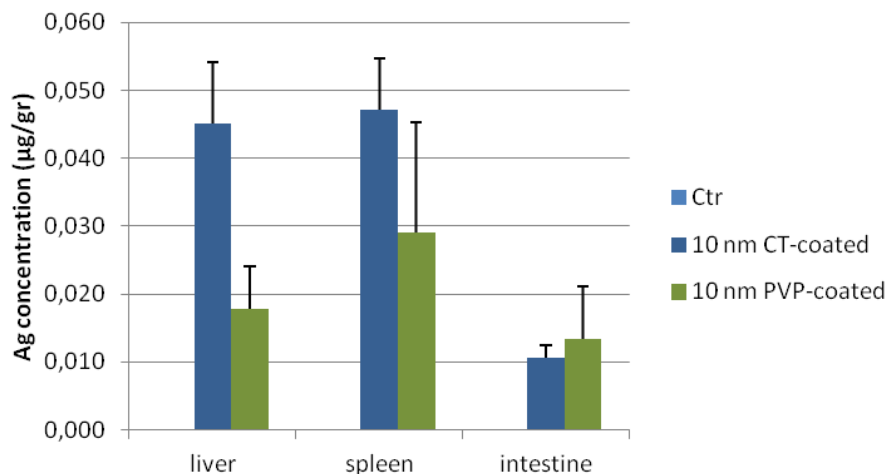


**Fig.16.** Silver concentration in liver, spleen and small intestine of mice after repeated oral administration of 10 nm-CT and PVP coated AgNPs at 5 mg/kg bw/day.

## Conclusion

- After ingestion, spleen and liver were the organs where the accumulation of silver was more evident, while only small amount of silver was detected in the intestine suggesting that AgNPs were already absorbed or excreted.
- Following oral administration a coating-dependent tissue distribution was observed, with increased accumulation of the CT-coated NPs in the spleen and liver, , suggesting a different mechanism of absorption, likely resulting from interaction with the biological membrane or fluids.
- Due to the higher silver accumulation in the analyzed organs, the CT-coated AgNPs were selected for the 28 days repeated oral administration.

#### **4.1.3. 28 days repeated oral administration of AgNPs: effect of repeated administration of low doses on accumulation and toxicity**

The aim of this study was to assess the biodistribution and effect of repeated oral administration of small AgNPs. An additional period of recovery to assess Ag persistence in organs was considered. Since no data about exposure are available, the two doses were selected as the lowest tested in literature studies.

##### **Physicochemical characterization**

10 nm AgNPs CT- coated were tested according to methods described in chapter 3 (3.1). Specifically, the following methods were applied:

- DLS
- UV-vis spectroscopy
- TEM

##### **Study design**

Mice were randomly assigned to four groups of treatments (n=6 animals per group) plus a vehicle control group. Mice received AgNPs 10 nm CT-coated at two doses of 0.25 and 1 mg/kg body weight (bw). For comparison, a group was treated with silver acetate (AgAc), used as source of silver ions, at a dose of 1.55 mg/kg bw, containing the equivalent dose of 1 mg Ag/kg bw. An aqueous solution of deionized water was administered as vehicle control. Mice were treated by oral gavage once a day for 28 days. For each group, 6 mice were sacrificed at the end of treatment while 6 animals were kept untreated, monitored and sacrificed after 28 days recovery period. At the sacrifice blood were collected by cardiac puncture for haematology and serum chemistry.

According to procedure described in chapter 3, organs (brain, liver, spleen, kidney, lung, brain, heart, small intestine) were sampled and the following determination was done:

- Haematology and serum chemistry
- Determination of silver content in tissues (liver, spleen, small intestine, testis, brain): ICP-MS;

- Visualization of silver in tissues: AMG
- Histopathological examination.
- Immunohistochemistry: Iba1 (microglial cells), GFAP (astrocytes), Albumin, Cleaved caspase-3
- TEM analysis of brain and intestine

## **Results and discussion**

### Physicochemical characterization

The physicochemical properties of AgNPs were monitored and evaluated during the treatment. Quality control was performed before the first administration and weekly (day 7, 14, 21), to ensure the adequate dispersion and absence of aggregation over the time (Tab. 10).

The correspondence between the optical properties given by the manufacturer and those measured in our laboratory appeared satisfactory; DLS and UV-vis spectroscopy as well as TEM indicated absence of aggregates and ensure the spherical shape of tested AgNPs (Fig.17)

Time (days)	DLS			UV-Vis	
	Mean size (nm)	peak (nm)	Pdl	$\lambda_{\max}$ (nm)	$H_{\max}$ (A.U.)
0	14.17±0.23	15.30±0.46	0.103±0.047	391.89±0.33	163.69±0.60
7	14.46±0.42	15.42±0.66	0.129±0.063	391.89±0.33	161.35±1.68
14	19.42±7.42	15.21±1.27	0.242±0.063	391.00±0.00	173.51±4.62
21	14.59±0.14	15.44±0.96	0.159±0.67	391.00±0.00	161.31±4.18

**Tab. 10.** Quality control of AgNPs in the as-received conditions (day 0) and at three other time points (day 7, 14, 21). For DLS analyses, the mean size of AgNPs is expressed in terms of hydrodynamic diameter. The maximum intensity peak is also reported to describe more comprehensively samples having multimodal distributions (for example, in the presence of AgNPs aggregates). The pdl provides a measure of particles uniformity. For UV-Vis analyses, the maximum wavelength ( $\lambda_{\max}$ , i.e. the wavelength corresponding to the highest absorbance of AgNPs) and the maximum absorbance value ( $H_{\max}$ ) are reported. The  $\lambda_{\max}$  and  $H_{\max}$  values were expressed as nanometer (nm) and arbitrary units (a.u.), respectively.

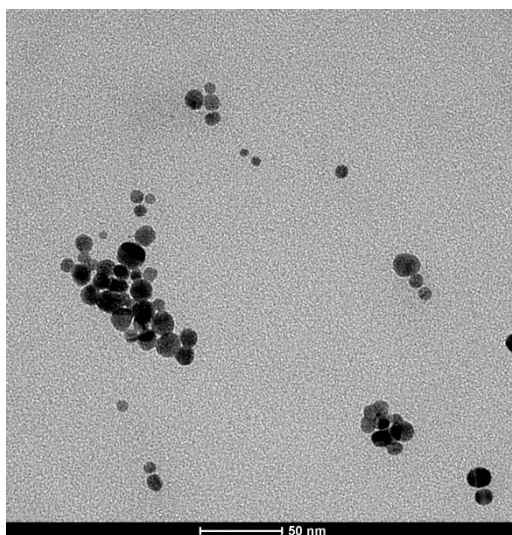


**Fig.17.** TEM of tested silver nanoparticles. All purchased particles were spherical in shape, and no stable aggregates were visible (scale bar = 50 nm).

### Hematology and serum chemistry

The hematological mean values of all the other groups were within reference intervals; however the group treated with AgNPs at a dose of 1 mg/kg showed a lymphocyte values slightly higher than the upper limit of the reference interval. The few hematological changes observed are consistent with a slight activation of inflammatory/immune response in individual mice (Tab. 11).

Concerning the clinical chemistry values, the group treated with AgNPs at a dose of 1 mg/kg has an increased in GLDH (glutamate dehydrogenase) suggesting an acute hepatocyte damage possibly associated with a slight impairment of liver function (Tab. 12).

When the results of hematology and clinical chemistry are evaluated together, it seems that treatment did not induce severe hematological or biochemical changes.

**Tab. 11.** Hematological values after oral exposure. Data expressed as median value.

Group	WBC x 10 <sup>3</sup> /μL	RBC 10 <sup>6</sup> /μL	Hb g/dL	Ht %	MCV fL	MCH pg	MCHC %	Plt 10 <sup>3</sup> /μL	Neutr 10 <sup>3</sup> /μL	Lymph x10 <sup>3</sup> /μL	Mono 10 <sup>3</sup> /μL	Eos 10 <sup>3</sup> /μL
<b>Ctrl</b>												
Mean	8,8	8,1	11,3	44,8	55,3	13,8	25	1586	1,15	7,34	0,27	0,03
± SD	± 1,7	± 0,7	± 1,1	± 3,0	± 2,2	± 0,3	± 1,0	± 318	± 0,61	± 1,41	± 0,14	± 0,05
<b>AgNPs 0,25 mg/kg</b>												
Mean	8,3	8,4	11,5	46,2	54,9	13,7	24,9	1448	1,19	6,4	0,58	0,14
± SD	± 1,6	± 0,3	± 0,5	± 2,4	± 0,8	± 0,1	± 0,3	± 605	± 0,38	± 0,88	± 0,54	± 0,23
<b>AgNPs 1 mg/kg</b>												
Mean	10	8,8	12,2	48,9	55,6	13,9	25	1480	0,88	8,76	0,33	0,08
± SD	± 2,9	± 0,3	± 0,5	± 2,1	± 1,3	± 0,4	± 0,4	± 306	± 0,35	± 2,97	± 0,23	± 0,11
<b>AgAc</b>												
Mean	9,3	8,2	11,6	46,6	56,7	14,2	25	1409	1,9	6,77	0,54	0,15
± SD	± 2,6	± 0,7	± 0,9	± 3,3	± 1,3	± 0,2	± 0,2	± 360	± 2,53	± 3,11	± 0,47	± 0,13
Ref. Int.	3.8-13.8	6.2- 11.6	10.3- 19.0	34.9- 65.0	47.1- 65.1	14.5- 18.3	24.1-34.9	744-2314	0.00-3.15	2.87- 10.31	0.12-0.86	0.00- 0.46

**Tab. 12.** Clinical chemistry values after oral exposure. Data expressed as median value.

Group	GLDH (U/L)	Urea (mg/dL)	Creatinine (mg/dL)	Triglycerides (mg/dL)	ALT (U/L)	Albumin (mg/dL)	Total protein (mg/dL)
<b>Ctrl</b>							
Mean ± SD	8,0 ± 3,5	39 ± 3	0,32 ± 0,03	155 ± 48	37 ± 28	2,31 ± 0,24	5,27 ± 0,79
<b>AgNPs 0,25 mg/kg</b>							
Mean ± SD	4,5 ± 2,4	34 ± 5	0,28 ± 0,01	93 ± 35	18 ± 6	2,40 ± 0,22	4,60 ± 0,29
<b>AgNPs 1 mg/kg</b>							
Mean ± SD	11,3 ± 3,7	44 ± 5	0,35 ± 0,11	157 ± 36	18 ± 5	2,45 ± 0,29	5,34 ± 0,42
<b>AgAc</b>							
Mean ± SD	13,3 ± 11,5	35 ± 4	0,30 ± 0,04	126 ± 101	24 ± 23	2,14 ± 0,55	4,54 ± 0,47
Ref. Int.	6.5-14.5	32 ± 8	0.40 ± 0.12	192 ± 67	45 ± 16	2.99 ± 0.62	5.38 ± 0.95



## Clinical signs

No changes in body weight were observed across the treated groups, control included. The body weight increased both during the treatment and the recovery period (Fig. 18). This is in line with most of the data reported by others investigators [97].

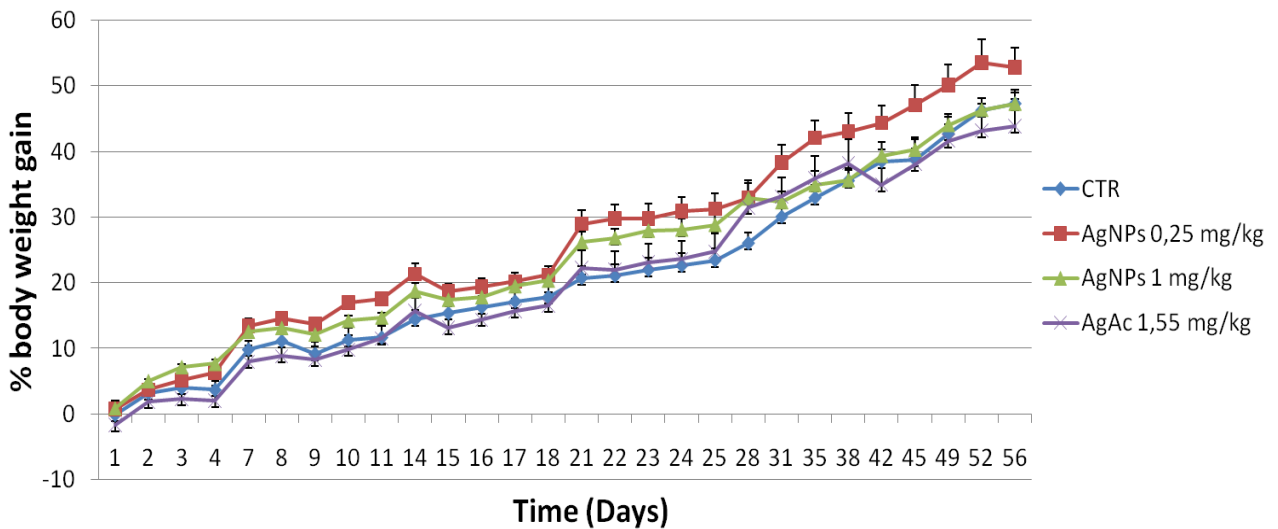


**Fig. 18.** Mean body weight gain (%) during PO administration and the recovery period. Data are expressed as means  $\pm$  SD

### Biodistribution

After 28 days of treatment the distribution pattern of silver was similar between the nano and the ionic form of silver. ICP-MS analysis demonstrated the highest silver concentration in the brain and in the liver, followed by spleen and small intestine. A very low concentration of silver was found in the kidney. The accumulation of silver in the organs was dose-dependent for the AgNPs, and was lower in comparison to the corresponding organs of mice exposed to AgAc treatment. Statistically significant differences were found in the brain and in the liver of mice treated with the high dose of AgNPs and in the brain, liver and spleen of mice treated with the high dose of AgAc in comparison to the tissues from control animals (Fig. 19).

The accumulation of Ag was dose-dependent and the ion form was present in a larger amount than AgNPs. This is possibly due to the lower bioavailability of the AgNPs compared to Ag ions[97].

After recovery period, Ag was still detected in the brain in all treated group (Fig. 20), however at lower amount, indicating that a time dependent clearance occurred.

### Histopathological examination

No histopathological changes were identified in control and treated groups. This supports the evidence reported by other authors that adverse effects on host tissues caused by oral administration of AgNP are inconsistent [63].

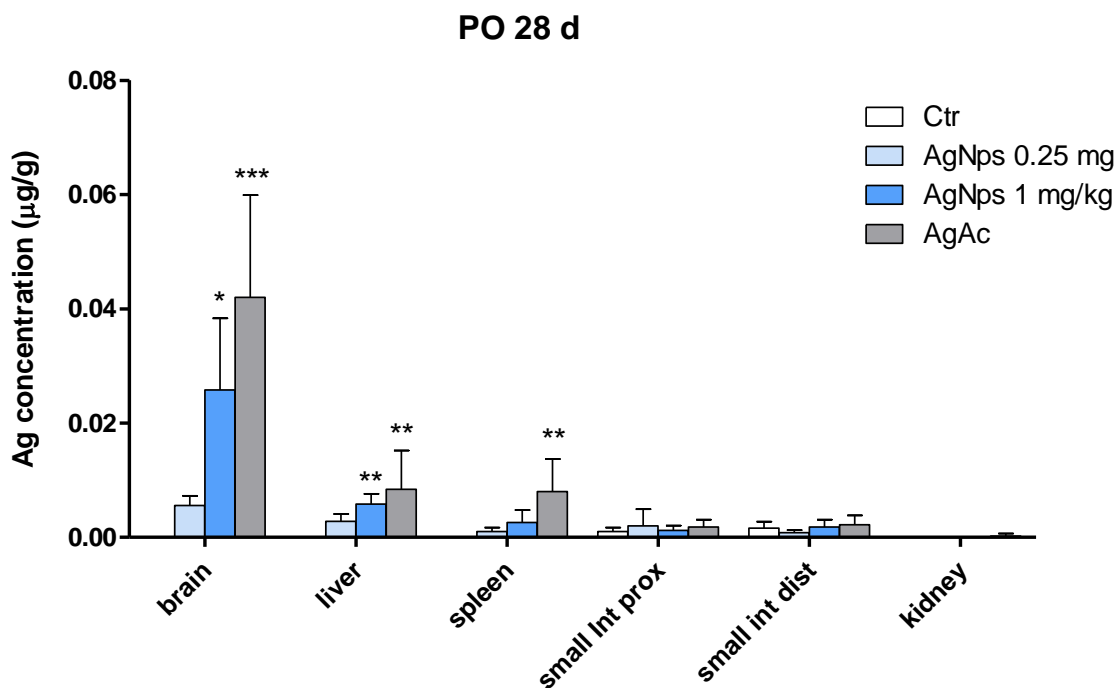


**Fig. 19.** Silver concentration in tissues after 28 days oral administration. Data are expressed as means  $\pm$  SD. Statistical significance: \* =  $p < 0.05$ ; \*\* =  $p < 0.01$ ; \*\*\* =  $p < 0.001$  vs control group.

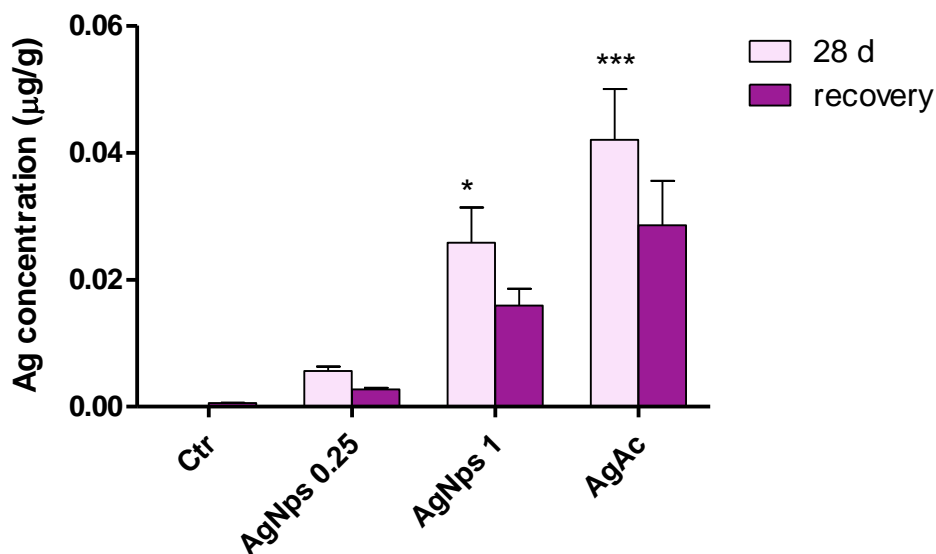


**Fig. 20.** Silver concentration in the brain 28 days after oral administration and after the recovery period. Data are expressed as means  $\pm$  SD. Statistical significance: \* =  $p < 0.05$ ; \*\* =  $p < 0.01$ ; \*\*\* =  $p < 0.001$  vs control group.

### Immunohistochemical evaluation

Since the brain was the organ with the highest Ag accumulation, immunohistochemical investigation was performed to evaluate changes in the cells involved in brain homeostasis and response to injury (astrocytes and microglia). In the hippocampus, an increase of GFAP (astrocytes marker) and Iba1 (microglia marker) immunostaining was observed in all treated groups in comparison to control animals; this was significantly higher for astrocytes in mice treated with AgNPs at 1 mg/kg and AgAc. After 28 days of treatment, an increase in the microglia positive area was detected in the same treated groups. After the recovery period, no differences in the morphology and density of astrocytes were observed however, a decrease of about 20% in Iba1 positive area was detected in the animals treated with the higher dose of AgNPs and of AgAc (Figs. 21-22). This decrease could correspond with the resolution phase of microglial activation; however, no morphological changes in glial cells were distinguished at histological magnification (Fig. 23).

The number of Iba1 positive cells in each field was also considered to relate the changes detected by digital image analysis to an increase or decrease in the number of cells. However, no changes in the cells number was observed in any treated groups. This suggests that the changes observed were possibly related to an increase/decrease of cell area. Additionally, no apoptotic glial cells were detected (Fig 24).

Albumin immunohistochemistry were performed to detect any BBB damage. Immunohistochemical staining did not reveal any signs of albumin extravasation from brain microvasculature in all controls and treated mice.

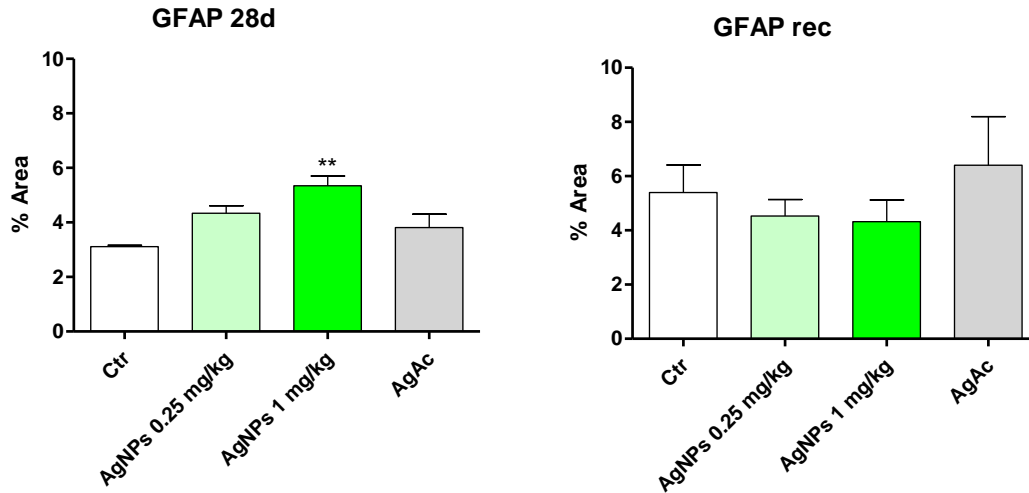


**Fig. 21.** Quantification of GFAP (astrocyte) positive cells after 28 days of AgNPs oral administration and at the end of the recovery period in the hippocampus. Data are expressed as means  $\pm$  SEM. Statistical significance: \*\* =  $p < 0.01$  vs control group.

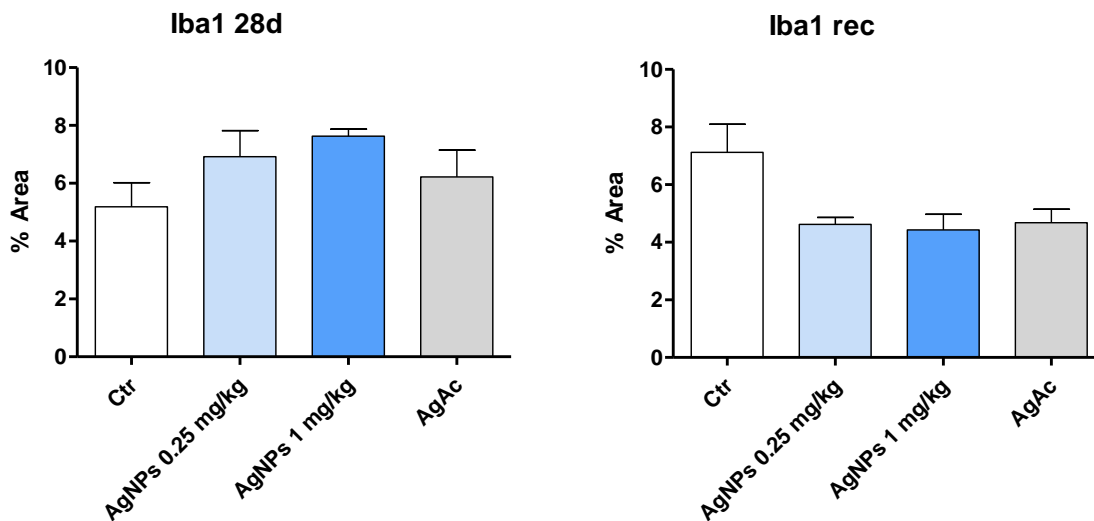


**Fig. 22.** Quantification of Iba1 (microglia) positive cells after 28 days of AgNPs oral administration and the end of the recovery period in the hippocampus. Data are expressed as means  $\pm$  SEM.

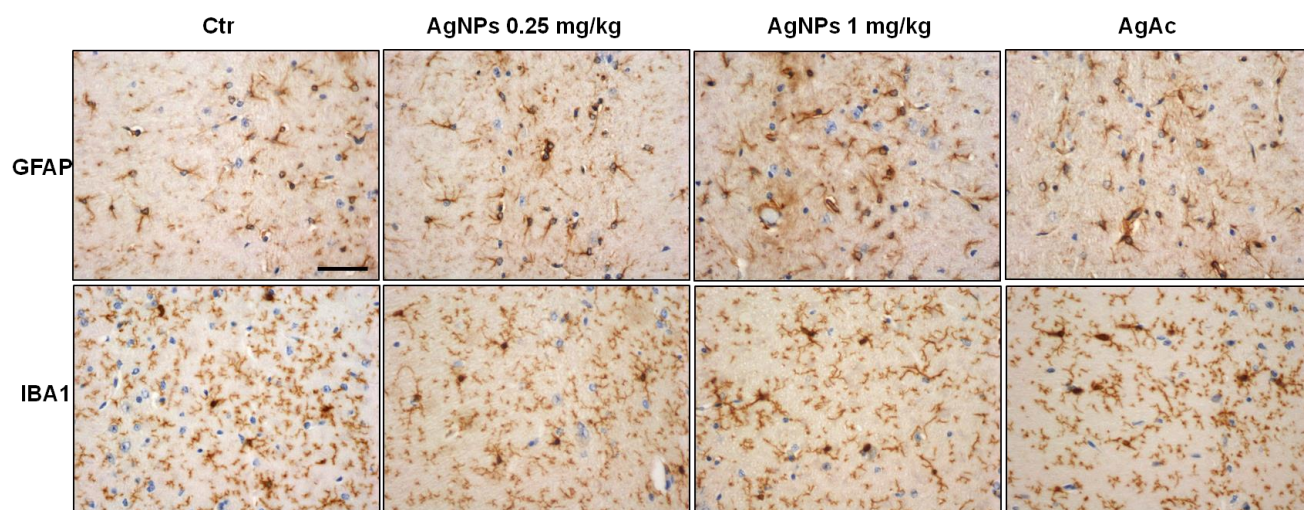


**Fig. 23.** IHC for GFAP and Iba1, 400x (scale bar 50  $\mu$ m). Hippocampus, glial cells after 28 days of oral administration.

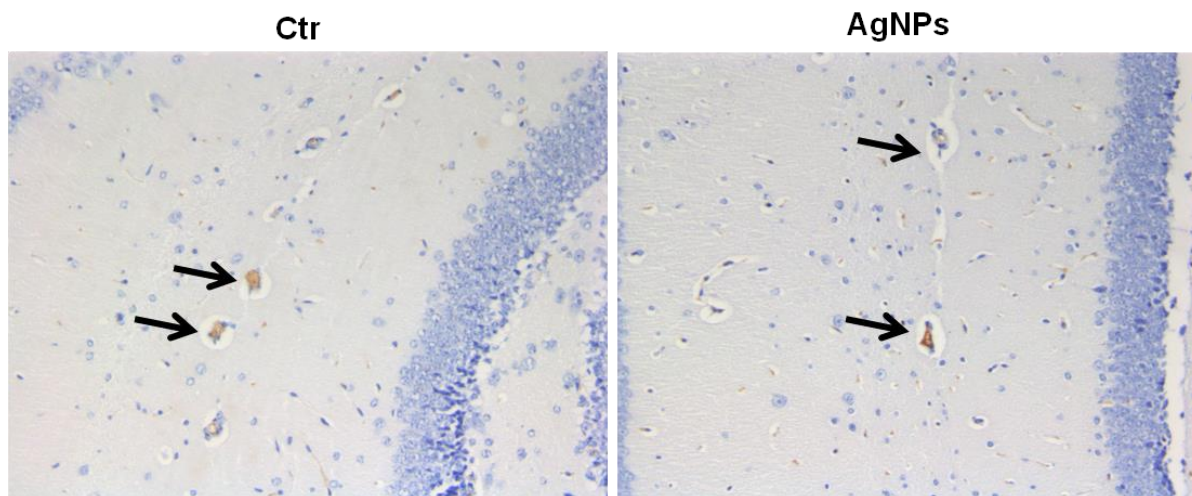


**Fig. 24.** IHC for Albumin, 400x (scale bar 50  $\mu$ m). No sign of albumin extravasations was observed.

## TEM analysis

TEM analysis of the hippocampus showed splitting of the basement membrane of the capillaries, and swelling of the perivascular end-feet of astrocytes in both AgNPs- and AgAc-treated mice (Fig. 25). These morphological changes were not observed at the end of the recovery period, suggesting that the change was reversible.

TEM analysis of the small intestine of control and treated mice showed no changes in the intestinal mucosa. Neither AgNPs nor Ag was detected.

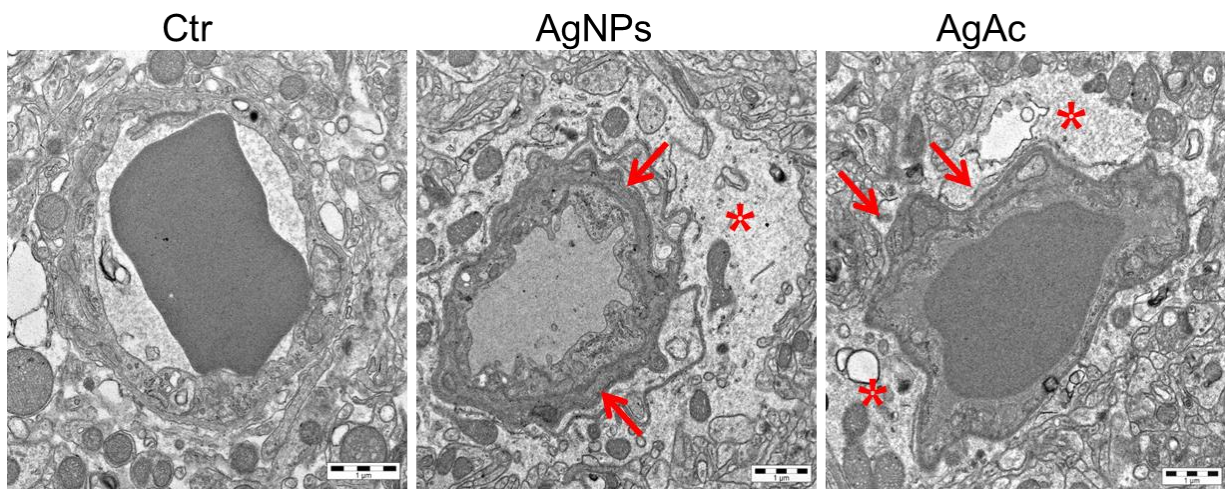


**Fig. 25.** Representative TEM images of the hippocampal capillary. Swelling of perivascular end-feet of astrocytes (asterisk) in AgNPs and AgAc treated mice. Splitting of capillary basement membrane in three and two different branches (arrows) in AgNPs and AgAc treated mouse.

## Conclusions

- Our study shows that the organ with the highest amount of Ag accumulation is the brain; differently from other the studies where it is reported that the main target organs for silver accumulation after repeated dose of orally administered NPs are liver, spleen and intestine [31], [32]. This evidence leads to hypothesize that the brain Ag accumulation could be due to the low clearance activity of this tissue, possibly indicating that the blood–brain barrier prevents the back transfer of Ag into the blood [84], [98].
- Ag persists in the brain also after the recovery period, even if a gradual reduction was observed. These data are in agreement with the results of few reported studies showing that Ag was still present in brain and testis 8 weeks after oral dosing (28 days oral exposure of 90 mg/kg bw of AgNPs < 15 nm in rats) [73].The persistence of AgNPs in the brain can lead to the release of Ag ions from the particle surface, triggering ROS production and oxidative stress in the cells[32].
- In all the organs analyzed, the higher Ag concentration was found in animal treated with AgAc, suggesting a different mechanism in cellular uptake and fate between Ag ionic and nanoparticulate form.
- We were not able to observe any cellular localization of AgNPs by TEM and to clarify if AgNPs were able to cross the blood–brain barrier (BBB).Recent studies showed that metallic and AgNPs can penetrate the BBB without affecting its permeability or conversely by inducing its destruction [80], [83], [99]. In our study, immunohistochemical staining for albumin did not reveal any sign of albumin extravasation (sign of blood brain barrier damage) from brain microvasculature in both control and treated animals.
- At the low doses, no histopathological findings were detected in most of the tissues evaluated supporting the evidences from other authors that adverse effects in the host tissues caused by oral administration of AgNP are low[63].
- The evaluation of glial cells showed the involvement of astrocytes and microglial cells in response to Ag; possibly in terms of activation of the cells protecting the brain from oxidative stress and metal toxicity.
- TEM analysis of the BBB showed ultrastructural morphological changes in astrocytes end-feet and capillary basement membrane. Swelling of astrocytic perivascular end-feet was observed



also in a study of a 2-week oral exposure to 1 mg/kg or 10 mg/kg of Ag-NPS in rats[100].It was hypothesized that extracellular potassium homeostasis and pH dysregulation play an important role in astrocytes swelling [101], [102]that could suggest a local increase in BBB permeability [103]. The splitting of capillary basement membrane was never reported before and this could be related to the Ag ions uptake.

- Ultrastructural changes and immunohistochemical investigations were similar in nano and ionic form of Ag, supporting the evidence that the effects induced by nano form of Ag are mediated by silver ions released from the particle surface[97].

## **4.2. BIODISTRIBUTION AND TOXICITY OF IRON OXIDE NPs (IONP)**

### **4.2..1. Single intravenous administration of IONPs: effect of dose and vehicle on distribution and toxicity**

(published paper Cappellini et al 2015)

The aim of the study was to assess the biodistribution and toxicity of newly synthesized IONP after single intravenous administration in mice.

The synthesis method of IONPs was fully described in the paper.

#### **Physicochemical characterization**

IONP were checked according to methods described in chapter 3 (3.1). The Following methods were applied:

- DLS
- Infra-red (IR) spectroscopy

#### **Study design**

Mice were intravenously injected with a single dose of IONP ( $\text{Fe}_3\text{O}_4$ -APTES-DAAO, 100 mg/kg bodyweight (bw) of NPs in NaCl 0.9%, and 20 mg/kg bw of NPs in NaPPi buffer at pH 7.4) (n= 3 per group) and sacrificed 24 h after the treatment. The control groups were treated with the corresponding vehicle (NaCl 0.9% or NaPPi buffer). Immediately after the treatment and the following hours, the general health and behavior of mice was monitored (Irwin test). The body weight of each mouse was measured before treatment and at sacrifice.

According to procedure described in chapter 3, organs (liver, spleen, kidney, lung, brain, heart) were sampled and the following determinations were done:

- Visualization of iron in tissues: Perl's iron staining
- Identification of cells containing iron aggregates: immunofluorescence for IBA1.
- Histopathological examination.

## **Results and discussion**

**(Additional details in the published paper Cappellini et al 2015, Appendix B and additional data in Appendix A)**

### Physicochemical characterization

#### **DLS**

DLS analyses showed that the population of Fe<sub>3</sub>O<sub>4</sub>-APTES-DAAO is stable around a dimension of 1 µm indicating that the enzyme conjugation process induces aggregation of NPs. However, more information on the hydrodynamic diameter of the iron core, the magnetization capabilities and the iron content would allow us to better compare these newly created particles and allow a comparison to others.

#### **Infra-red (IR) spectroscopy**

Fe<sub>3</sub>O<sub>4</sub>NP-APTES-DAAO were characterized by IR analysis to assess the functionalization of ligands in the newly synthesized system. All conjugation sites of Fe<sub>3</sub>O<sub>4</sub> NPs are saturated, obtaining an absolute APTES functionalization.

### Clinical signs

Immediately after the administration of NPs, and during the following hours, all mice appeared healthy and no relevant behavioral alterations were observed (data on Irwin test, appendix A). No significant differences in body weight gain and relative organ weights of liver, spleen and kidney were observed between control and Fe<sub>3</sub>O<sub>4</sub>-APTES-DAAO treated group (Tab. 13).

Group	TOTAL WEIGHT				RELATIVE WEIGHT		
	Body weight	liver	spleen	kydneys	liver	spleen	kidneys
CTR							
mean	30,14	1,99	0,15	0,58	6,55	0,48	1,91
SD	1,99	0,50	0,05	0,04	1,23	0,13	0,01
IONP 100 mg/kg							
mean	29,46	2,11	0,17	0,48	7,18	0,57	1,63
SD	2,35	0,07	0,03	0,02	0,35	0,06	0,09
CTR (NaPPi pH7,4)							
mean	28,9	1,93	0,15	0,51	6,66	0,50	1,75
SD	0,5	0,0	0,0	0,0	0,1	0,1	0,1
IONP 20 mg/kg							
	28,6	2,0	0,2	0,5	6,90	0,54	1,59
	1,4	0,1	0,0	0,0	0,2	0,1	0,2

**Tab. 13.** Total and relative weight

### Biodistribution

In treated group, intracytoplasmic brown granular material (consistent with iron pigment, as confirmed by Perls iron staining) was found in HE stained sections of the liver, spleen and lungs, and only occasionally in the kidney (at level of blood vessels). In the liver the iron pigments was found mainly in the cytoplasm of Kupffer cells (immunostained with Iba1)(Fig. 26). In the lungs, there were moderate numbers of cells (monocytes/macrophages) with intracytoplasmic iron pigments infiltrating the alveolar septa, throughout the pulmonary parenchyma. In the spleen, large numbers of histiocytes with intracytoplasmic iron pigment were found in the red pulp, marginal zone, and PALS/germinal center (Fig. 25). No iron deposits were observed in the heart, testis and brain. Reduced amount of iron-containing deposits were detected in liver and spleen of mice treated with 20 mg/kg compared with those found in mice treated with 100 mg NP/kg. Mainly, iron deposits were found in the cytoplasm of monocytes/macrophages/histiocytes, indicating that most of injected particles were removed from blood circulation by phagocytic cells.

The results of the quantitative evaluation of the iron deposits detected in Perls iron stained sections of examined organs is reported in Table 14.

Group	Liver	Spleen	Lung	Kidney	Brain	Heart
Vehicle	0,02 ±0,02	0,02 ±0,00	0,05 ±0,02	0,04 ±0,01	0,00 ±0,00	0,00 ±0,00
IONP 100 mg/kg	2,98 ±1,11	1,40 ±0,55	0,51 ±0,13	0,09 ±0,05	0,00 ±0,00	0,00 ±0,00
IONP 20 mg/kg	0,23 ±0,07	0,17 ±0,06	0,13 ±0,08	0,04 ±0,02	0,00 ±0,00	0,00 ±0,00

**Tab 14.**Quantitative evaluation of iron deposits detected in Perls iron stained sections

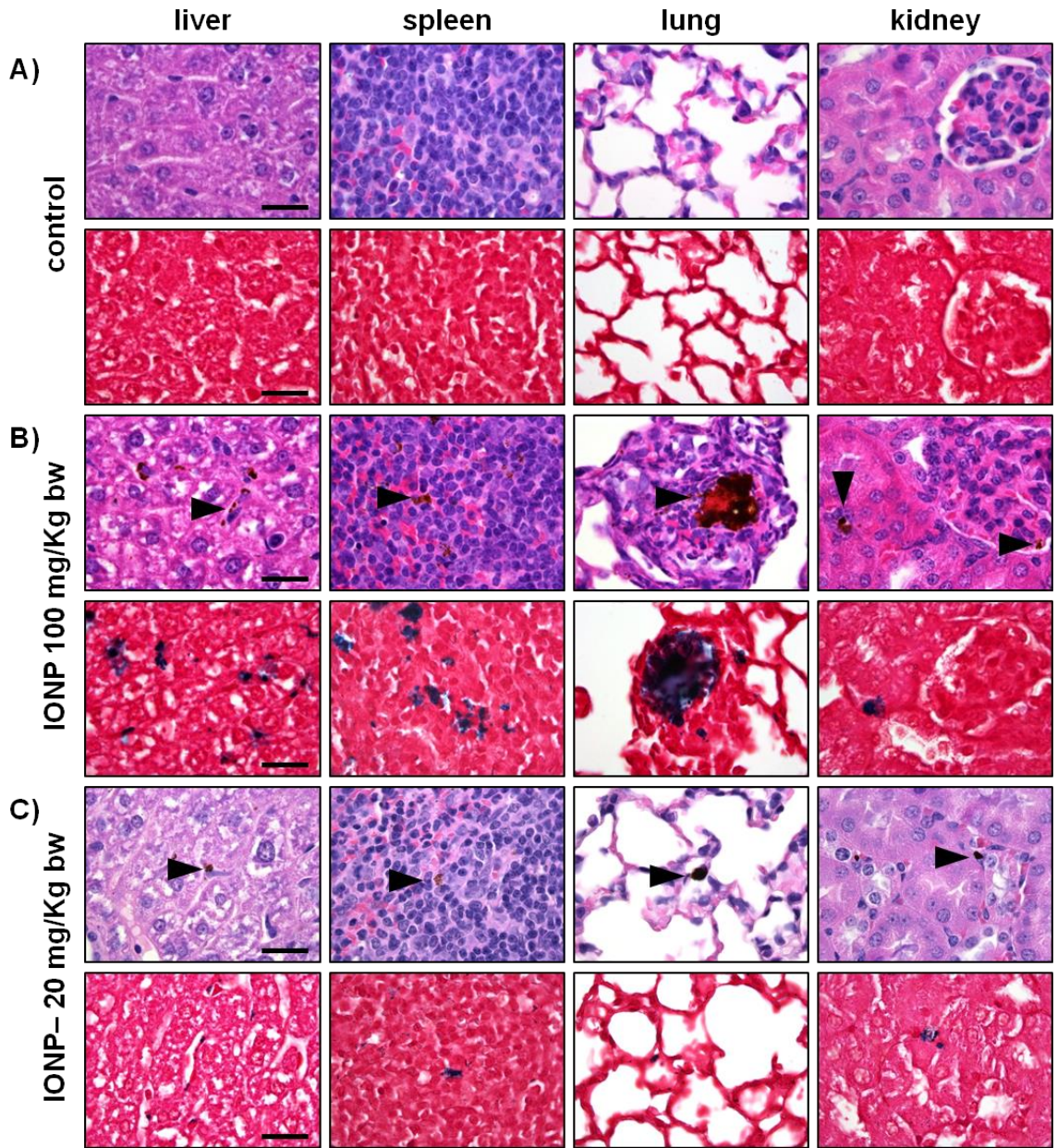


**Fig. 25.** Histology of liver, spleen, lung, and kidney of mice treated with vehicle (A, control), 20 mg/kg (B, EXP 1), and 100 mg/kg (C, EXP 2) of NPs (upper panel: H&E; lower panel: Perls stain; scale bar = 25  $\mu$ m). Brown granular material is evident in H&E stained sections (arrowheads) of NP treated mice, consistent with iron aggregates, as confirmed by Perls stain (blue).

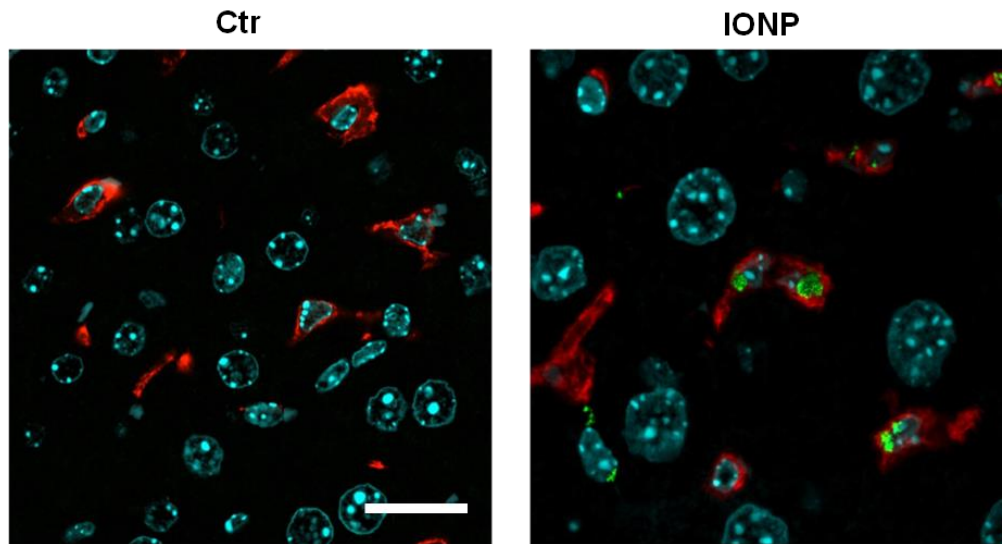


**Fig. 26.** IF stain, 400x (scale bar 20  $\mu\text{m}$ ). Iron-containing NPs (green) are mainly found in the cytoplasm of Iba1+ Kupffer cells (red) of liver. Nuclei stained with DAPI (cyan).

### Histopathological evaluation

In lungs of mice treated with the highest dose, multifocally, intravascular up to 100  $\mu\text{m}$  in diameter iron aggregates (emboli) surrounded by granulocytes, were found in association with interstitial infiltrates of histiocytes expanding the alveolar septa after higher dose administration (Fig. 27). The presence of pulmonary embolization of iron aggregates is due to the nanoparticles aggregation. The presence of intravascular iron deposits associated with interstitial inflammation indicated that pulmonary embolization occurred after intravenous administration of aggregated NPs, as confirmed by the results of DLS analysis. The white pulp was affected by mild-to-moderate follicular reactive hyperplasia. This finding may be interpreted as an antigenic response, likely directed against the enzymatic portion of the NP system.

Any adverse effect was observed after intravenous administration of a lower dose of NPs, containing a different vehicle (NaPPi buffer instead of 0.9% NaCl) that prevents NPs aggregation.

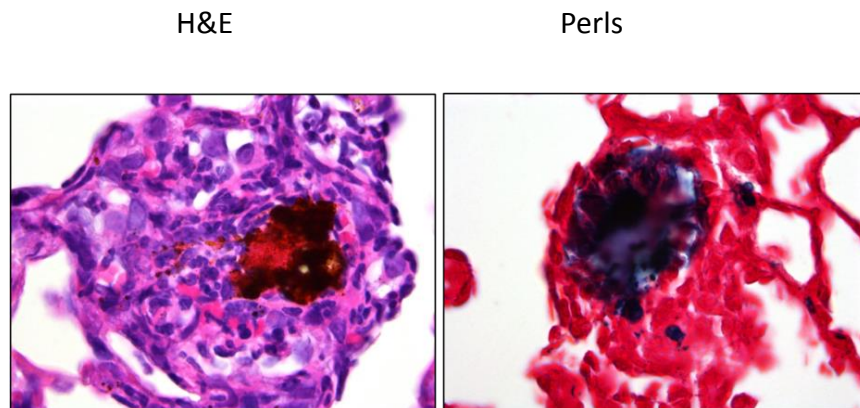


**Fig. 27.** Histology and Perls stain (400x). Alveolar septa infiltrated by macrophages and neutrophils surrounding a brown-black aggregate of iron-containing nanoparticles.



## Conclusions

- The physicochemical properties of NPs as well as of the vehicle used during synthesis processes and inoculation strongly influence their fate, organ/cellular distribution and toxicity.
- Particularly for nanoparticles designed for clinical applications, the structure-property relations are critical to achieve long circulation time, efficient extravasation and site accumulation. Furthermore in NPs based drug-delivery platforms an additional concerns to be considered is the potential toxicity of the component of the platform other than the drug [53].
- Finally, the potential toxic effects due to the chronic persistence of NPs in MPS and the likely transformation of NPs *in vivo* remains to be determined and should be further investigated.

## 5. DISCUSSION

The effects of engineered nanoparticle (NPs) and nanomaterials (NMs) need to be thoroughly investigated to ensure a better understanding of nanoparticle toxicology, of their fate and behavior and of the life cycle of nanomaterial-embedded products. With a better knowledge of all these aspects, the potential hazards can be minimized for consumers, workers and the environment and proper risk management be developed[7].

One of the main limitations in the risk assessment of NMs is the general lack of high quality exposure and dosimetry data for humans. A strategy to identify the proper metrics that can best relate exposure levels to human health effects has not yet identified. Indeed, there are no health-based recommendations for evaluating occupational exposures to NMs. One of the issues is the difficulty to determine the presence on NMs and properly measure them [104].

Another issue is the difficulty to compare different studies in terms of NPs type, source dosing and exposure methodologies. Since there is a general need for harmonization of the methodologies used for the characterization of NMs, the OECD working Party on Manufactured NMs aims to provide appropriate testing methods to assess physical chemicals properties, environmental fate and behaviour, and toxicity of NMs.

As a starting point, the detailed description of the NMs is very important to assess the physical-chemical properties of the NMs with regard to their potential adverse effects [7]. Moreover selected doses of administered NMs should ensure adequate exposure, they need to be scientifically justified and they must reflect possible exposure scenarios in human toxicology[105].

In our studies, the physicochemical properties of NPs were fully characterized in order to correlate any observed effects to the nanoparticles' properties. Moreover, the dissolution study performed for AgNPs ensured an adequate internal exposure to AgNPs, as it is demonstrated that NMs may change form during and after release [105].

The dosing for i.v. exposure was based on the literature data. Comparing to them, very low doses and doses that previously demonstrated mild or low adverse effects were chosen. Despite the low doses administered the main findings observed were the marked hepatotoxicity and pulmonary

embolization of iron aggregates after AgNPs and IONP administration respectively. Both biodistribution and toxicity were related to size and size distribution as well as the vehicle used for the synthesis. Of note, the pulmonary embolization observed is due to the aggregation of IONPs and not related to the NPs itself. The use of a vehicle capable to prevent NPs aggregation is fundamental for a proper evaluation of adverse effects that may occur.

Even if it is well known that the relationship of size and/or shape to NPs toxicity or nano medicine efficacy should be investigated on a case by case basis, because of the wide differences in the behavior of different NPs, the identification of physicochemical parameters that most affect NPs toxicity could help in the prediction of the *in vivo* behaviour of NPs.

Another limit of current literature studies is the lack of long term exposure studies, useful to mimic the human exposure scenario[7]. In our preliminary study of 28 days repeated oral administration of AgNPs, we demonstrated that NPs accumulate in the brain and some morphological changes occurred in astrocytes and basement membrane of capillaries and in glial cells, specifically involved in brain homeostasis and response to injury. Since it was demonstrated an induction of inflammation and oxidative stress in brain after NPs exposure, and since oxidative stress is involved in the pathogenesis of many neurodegenerative diseases, such as Alzheimer's disease (AD), Parkinson's disease (PD), or Huntington's disease, the effects of NPs in neural cells should be carefully analyzed [106], [107]. It was also demonstrated the role of trace metals in development of neurodegenerative diseases. Increased iron levels have been reported to be elevated in the PD midbrain, leading to subsequent neurodegeneration. Moreover the central tenet of amyloid beta toxicity in AD is linked with the presence of redox metals, mainly copper and non-redox zinc[107].Based on these observations the effects of metal NPs on the development of neurodegenerative disease should be further studied.

In nanomedicine the application of NPs (especially IONP) in brain imaging, brain-targeted drug or gene delivery is a promising field, however little is known about the accumulation, retention, and adverse effects of NPs in the brain. Also in that case, it should be considered the metal release resulting in an accumulation of free metals in brain and other organs that may lead to an increase

in ROS production and oxidative stress, subsequently leading to mitochondrial damage and cytotoxicity. [108].

The association of NPs with various brain diseases or their translocation using models that express a compromised BBB should also be investigated.

Another important issue associated to the use of NPs is their persistence in tissues. The few studies performed indicate brain and testis as organs where Ag is still present after a recovery period. For bulk materials, it has already been known for a long time that certain elements such as silver have a prolonged half-life in the CNS compared with other organs [75]. Concerning other tissues, very little is known about the cellular elimination of NPs and bulk materials. The cellular retention of NPs may cause adverse effects and it is a relevant issue considering that NPs localized in the cells of the mononuclear phagocyte system (MPS), the professional macrophages involved in the clearance and processing of larger NPs from the blood flow. In general, liver, spleen and lung are usually the dominant organs for clearance of the NPs from the bloodstream where specialized tissue-resident macrophages (Kupffer cells in liver, marginal zones macrophages in spleen and alveolar macrophages in lungs) are localized [109]. NPs, unlike small molecular weight, soluble therapeutics, approximate the same size scale as biologics, do not permeate epithelial membranes efficiently and often are decorated with diverse non-specifically adsorbed host proteins, increasing their non-specific cellular interactions. Both size and physical properties increase cellular recognition that prompts host recognition, NPs clearance and associated inflammatory effects[110]. *In vivo* recognition of NPs by phagocytes is a complex phenomenon depending on the combination of the various physicochemical parameters, i.e. size, shape, charge and the nature and density of coating molecules. Uptake of the NPs by the macrophages of liver and spleen is usually preceded by opsonization, recognition by the macrophages and phagocytosis. Among these processes, the adsorbed protein coating, referred to as “corona” in the NPs influence the presentation of NPs to phagocytes and is increasingly important to understand as a determinant of their clearance[110]. Many *in vitro* studies investigated the role of macrophages in uptake of NPs. They show that the cytokines release can accurately predict the *in vivo* outcomes, but it was difficult to study the mechanisms of NPs elimination [110], [111]. Lysosomes play a central role in the cellular elimination of NPs either by dissolution or degradation or by exocytosis. Lysosomes are

able to degrade not only biodegradable polymers, but also metal oxide NPs such as iron oxide NPs [111].

The investigations of the uptake and retention of NPs in MPS should be taken in consideration in nanomedicine during the design of NPs that should avoid MPS uptake to maximize NPs accumulation in the delivery sites, such as tumors. Modification of the surface with polyethylene glycol (PEG) is commonly used for this purpose and to induce a longer circulation time [112]. On the other hand, for some other imaging applications such as evaluation of brain lesions, assessment of rejection of the transplants or grafts, higher uptake rates of the injected NPs (i.e. IONP) by specific macrophages (other than the Kupffer cells) or circulating monocytes and their subsequent homing to specific tissues is desired. Recent reports also demonstrate that either NPs or monocyte–macrophages can be selectively manipulated to facilitate their phagocytosis and targeting abilities. For instance, by either specific coating of NPs or by pretreating phagocytic cells with specific cytokines the phagocytic and tissue or lesion homing capabilities of particle containing phagocytes can be influenced. It is important to note that macrophage uptake can have either beneficial or detrimental effects, based on the desired application [109].

Developing correlations between NPs physicochemical characteristics and NPs uptake, processing and clearance mechanisms in macrophages would provide a basis to overcome particle systemic delivery and targeting, and facilitate design of new, more efficacious and safer nanomaterial platforms.

In conclusion, comparing to other literature studies, unusual findings concerning the toxic effects after NPs i.v. and PO exposure and at low doses were highlighted in our experiments. These findings were strictly related to the physicochemical properties of NPs and strongly confirmed that a complete NPs characterization is fundamental to ensure the NPs changes before the administration that could affect the *in vivo* outcomes. The brain was the organ most involved in Ag accumulation after repeated oral exposure due to a low clearance, confirming previous results. Moreover, the involvement of glial cells and changes at the BBB level observed, added new knowledge about brain changes occurred. Finally, the involvement of MPs in NPs biodistribution and toxic effects due to the persistence of NPs in MPS was considered.

One of the limits of the studies reported was the low number of animal used in each experiment. However, these studies should be considered as preliminary investigative studies and based on the observation obtained, more specific studies to confirm the evidences described should be planned.

## 6. ACKNOWLEDGEMENT

This research was supported by Fondazione Cariplo for the project “Toxicology of chronic exposure to engineered silver nanoparticles”, under the 2011 call “Nanoparticles, nanotechnologies and ultrafine particles”.

I wish to express my gratitude to all those Colleagues from the following institutions that contributed to this project:

- Dr Camilla Recordati, Mouse and animal pathology laboratory, Fondazione Filarete, Milan, for her contribution in conceive the experiments, critically reviewing of the results and histopathological evaluation.
- Prof.ssa Cristina Lenardi, Dr SimonaArgentiere and Dr Claudia Cella- C.I.Ma.I.Na. CENTRO INTERDISCIPLINARE MATERIALI E INTERFACCE NANOSTRUTTURATI, University of Milan-for their contribution to the physicochemical characterization of NPs.
- Dr Francesco Cubadda and his group- Department of Food Safety and Veterinary Public Health, Istituto Superiore di Sanità-National Health Institute, Rome- for its contribution in the Ag determination in tissues.
- Dr Fabio Fiordaliso and his group- Unit of Bio-imaging. IRCCS - Istituto di Ricerche Farmacologiche "Mario Negri", Milan- that performed TEM analysis.
- Prof. Saverio Paltrinieri, Dipartimento di medicina veterinaria, University of Milan, for hematology and clinical chemistry analysis.
- Dr Paolo Bigini,Department of Biochemistry and Molecular Pharmacology Istituto di Ricerche Farmacologiche "Mario Negri" and Dr Andrea Terron- EFSA European Food Safety Authority, Parma- for the thesis revisions.

## 7. REFERENCES

- [1] J. Potočník, "Commission recommendation of 18 October 2011 on the definition of nanomaterial (2011/696/EU).," *Off. J. Eur. Union*, vol. L275, no. June 2010, pp. 38–40, 2011.
- [2] M. A. Munger, P. Radwanski, G. C. Hadlock, G. Stoddard, A. Shaaban, J. Falconer, D. W. Grainger, and C. E. Deering-rice, "In vivo human time-exposure study of orally dosed commercial silver nanoparticles," *Nanomedicine Nanotechnology, Biol. Med.*, vol. 10, no. 1, pp. 1–9, 2014.
- [3] C. Gerber and H. P. Lang, "How the doors to the nanoworld were opened," *Nat. Nanotechnol.*, vol. 1, no. 1, pp. 3–5, 2006.
- [4] S. Horikoshi and N. Serpone, "Introduction to Nanoparticles," *Microwaves Nanoparticle Synth. Fundam. Appl.*, pp. 1–24, 2013.
- [5] and R. S. Ping-Chang Lin, Stephen Lin, Paul C. Wang, "Techniques for physicochemical characterization of nanomaterials," vol. 32, no. 4, pp. 711–726, 2014.
- [6] G. Oberdörster, E. Oberdörster, and J. Oberdörster, "Nanotoxicology: An emerging discipline evolving from studies of ultrafine particles," *Environ. Health Perspect.*, vol. 113, no. 7, pp. 823–839, 2005.
- [7] SCENIHR (Scientific Committee on Emerging and Newly Identified Health Risks), "Risk Assessment of Products of Nanotechnologies," no. 19 January, p. 71, 2009.
- [8] M. Baldo, "Introduction to Nanoelectronics MIT OpenCourseWare Publication May 2011," *Quantum*, no. May, 2011.
- [9] D. Bhattacharyya, S. Singh, and N. Satnalika, "Nanotechnology , Big things from a Tiny World : a Review," *Sci. Technol.*, vol. 2, no. 3, pp. 29–38, 2009.
- [10] T. N. Science, G. Holdridge, and W. Zhang, "Nanotechnology and the Environment: Report of a National Nanotechnology Initiative Workshop," *Nanotechnology*.
- [11] R. Kessler, "Engineered nanoparticles in consumer products: understanding a new ingredient.," *Environ. Health Perspect.*, vol. 119, no. 3, 2011.
- [12] M. E. Vance, T. Kuiken, E. P. Vejerano, S. P. McGinnis, M. F. Hochella, and D. R. Hull, "Nanotechnology in the real world: Redeveloping the nanomaterial consumer products inventory," *Beilstein J. Nanotechnol.*, vol. 6, no. 1, pp. 1769–1780, 2015.
- [13] J. Miller, "Beyond biotechnology: FDA regulation of nanomedicine.," *Columbia Sci. Technol. Law Rev.*, vol. 4, p. E5, 2003.
- [14] D. Bobo, K. J. Robinson, J. Islam, K. J. Thurecht, S. R. Corrie, and S. R. Corrie, "Nanoparticle-Based Medicines : A Review of FDA-Approved Materials and Clinical Trials to Date," *Pharm. Res.*, pp. 2373–2387, 2016.
- [15] V. S. W. Chan, "Nanomedicine : An unresolved regulatory issue &," vol. 46, pp. 218–224, 2006.
- [16] L. Yildirimer, N. T. K. Thanh, M. Loizidou, and A. M. Seifalian, "Toxicological considerations of clinically applicable nanoparticles," 2011.
- [17] G. Pattan and G. Kaul, "Health hazards associated with nanomaterials.," *Toxicol. Ind. Health*, vol. 30, no. 6, pp. 499–519, Sep. 2012.
- [18] C. From, T. H. E. Commission, T. O. The, T. H. E. Council, and T. H. E. E. Economic, "COMMUNICATION FROM THE COMMISSION TO THE EUROPEAN PARLIAMENT, THE COUNCIL AND THE EUROPEAN ECONOMIC AND SOCIAL COMMITTEE Second Regulatory



- Review on Nanomaterials,” 2012.
- [19] J. E. Lee, N. Lee, T. Kim, J. Kim, and T. Hyeon, “Multifunctional mesoporous silica nanocomposite nanoparticles for theranostic applications,” *Acc. Chem. Res.*, vol. 44, no. 10, pp. 893–902, 2011.
- [20] B. Kiss, T. Bíró, G. Czifra, B. I. Tóth, Z. Kertész, Z. Szikszai, Á. Z. Kiss, I. Juhász, C. C. Zouboulis, and J. Hunyadi, “Investigation of micronized titanium dioxide penetration in human skin xenografts and its effect on cellular functions of human skin-derived cells,” *Exp. Dermatol.*, vol. 17, no. 8, pp. 659–667, 2008.
- [21] S. Vardharajula, S. Z. Ali, P. M. Tiwari, E. Eroğlu, K. Vig, V. A. Dennis, and S. R. Singh, “Functionalized carbon nanotubes: Biomedical applications,” *Int. J. Nanomedicine*, vol. 7, pp. 5361–5374, 2012.
- [22] M. J. R. Virlan, D. Miricescu, R. Radulescu, C. M. Sabliov, A. Totan, B. Calenic, and M. Greabu, “Organic Nanomaterials and Their Applications in the Treatment of Oral Diseases,” *Molecules*, vol. 21, no. 2, pp. 1–23, 2016.
- [23] E. Abbasi, S. Aval, A. Akbarzadeh, M. Milani, H. Nasrabadi, S. Joo, Y. Hanifehpour, K. Nejati-Koshki, and R. Pashaei-Asl, “Dendrimers: synthesis, applications, and properties,” *Nanoscale Res. Lett.*, vol. 9, no. 1, p. 247, 2014.
- [24] M. Umair, I. Javed, M. Rehman, A. Madni, A. Javeed, and A. Ghafoor, “Nanotoxicity of Inert Materials : The Case of Gold , Silver and Iron,” vol. 19, no. 2, pp. 161–180, 2016.
- [25] Y. Tauran, A. Brioude, A. W. Coleman, M. Rhimi, and B. Kim, “Molecular recognition by gold, silver and copper nanoparticles,” *World J. Biol. Chem.*, vol. 4, no. 3, pp. 35–63, 2013.
- [26] L. Wei, J. Lu, H. Xu, A. Patel, Z. Chen, and G. Chen, “Silver nanoparticles : synthesis , properties , and therapeutic applications,” *Drug Discov. Today*, vol. 20, no. 5, pp. 595–601, 2015.
- [27] L. A. Austin, M. A. Mackey, E. C. Dreaden, and M. A. El-Sayed, “The optical, photothermal, and facile surface chemical properties of gold and silver nanoparticles in biodiagnostics, therapy, and drug delivery,” *Arch Toxicol.*, vol. 88, no. 7, pp. 1391–1417, 2014.
- [28] K. Mijndonckx, N. Leys, J. Mahillon, S. Silver, and R. Van Houdt, “Antimicrobial silver: Uses, toxicity and potential for resistance,” *BioMetals*, vol. 26, no. 4, pp. 609–621, 2013.
- [29] C. You, C. Han, and X. Wang, “The progress of silver nanoparticles in the antibacterial mechanism , clinical application and cytotoxicity,” pp. 9193–9201, 2012.
- [30] E. Marambio-Jones, Catalina Hoek, “A review of the antibacterial effects of silver nanomaterials and potential implications for human health and the environment,” *J. Nanoparticle Res.*, vol. 12, p. 21, 2010.
- [31] Y. S. Kim, M. Y. Song, J. D. Park, K. S. Song, H. R. Ryu, Y. H. Chung, H. K. Chang, J. H. Lee, K. H. Oh, B. J. Kelman, I. K. Hwang, and I. J. Yu, “Subchronic oral toxicity of silver nanoparticles,” vol. 408, pp. 1–11, 2010.
- [32] S. Gaillet and J.-M. Rouanet, “Silver nanoparticles: Their potential toxic effects after oral exposure and underlying mechanisms - A review,” *Food Chem. Toxicol.*, vol. 77C, pp. 58–63, 2014.
- [33] H. Bouwmeester, J. Poortman, R. J. Peters, E. Wijma, E. Kramer, S. Makama, K. Puspitaninganindita, H. J. P. Marvin, A. A. C. M. Peijnenburg, and P. J. M. Hendriksen, “Characterization of translocation of silver nanoparticles and effects on whole-genome gene expression using an in vitro intestinal epithelium coculture model,” *ACS Nano*, vol. 5, no. 5,

- pp. 4091–4103, 2011.
- [34] S. Galdiero, M. Galdiero, A. Gade, and M. Rai, “Silver Nanoparticles : Therapeutical Uses , Toxicity , and Safety Issues,” pp. 1931–1944, 2014.
- [35] K. Chaloupka, Y. Malam, and A. M. Seifalian, “Nanosilver as a new generation of nanoparticle in biomedical applications,” *Trends Biotechnol.*, vol. 28, no. 11, pp. 580–588, 2010.
- [36] L. Pineda, A. Chwalibog, E. Sawosz, C. Lauridsen, R. Engberg, J. Elnif, A. Hotowy, F. Sawosz, Y. Gao, A. Ali, and H. S. Moghaddam, “Effect of silver nanoparticles on growth performance, metabolism and microbial profile of broiler chickens,” *Arch. Anim. Nutr.*, vol. 66, no. 5, pp. 416–429, 2012.
- [37] M. Fondevila, R. Herrero, M. C. Casallas, L. Abecia, and J. J. Duchá, “Silver nanoparticles as a potential antimicrobial additive for weaned pigs,” *Anim. Feed Sci. Technol.*, vol. 150, no. 3–4, pp. 259–269, Apr. 2009.
- [38] T. C. Dakal, A. Kumar, R. S. Majumdar, and V. Yadav, “Mechanistic Basis of Antimicrobial Actions of Silver Nanoparticles.,” *Front. Microbiol.*, vol. 7, no. November, p. 1831, 2016.
- [39] S. Belluco, C. Losasso, I. Patuzzi, L. Rigo, D. Conficoni, F. Gallochio, V. Cibir, P. Catellani, S. Segato, and A. Ricci, “Silver as antibacterial toward *Listeria monocytogenes*,” *Front. Microbiol.*, vol. 7, no. MAR, pp. 1–9, 2016.
- [40] G. G. Lin and J. G. Scott, “Molecular Toxicity Mechanism of Nanosilver,” vol. 100, no. 2, pp. 130–134, 2012.
- [41] J. R. Morones, J. L. Elechiguerra, A. Camacho, K. Holt, J. B. Kouri, J. T. Ramírez, and M. J. Yacaman, “The bactericidal effect of silver nanoparticles,” *Nanotechnology*, vol. 16, no. 10, pp. 2346–2353, Oct. 2005.
- [42] Z. R. Panacek A, Kvítek L, Pucek R, Kolar M, Vecerova R, Pizúrova N, Sharma VK, Nevecna T, “Silver Colloid Nanoparticles : Synthesis , Characterization , and Their Antibacterial Activity,” *J Phys. Chem. B*, vol. 110, pp. 16248–16253, 2006.
- [43] G. A. Sotiriou and S. E. Pratsinis, “Antibacterial activity of nanosilver ions and particles,” *Environ. Sci. Technol.*, vol. 44, no. 14, pp. 5649–5654, 2010.
- [44] M. A. Ansari, H. M. Khan, A. A. Khan, M. K. Ahmad, A. A. Mahdi, R. Pal, and S. S. Cameotra, “Interaction of silver nanoparticles with *Escherichia coli* and their cell envelope biomolecules,” *J. Basic Microbiol.*, vol. 54, no. 9, pp. 905–915, 2014.
- [45] M. Zia, A. R. Phull, and J. S. Ali, “Synthesis, characterisation, applications and challenges of Iron Oxide Nanoparticles,” *Nanotechnol. Sci. Appl.*, vol. 9, pp. 49–67, 2016.
- [46] C. Felton, A. Karmakar, Y. Gartia, P. Ramidi, A. S. Biris, and A. Ghosh, “Magnetic nanoparticles as contrast agents in biomedical imaging: recent advances in iron- and manganese-based magnetic nanoparticles.,” *Drug Metab. Rev.*, vol. 46, no. 2, pp. 142–54, 2014.
- [47] and G. L. Shouheng Sun, Hao Zeng, David B. Robinson, Simone Raoux, Philip M. Rice, Shan X. Wang, “Monodisperse MFe<sub>2</sub>O<sub>4</sub> (M ) Fe, Co, Mn) Nanoparticles,” *J. Am. Chem. Soc.*, vol. 126, no. 1, pp. 273–279, 2004.
- [48] P. B. Santhosh and N. P. Ulrich, “Multifunctional superparamagnetic iron oxide nanoparticles: Promising tools in cancer theranostics,” *Cancer Lett.*, vol. 336, no. 1, pp. 8–17, 2013.
- [49] K. Maier-Hauff, F. Ulrich, D. Nestler, H. Niehoff, P. Wust, B. Thiesen, H. Orawa, V. Budach, and A. Jordan, “Efficacy and safety of intratumoral thermotherapy using magnetic iron-oxide

- nanoparticles combined with external beam radiotherapy on patients with recurrent glioblastoma multiforme," *J. Neurooncol.*, vol. 103, no. 2, pp. 317–324, 2011.
- [50] R. A. Revia and M. Zhang, "Magnetite nanoparticles for cancer diagnosis , treatment , and treatment monitoring : recent advances," *Biochem. Pharmacol.*, vol. 19, no. 3, pp. 157–168, 2016.
- [51] Y.-W. Jun, Y.-M. Huh, J.-S. Choi, J.-H. Lee, H.-T. Song, S. Kim, S. Yoon, K.-S. Kim, J.-S. Shin, J.-S. Suh, and J. Cheon, "Nanoscale size effect of magnetic nanocrystals and their utilization for cancer diagnosis via magnetic resonance imaging.," *J. Am. Chem. Soc.*, vol. 127, no. 16, pp. 5732–3, 2005.
- [52] M. R. Bashir, L. Bhatti, D. Marin, and R. C. Nelson, "Emerging applications for ferumoxytol as a contrast agent in MRI," *J. Magn. Reson. Imaging*, vol. 41, no. 4, pp. 884–898, 2015.
- [53] N. Feliu, D. Docter, M. Heine, P. del Pino, S. Ashraf, J. Kolosnjaj-Tabi, P. Macchiarini, P. Nielsen, D. Alloeyau, F. Gazeau, R. H. Stauber, and W. J. Parak, "In vivo degeneration and the fate of inorganic nanoparticles," *Chem. Soc. Rev.*, vol. 5, no. 9, pp. 33–37, 2016.
- [54] G. Pattan and G. Kaul, "Health hazards associated with nanomaterials," no. September 2012, 2013.
- [55] H. F. Krug, "Nanosafety Research — Are We on the Right Track ? *Angewandte*," pp. 12304–12319, 2014.
- [56] S. M. Hussain, D. B. Warheit, S. P. Ng, K. K. Comfort, C. M. Grabinski, and L. K. Braydich-Stolle, "At the crossroads of nanotoxicology in vitro: Past achievements and current challenges," *Toxicol. Sci.*, vol. 147, no. 1, pp. 5–16, 2015.
- [57] E. P. and Chavon Walters and V. Somerset, "Nanotoxicology: A Review."
- [58] A. Ivask, K. Kasemets, M. Mortimer, and A. Kahru, "Toxicity of Ag , CuO and ZnO nanoparticles to selected environmentally relevant test organisms and mammalian cells in vitro : a critical review," pp. 1181–1200, 2013.
- [59] N. Khlebtsov and L. Dykman, "Biodistribution and toxicity of engineered gold nanoparticles : a review of in vitro and in vivo studies," pp. 1647–1671, 2011.
- [60] B. J. Marquis, S. A. Love, K. L. Braun, and C. L. Haynes, "Analytical methods to assess nanoparticle toxicity a current summary of the analytical techniques used in," pp. 425–439, 2009.
- [61] C. S. Yah, G. S. Simate, and S. E. Iyuke, "Nanoparticles toxicity and their routes of exposures," vol. 25, no. 2, pp. 477–491, 2012.
- [62] F. Ehrhart, C. T. Evalo, and E. Willighagen, "Current systems biology approaches in hazard assessment of nanoparticles," *bioRxiv*, 2015.
- [63] Bergin, "Nanoparticle toxicity by the gastrointestinal route: evidence and knowledge gaps," 2013.
- [64] Q. Mu, G. Jiang, L. Chen, H. Zhou, D. Fourches, A. Tropsha, and B. Yan, "Chemical Basis of Interactions Between Engineered Nanoparticles and Biological Systems," *Chem. Rev.*, vol. i, no. 15, pp. 7740–7781, 2016.
- [65] S. R. Saptarshi, A. Duschl, A. L. Lopata, A. Duschl, and A. L. Lopata, "Interaction of nanoparticles with proteins: relation to bio-reactivity of the nanoparticle.," *J. Nanobiotechnology*, vol. 11, no. 1, p. 26, 2013.
- [66] SCENIHR (Scientific Committee on Emerging and Newly Identified Health Risks), *Nanosilver: safety, health and environmental effects and role in antimicrobial resistance*, vol. 18, no.

- December. 2013.
- [67] G. Oberdörster, A. Maynard, K. Donaldson, V. Castranova, J. Fitzpatrick, K. Ausman, J. Carter, B. Karn, W. Kreyling, D. Lai, and S. Olin, "Principles for characterizing the potential human health effects from exposure to nanomaterials : elements of a screening strategy," vol. 35, pp. 1–35, 2005.
- [68] H. Cho, J. Sung, K. Song, J. Kim, J. Ji, J. Lee, H. Ryu, K. Ahn, and I. Yu, "Genotoxicity of Silver Nanoparticles in Lung Cells of Sprague Dawley Rats after 12 Weeks of Inhalation Exposure," *Toxics*, vol. 1, no. 1, pp. 36–45, 2013.
- [69] K. S. Song, J. H. Sung, J. H. Ji, J. H. Lee, J. S. Lee, H. R. Ryu, J. K. Lee, Y. H. Chung, H. M. Park, B. S. Shin, H. K. Chang, B. Kelman, and I. J. Yu, "Recovery from silver-nanoparticle-exposure-induced lung inflammation and lung function changes in Sprague Dawley rats," *Nanotoxicology*, vol. 7, no. 2, pp. 169–180, 2013.
- [70] Z. Lin, N. A. Monteiro-riviere, and J. E. Riviere, "Pharmacokinetics of metallic nanoparticles," vol. 7, no. April, pp. 189–217, 2015.
- [71] W. H. De Jong, L. T. M. Van Der Ven, A. Sleijffers, M. V. D. Z. Park, E. H. J. M. Jansen, H. Van Loveren, and R. J. Vandebriel, "Systemic and immunotoxicity of silver nanoparticles in an intravenous 28 days repeated dose toxicity study in rats," *Biomaterials*, vol. 34, no. 33, 2013.
- [72] Y. Xue, S. Zhang, Y. Huang, T. Zhang, X. Liu, Y. Hu, Z. Zhang, and M. Tang, "Acute toxic effects and gender-related biokinetics of silver nanoparticles following an intravenous injection in mice," *J. Appl. Toxicol.*, vol. 32, no. 11, pp. 890–899, Nov. 2012.
- [73] M. Van Der Zande, R. J. Vandebriel, E. Van Doren, E. Kramer, Z. Herrera Rivera, C. S. Serrano-Rojero, E. R. Gremmer, J. Mast, R. J. B. Peters, P. C. H. Hollman, P. J. M. Hendriksen, H. J. P. Marvin, A. A. C. M. Peijnenburg, and H. Bouwmeester, "Distribution, elimination, and toxicity of silver nanoparticles and silver ions in rats after 28-day oral exposure," *ACS Nano*, vol. 6, no. 8, pp. 7427–7442, 2012.
- [74] K. Loeschner, N. Hadrup, K. Qvortrup, A. Larsen, X. Gao, U. Vogel, A. Mortensen, H. R. Lam, and E. H. Larsen, "Distribution of silver in rats following 28 days of repeated oral exposure to silver nanoparticles or silver acetate," *Part. Fibre Toxicol.*, vol. 8, no. 1, p. 18, 2011.
- [75] J. Rungby and G. Danscher, "Localization of exogenous silver in brain and spinal cord of silver exposed rats.," *Acta Neuropathol.*, vol. 60, no. 1–2, pp. 92–8, 1983.
- [76] R. R. R. Sardari, S. R. Zarchi, A. Talebi, S. Nasri, S. Imani, A. Khoradmehr, and S. A. R. Sheshde, "Toxicological effects of silver nanoparticles in rats," *African J. Microbiol. Res.*, vol. 6, no. 27, pp. 5587–5593, Jul. 2012.
- [77] G. N. Jeong, U. B. Jo, H. Y. Ryu, Y. S. Kim, K. S. Song, and I. J. Yu, "Histochemical study of intestinal mucins after administration of silver nanoparticles in Sprague-Dawley rats," *Arch. Toxicol.*, vol. 84, no. 1, pp. 63–69, 2010.
- [78] Y. S. Kim, J. S. Kim, H. S. Cho, D. S. Rha, J. M. Kim, J. D. Park, B. S. Choi, R. Lim, H. K. Chang, Y. H. Chung, I. H. Kwon, J. Jeong, B. S. Han, and I. J. Yu, "Twenty-eight-day oral toxicity, genotoxicity, and gender-related tissue distribution of silver nanoparticles in Sprague-Dawley rats.," *Inhal. Toxicol.*, vol. 20, no. 6, pp. 575–583, 2008.
- [79] B. Shahare and M. Yashpal, "Toxic effects of repeated oral exposure of silver nanoparticles on small intestine mucosa of mice.," *Toxicol. Mech. Methods*, vol. 23, no. 3, pp. 161–7, Mar. 2013.
- [80] Z. Yang, Z. W. Liu, R. P. Allaker, P. Reip, J. Oxford, Z. Ahmad, and G. Ren, "A review of

- nanoparticle functionality and toxicity on the central nervous system.," *J. R. Soc. Interface*, vol. 7 Suppl 4, pp. S411-22, Aug. 2010.
- [81] J. Tang, L. Xiong, S. Wang, J. Wang, L. Liu, J. Li, F. Yuan, and T. Xi, "Distribution, Translocation and Accumulation of Silver Nanoparticles in Rats," *J. Nanosci. Nanotechnol.*, vol. 9, no. 8, pp. 4924–4932, 2009.
- [82] N. Hadrup, K. Loeschner, A. Mortensen, A. K. Sharma, K. Qvortrup, E. H. Larsen, and H. R. Lam, "The similar neurotoxic effects of nanoparticulate and ionic silver in vivo and in vitro," *Neurotoxicology*, vol. 33, no. 3, pp. 416–423, Jun. 2012.
- [83] H. S. Sharma and A. Sharma, "Nanoparticles aggravate heat stress induced cognitive deficits, blood-brain barrier disruption, edema formation and brain pathology," *Progress in Brain Research*, vol. 162. pp. 245–273, 2007.
- [84] J. Skalska, M. Frontczak-Baniewicz, and L. Struzyńska, "Synaptic degeneration in rat brain after prolonged oral exposure to silver nanoparticles," *Neurotoxicology*, vol. 46, pp. 145–154, 2015.
- [85] B. Reidy, A. Haase, A. Luch, K. A. Dawson, and I. Lynch, "Mechanisms of silver nanoparticle release, transformation and toxicity: A critical review of current knowledge and recommendations for future studies and applications," *Materials (Basel)*, vol. 6, no. 6, pp. 2295–2350, 2013.
- [86] P. L. Drake and K. J. Hazelwood, "Exposure-related health effects of silver and silver compounds: A review," *Ann. Occup. Hyg.*, vol. 49, no. 7, pp. 575–585, 2005.
- [87] S. C. Hong, J. H. Lee, J. Lee, H. Y. Kim, J. Y. Park, J. Cho, J. Lee, and D. W. Han, "Subtle cytotoxicity and genotoxicity differences in superparamagnetic iron oxide nanoparticles coated with various functional groups.," *Int. J. Nanomedicine*, vol. 6, pp. 3219–3231, 2011.
- [88] C. K. Huynh KA1, "Aggregation Kinetics of Citrate and Polyvinylpyrrolidone Coated Silver Nanoparticles in Monovalent and Divalent Electrolyte Solutions," vol. 45, no. 13, pp. 5564–5571, 2012.
- [89] C. E. Román-velázquez, C. Noguez, C. E. Román-velázquez, and C. Noguez, "Designing the plasmonic response of shell nanoparticles : Spectral representation Designing the plasmonic response of shell nanoparticles :," vol. 44116, 2011.
- [90] G. Bachler, N. von Goetz, and K. Hungerbuhler, "A physiologically based pharmacokinetic model for ionic silver and silver nanoparticles," *Int J Nanomedicine*, vol. 8, pp. 3365–3382, 2013.
- [91] K. Loza, J. Diendorf, C. Sengstock, L. Ruiz-Gonzalez, J. M. Gonzalez-Calbet, M. Vallet-Regi, M. Köller, and M. Epple, "The dissolution and biological effects of silver nanoparticles in biological media," *J. Mater. Chem. B*, vol. 2, 2014.
- [92] W. Utembe, K. Potgieter, A. B. Stefaniak, and M. Gulumian, "Dissolution and biodurability : Important parameters needed for risk assessment of nanomaterials," ???, pp. 1–12, 2015.
- [93] D. P. Lankveld, A. G. Oomen, P. Krystek, A. Neigh, A. Troost-de Jong, C. W. Noorlander, J. C. Van Eijkeren, R. E. Geertsma, and W. H. De Jong, "The kinetics of the tissue distribution of silver nanoparticles of different sizes," *Biomaterials*, vol. 31, no. 32, pp. 8350–8361, 2010.
- [94] H. H. Gustafson, D. Holt-Casper, D. W. Grainger, and H. Ghandehari, "Nanoparticle uptake: The phagocyte problem," *Nano Today*, vol. 10, no. 4. Elsevier, pp. 487–510, 01-Aug-2015.
- [95] C. Recordati, M. De Maglie, S. Bianchessi, S. Argenti, C. Cella, S. Mattiello, F. Cubadda, F. Aureli, M. D'Amato, A. Raggi, C. Lenardi, P. Milani, and E. Scanziani, "Tissue distribution and

- acute toxicity of silver after single intravenous administration in mice: nano-specific and size-dependent effects.," *Part. Fibre Toxicol.*, vol. 13, no. 1, p. 12, 2016.
- [96] C. Beer, R. Foldbjerg, Y. Hayashi, D. S. Sutherland, and H. Autrup, "Toxicity of silver nanoparticles — Nanoparticle or silver ion?," *Toxicol. Lett.*, vol. 208, no. 3, pp. 286–292, 2012.
- [97] N. Hadrup and H. R. Lam, "Oral toxicity of silver ions , silver nanoparticles and colloidal silver – A review," *Regul. Toxicol. Pharmacol.*, vol. 68, no. 1, pp. 1–7, 2014.
- [98] J. H. Lee, Y. S. Kim, K. S. Song, H. R. Ryu, J. H. Sung, J. D. Park, H. M. Park, N. W. Song, B. S. Shin, D. Marshak, K. Ahn, J. E. Lee, and I. J. Yu, "Biopersistence of silver nanoparticles in tissues from Sprague–Dawley rats," *Part. Fibre Toxicol.*, vol. 10, no. 1, pp. 1–14, 2013.
- [99] J. S. Kim, T. J. Yoon, K. N. Yu, B. G. Kim, S. J. Park, H. W. Kim, K. H. Lee, S. B. Park, J. K. Lee, and M. H. Cho, "Toxicity and tissue distribution of magnetic nanoparticles in mice," *Toxicol Sci*, vol. 89, no. 1, pp. 338–347, 2006.
- [100] L. Xu, A. Shao, Y. Zhao, Z. Wang, C. Zhang, Y. Sun, J. Deng, and L. L. Chou, "Neurotoxicity of Silver Nanoparticles in Rat Brain After Intra-gastric Exposure," *J. Nanosci. Nanotechnol.*, vol. 15, no. 6, pp. 4215–4223, 2015.
- [101] J. Xiang, Y. Tang, C. Li, E. J. Su, D. A. Lawrence, and R. F. Keep, "Mechanisms underlying astrocyte endfeet swelling in stroke," in *Acta Neurochirurgica, Supplementum*, vol. 121, Springer-Verlag Wien, 2016, pp. 19–22.
- [102] C. M. Florence, L. D. Baillie, and S. J. Mulligan, "Dynamic Volume Changes in Astrocytes Are an Intrinsic Phenomenon Mediated by Bicarbonate Ion Flux," *PLoS One*, vol. 7, no. 11, Nov. 2012.
- [103] P. O. Gerrits, H. de Weerd, J. J. L. van der Want, R. Kortekaas, P. G. M. Luiten, and J. G. Veening, "Microvascular changes in estrogen-?? sensitive brainstem structures of aging female hamsters," *Neurosci. Res.*, vol. 67, no. 4, pp. 267–274, 2010.
- [104] M. Debia, B. Bakhiyi, C. Ostiguy, J. H. Verbeek, D. H. Brouwer, and V. Murashov, "A Systematic Review of Reported Exposure to Engineered Nanomaterials," pp. 1–20, 2016.
- [105] OECD, "GUIDANCE MANUAL FOR THE TESTING OF MANUFACTURED NANOMATERIALS: OECD's SPONSORSHIP PROGRAMME; FIRST REVISION," *Development*, no. 2009, pp. 1–92, 2010.
- [106] A. Haase, S. Rott, A. Mantion, P. Graf, J. Plendl, A. F. Thu, W. P. Meier, A. Taubert, A. Luch, and G. Reiser, "Effects of Silver Nanoparticles on Primary Mixed Neural Cell Cultures : Uptake , Oxidative Stress and Acute Calcium Responses," vol. 126, no. 2, pp. 457–468, 2012.
- [107] K. Jomova, D. Vondrakova, M. Lawson, and M. Valko, "Metals, oxidative stress and neurodegenerative disorders," *Mol. Cell. Biochem.*, vol. 345, no. 1–2, pp. 91–104, 2010.
- [108] S. Z. Imam, S. M. Lantz-McPeak, E. Cuevas, H. Rosas-Hernandez, S. Liachenko, Y. Zhang, S. Sarkar, J. Ramu, B. L. Robinson, Y. Jones, B. Gough, M. G. Paule, S. F. Ali, and Z. K. Binienda, "Iron Oxide Nanoparticles Induce Dopaminergic Damage: In vitro Pathways and In Vivo Imaging Reveals Mechanism of Neuronal Damage," *Mol. Neurobiol.*, vol. 52, no. 2, pp. 913–926, 2015.
- [109] H. Arami, A. Khandhar, D. Liggitt, and K. M. Krishnan, "Chem Soc Rev," *Chem. Soc. Rev.*, vol. 44, pp. 8576–8607, 2015.
- [110] H. H. Gustafson, D. Holt-Casper, D. W. Grainger, and H. Ghandehari, "Nanoparticle uptake: The phagocyte problem," *Nano Today*, vol. 10, no. 4, pp. 487–510, 2015.

- [111] E. Fröhlich, "Cellular elimination of nanoparticles," *Environ. Toxicol. Pharmacol.*, vol. 46, pp. 90–94, 2016.
- [112] J. M. Chalovich and E. C. Eisenberg, "State-of-the-Art in Design Rules for Drug Delivery Platforms: Lessons from FDA-approved Nanomedicines," *Biophys. Chem.*, vol. 257, no. 5, pp. 2432–2437, 2005.
- [113] Danscher G. Light and electron microscopic localization of silver in biological tissue. *Histochemistry*. 1981;71:177–86.
- [114] Peophet EB. Armed Forces Institute of Pathology Staf. In: AFIP Laboratory Methods in Histotechnology. Prophet EB, Mills B, Arrington JB, Sobin LH (Eds). American Registry of Pathology Publisher, Washington, DC, USA, 1–279 (1994).

**Appendix A: ADDITIONAL DATA**

**4.1.1 Single intravenous administration: effect of size and coating on biodistribution and toxicity**

**Behavioural observation: Irwin test**

No relevant behavioral alterations were observed.

<b>Time: + 5 min</b>		<b>CTR</b>		<b>AgNPs 10 nm Ct-coated</b>		
Undisturbed animal	Ref value	C3	C4	C1	C2	C5
1) Body position	4	4	4	4	4	4
2) Mobility	4	0	0	4	0	4
3) Eye prominence	-	-	-	-	-	-
4) Respiration	4	4	4	4	4	4
5) Tremors	0	0	0	0	0	0
6) Convulsions	-	-	-	-	-	-
7) Grooming	4	0	0	0	0	0
8) Stereotypies	0	0	0	0	0	0
9) Piloerection	0	0	0	0	0	0
Disturbed animal						
1) Touch response	4	4	4	4	4	4
2) Positional passivity	0	0	0	0	0	0
3) Catatonia	0	0	0	0	0	0
4) Grip strenght	4	4	4	4	4	2
5) Abdomen tone	4	4	4	4	4	4
6) Corneal reflex	4	4	4	4	4	4
7) Pinna reflex	4	4	4	4	4	4
8) Tail pinch response	4	4	4	4	4	4
9) Righting reflex	0	0	0	0	0	0
Neurovegetative profile						
1) Skin color	4	4	4	4	4	4
2) Stools						
3) Urines	-	-	-	-	-	-
4) Lacrimation	0	0	0	0	0	0
5) Salivation	0	0	0	0	0	0
6) Rhinorrhea	0	0	0	0	0	0
7) Temperature	/	/	/	/	/	/

<b>Time: + 5 min</b>		<b>CTR</b>		<b>AgNPs 10 nm Ct-coated</b>		
Undisturbed animal	Ref value	C3	C4	C1	C2	C5
1) Body position	4	4	4	4	4	4
2) Mobility	0	0	0	0	0	0



3) Eye prominence	-	-	-	-	-	-
4) Respiration	4	4	4	4	4	4
5) Tremors	0	0	0	0	0	0
6) Convulsions	-	-	-	-	-	-
7) Grooming	4	0	0	0	0	0
8) Stereotypies	0	0	0	0	0	0
9) Piloerection	0	0	0	0	0	0
Disturbed animal						
1) Touch response	4	4	4	2	4	4
2) Positional passivity	0	0	0	0	0	0
3) Catatonia	0	0	0	0	0	0
4) Grip strenght	4	4	4	4	4	4
5) Abdomen tone	4	4	4	4	4	4
6) Corneal reflex	4	4	4	4	4	4
7) Pinna reflex	4	4	4	4	4	4
8) Tail pinch response	4	4	4	4	4	0
9) Righting reflex	0	0	0	0	0	0
Neurovegetative profile						
1) Skin color	4	4	4	4	4	4
2) Stools						
3) Urines	-	-	-	-	-	-
4) Lacrimation	0	0	0	0	0	0
5) Salivation	0	0	0	0	0	0
6) Rhinorrhea	0	0	0	0	0	0
7) Temperature	/	/	/	/	/	/

Time: +30 min		CTR		AgNPs 10 nm Ct-coated		
Undisturbed animal	Ref value	C3	C4	C1	C2	C5
1) Body position	4	6	4	4	4	4
2) Mobility	4	0	0	0	0	0
3) Eye prominence	-	-	-	-	-	-
4) Respiration	4	4	4	4	4	4
5) Tremors	0	0	0	0	0	0
6) Convulsions	-	-	-	-	-	-
7) Grooming	4	0	0	4	0	0
8) Stereotypies	0	0	0	0	0	0
9) Piloerection	0	0	0	0	0	0
Disturbed animal						
1) Touch response	4	4	4	2	4	4

2) Positional passivity	0	0	0	0	0	0
3) Catatonia	0	0	0	0	0	0
4) Grip strenght	4	4	4	4	2	4
5) Abdomen tone	4	4	4	4	4	4
6) Corneal reflex	4	4	4	4	4	4
7) Pinna reflex	4	4	4	4	4	4
8) Tail pinch response	4	4	4	4	4	4
9) Righting reflex	0	0	0	0	0	0
Neurovegetative profile						
1) Skin color	4	4	4	4	4	4
2) Stools						
3) Urines	-	+	-	-	-	-
4) Lacrimation	0	0	0	0	0	0
5) Salivation	0	0	0	0	0	0
6) Rhinorrhea	0	0	0	0	0	0
7) Temperature	/	/	/	/	/	/

Time: +60 min		CTR		AgNPs 10 nm Ct-coated		
Undisturbed animal	Ref value	C3	C4	C1	C2	C5
1) Body position	4	6	4	4	4	4
2) Mobility	4	0	0	0	0	0
3) Eye prominence	-	-	-	-	-	-
4) Respiration	4	4	4	4	4	4
5) Tremors	0	0	0	0	0	0
6) Convulsions	-	-	-	-	-	-
7) Grooming	4	0	0	0	0	0
8) Stereotypies	0	0	0	0	0	0
9) Piloerection	0	0	0	0	0	0
Disturbed animal						
1) Touch response	4	6	4	2	2	4
2) Positional passivity	0	0	0	0	0	0
3) Catatonia	0	0	0	0	0	0
4) Grip strenght	4	4	4	4	4	4
5) Abdomen tone	4	4	4	4	4	4
6) Corneal reflex	4	4	4	4	4	4
7) Pinna reflex	4	4	4	4	4	4
8) Tail pinch response	4	4	4	4	4	4
9) Righting reflex	0	0	0	0	0	0
Neurovegetative						

profile						
1) Skin color	4	4	4	4	4	4
2) Stools		11	12	6	4	2
3) Urines	-	-	-	-	-	-
4) Lacrimation	0	0	0	0	0	0
5) Salivation	0	0	0	0	0	0
6) Rhinorrhea	0	0	0	0	0	0
7) Temperature	/	/	/	/	/	/

### Histopathological examination

Grading of most relevant histopathological lesions observed in mice following i.v. exposure to 10 mg/kg of AgNPs, evaluated as follows: 0 = absence of lesions; 1 = minimal lesions; 2 = mild lesions; 3 = moderate lesions; 4 = severe lesions. Results are expressed as median score per group (range).

Group	Hepatobiliary tract			Spleen	Kidney
	Hepatocellular	Portal vein	Gall bladder	Red pulp	Tubuar
	necrosis and hemorrhage	Peribiliary hemorrhage	endothelial damage	hyperemia	necrosis
Control	0 (0-0)	0 (0-0)	0 (0-0)	1 (0-2)	0 (0-0)
10 nm AgNP-CT	4 (3-4)	2 (1-4)	1 (0-4)	2 (2-3)	0 (0-0)
10 nm AgNP-PVP	4 (2-4)	2 (1-4)	2 (0-4)	3 (3-4)	0 (0-0)
40 nm AgNP-CT	0 (0-1)	0 (0-1)	0 (0-0)	2 (2-3)	0 (0-0)
40 nm AgNP-PVP	0 (0-0)	0 (0-0)	0 (0-0)	2 (1-2)	0 (0-0)
100 nm AgNP-CT	0 (0-0)	0 (0-0)	0 (0-0)	0 (0-1)	0 (0-0)
100 nm AgNP-PVP	0 (0-0)	0 (0-0)	0 (0-0)	1 (0-2)	0 (0-0)
AgAc	0 (0-0)	0 (0-0)	0 (0-0)	1 (0-2)	4 (3-4)

## ICP-MS

Silver concentration ( $\mu\text{g/g}$  wet organ) determined by ICP-MS in blood and organs following i.v. exposure to 10 mg/kg bw of AgNPs in mice.

Group	Mouse ID	Organ					
		Spleen	Liver	Lung	Kidney	Brain	Blood
Control	B1	0.002	0.004	0.039	0.005	0.001	0.000
	C2	0.006	0.005	0.017	0.002	0.001	0.000
	A3	0.002	0.002	0.002	0.001	0.003	0.000
	<b>Mean</b>	<b>0.003</b>	<b>0.004</b>	<b>0.003</b>	<b>0.001</b>	<b>0.020</b>	<b>0.000</b>
	SD	0.002	0.001	0.001	0.000	0.018	0.000
AgAc	H4	11,8	55,2	3,3	16,5	0,36	n.a.
	H5	19,1	63,2	4,1	13,8	0,43	n.a.
	H6	10,6	78,6	4,3	10,2	0,36	n.a.
	<b>Mean</b>	<b>13,9</b>	<b>65,7</b>	<b>3,9</b>	<b>13,5</b>	<b>0,38</b>	<b>n.a.</b>
	SD	4,6	11,9	0,5	3,2	0,04	n.a.
10 nm AgNP-CT	A1	113.6	77.6	73.6	2.2	0.4	2.7
	B2	112.4	71.3	62.9	3.3	0.3	n.a.
	C3	139.1	85.7	66.1	4.0	0.3	2.4
	<b>Mean</b>	<b>121.7</b>	<b>78.2</b>	<b>67.5</b>	<b>3.2</b>	<b>0.3</b>	<b>2.6</b>
	SD	15.1	7.2	5.5	0.9	0.1	0.3
40 nm AgNP-CT	E5	70.9	62.9	8.4	0.5	0.2	1.5
	G3	109.7	79.3	10.1	1.0	0.2	1.1
	H1	72.0	70.8	5.6	0.9	0.2	2.7
	<b>Mean</b>	<b>84.2</b>	<b>71.0</b>	<b>8.0</b>	<b>0.8</b>	<b>0.2</b>	<b>1.8</b>
	SD	22.1	8.2	2.3	0.3	0.0	0.8
100 nm AgNP-CT	C5	67.6	51.4	7.6	0.4	0.2	0.8
	E6	61.9	56.9	10.9	0.5	0.2	0.7
	D4	78.2	51.5	5.9	0.6	0.2	0.7
	<b>Mean</b>	<b>69.2</b>	<b>53.2</b>	<b>8.1</b>	<b>0.5</b>	<b>0.2</b>	<b>0.7</b>
	SD	8.3	3.1	2.5	0.1	0.0	0.0
10 nm AgNP-PVP	F1	81.6	63.8	34.8	3.0	0.2	n.a.
	G2	100.0	69.5	32.1	2.5	0.4	2.2
	H3	82.3	74.2	31.3	2.9	0.3	2.1
	<b>Mean</b>	<b>88.0</b>	<b>69.2</b>	<b>32.8</b>	<b>2.8</b>	<b>0.3</b>	<b>2.2</b>
	SD	10.5	5.2	1.8	0.3	0.1	0.1
40 nm AgNP-PVP	A5	80.9	69.3	6.0	1.2	0.2	1.3
	A6	68.6	67.7	4.9	0.9	0.2	0.8
	E1	59.6	58.2	4.7	0.9	0.2	1.0
	<b>Mean</b>	<b>69.7</b>	<b>65.0</b>	<b>5.2</b>	<b>1.0</b>	<b>0.2</b>	<b>1.0</b>
	SD						

	SD	10.7	6.0	0.7	0.2	0.0	0.2
100 nm AgNP-PVP	D3	60.5	61.6	1.9	0.9	0.2	0.6
	F4	54.8	62.7	2.8	0.7	0.2	0.7
	G5	68.3	71.9	2.9	0.6	0.2	0.6
	<b>Mean</b>	<b>61.2</b>	<b>65.4</b>	<b>2.5</b>	<b>0.7</b>	<b>0.2</b>	<b>0.6</b>
	SD	6.8	5.7	0.5	0.1	0.0	0.0

#### 4.1.2 Single intravenous administration of AgNPs: batch dependent biodistribution and toxicity

##### Histopathological examination

Summary of histopathological examination.

Size	Lot. ID	Administration	Dose	Mouse ID	Histopathological grading			
					Hepaocellular necrosis/hemorrhage	Median	Gall bladder hemorrhage	Median
10 nm	A	IV 24h	5 mg/kg	E2	4	1	4	2,5
				F5	0		1	
				G1	1		0	
			10 mg/kg	A1	3	4	2	2
				B2	4		4	
				C3	4		2	
10 nm	B	IV 24h	5 mg/kg	A2	1	1	0	1
				C4	1		1	
				C5	0		1	
			10 mg/kg	B4	3	2	3	2
				B5	1		2	
				B6	2		1	
10 nm	C	IV 24h	5 mg/kg	B1	3	2	np	0
				B2	2		0	
				B3	2		1	
			10 mg/kg	B4	3	4	0	0
				B5	4		np	
				B6	4		0	
5 nm	\	IV 24h	10 mg/kg	A1	4	4	4	3
				A3	4		2	
				A4	3		3	

#### 4.2.1 Single intravenous administration of IONPs: effect of dose and vehicle on distribution and toxicity

##### Behavioural observation: Irwin test

No relevant behavioral alterations were observed.

<b>Time: + 5 min</b>		<b>CTR</b>		<b>Fe3O4-DAAO 100mg/kg</b>		
Undisturbed animal	Ref value	C3	C4	C1	C2	C5
1) Body position	4	4	4	4	4	4
2) Mobility	4	0	0	4	0	4
3) Eye prominence	-	-	-	-	-	-
4) Respiration	4	4	4	4	4	4
5) Tremors	0	0	0	0	0	0
6) Convulsions	-	-	-	-	-	-
7) Grooming	4	0	0	0	0	0
8) Stereotypies	0	0	0	0	0	0
9) Piloerection	0	0	0	0	0	0
Disturbed animal						
1) Touch response	4	4	4	4	4	4
2) Positional passivity	0	0	0	0	0	0
3) Catatonia	0	0	0	0	0	0
4) Grip strenght	4	4	4	4	4	2
5) Abdomen tone	4	4	4	4	4	4
6) Corneal reflex	4	4	4	4	4	4
7) Pinna reflex	4	4	4	4	4	4
8) Tail pinch response	4	4	4	4	4	4
9) Righting reflex	0	0	0	0	0	0
Neurovegetative profile						
1) Skin color	4	4	4	4	4	4
2) Stools						
3) Urines	-	-	-	-	-	-
4) Lacrimation	0	0	0	0	0	0
5) Salivation	0	0	0	0	0	0
6) Rhinorrhea	0	0	0	0	0	0
7) Temperature	/	/	/	/	/	/

<b>Time: +15 min</b>		<b>CTR</b>		<b>Fe3O4-DAAO 100mg/kg</b>		
Undisturbed animal	Ref value	C3	C4	C1	C2	C5

1) Body position	4	4	4	4	4	4
2) Mobility	0	0	0	0	0	0
3) Eye prominence	-	-	-	-	-	-
4) Respiration	4	4	4	4	4	4
5) Tremors	0	0	0	0	0	0
6) Convulsions	-	-	-	-	-	-
7) Grooming	4	0	0	0	0	0
8) Stereotypies	0	0	0	0	0	0
9) Piloerection	0	0	0	0	0	0
Disturbed animal						
1) Touch response	4	4	4	2	4	4
2) Positional passivity	0	0	0	0	0	0
3) Catatonia	0	0	0	0	0	0
4) Grip strenght	4	4	4	4	4	4
5) Abdomen tone	4	4	4	4	4	4
6) Corneal reflex	4	4	4	4	4	4
7) Pinna reflex	4	4	4	4	4	4
8) Tail pinch response	4	4	4	4	4	0
9) Righting reflex	0	0	0	0	0	0
Neurovegetative profile						
1) Skin color	4	4	4	4	4	4
2) Stools						
3) Urines	-	-	-	-	-	-
4) Lacrimation	0	0	0	0	0	0
5) Salivation	0	0	0	0	0	0
6) Rhinorrhea	0	0	0	0	0	0
7) Temperature	/	/	/	/	/	/

<b>Time: +30 min</b>		<b>CTR</b>		<b>Fe3O4-DAAO 100mg/kg</b>		
Undisturbed animal	Ref value	C3	C4	C1	C2	C5
1) Body position	4	6	4	4	4	4
2) Mobility	4	0	0	0	0	0
3) Eye prominence	-	-	-	-	-	-
4) Respiration	4	4	4	4	4	4
5) Tremors	0	0	0	0	0	0
6) Convulsions	-	-	-	-	-	-
7) Grooming	4	0	0	4	0	0
8) Stereotypies	0	0	0	0	0	0
9) Piloerection	0	0	0	0	0	0
Disturbed animal						

1) Touch response	4	8	4	2	4	4
2) Positional passivity	0	0	0	0	0	0
3) Catatonia	0	0	0	0	0	0
4) Grip strenght	4	4	4	4	2	4
5) Abdomen tone	4	4	4	4	4	4
6) Corneal reflex	4	4	4	4	4	4
7) Pinna reflex	4	4	4	4	4	4
8) Tail pinch response	4	4	4	4	4	4
9) Righting reflex	0	0	0	0	0	0
Neurovegetative profile						
1) Skin color	4	4	4	4	4	4
2) Stools						
3) Urines	-	+	-	-	-	-
4) Lacrimation	0	0	0	0	0	0
5) Salivation	0	0	0	0	0	0
6) Rhinorrhea	0	0	0	0	0	0
7) Temperature	/	/	/	/	/	/

<b>Time: +60 min</b>		<b>CTR</b>		<b>Fe3O4-DAAO 100mg/kg</b>		
Undisturbed animal	Ref value	C3	C4	C1	C2	C5
1) Body position	4	6	4	4	4	4
2) Mobility	4	0	0	0	0	0
3) Eye prominence	-	-	-	-	-	-
4) Respiration	4	4	4	4	4	4
5) Tremors	0	0	0	0	0	0
6) Convulsions	-	-	-	-	-	-
7) Grooming	4	0	0	0	0	0
8) Stereotypies	0	0	0	0	0	0
9) Piloerection	0	0	0	0	0	0
Disturbed animal						
1) Touch response	4	8	4	2	2	4
2) Positional passivity	0	0	0	0	0	0
3) Catatonia	0	0	0	0	0	0
4) Grip strenght	4	4	4	4	4	4
5) Abdomen tone	4	4	4	4	4	4
6) Corneal reflex	4	4	4	4	4	4
7) Pinna reflex	4	4	4	4	4	4
8) Tail pinch response	4	4	4	4	4	4
9) Righting reflex	0	0	0	0	0	0
Neurovegetative						



profile						
1) Skin color	4	4	4	4	4	4
2) Stools		11	12	6	4	2
3) Urines	-	-	-	-	-	-
4) Lacrimation	0	0	0	0	0	0
5) Salivation	0	0	0	0	0	0
6) Rhinorrhea	0	0	0	0	0	0
7) Temperature	/	/	/	/	/	/


**Appendix B: PUBLISHED PAPER**

RESEARCH

Open Access



# Tissue distribution and acute toxicity of silver after single intravenous administration in mice: nano-specific and size-dependent effects

Camilla Recordati<sup>1\*†</sup> , Marcella De Maglie<sup>1,2†</sup>, Silvia Bianchessi<sup>1</sup>, Simona Argentiere<sup>1</sup>, Claudia Cella<sup>1,3</sup>, Silvana Mattiello<sup>2</sup>, Francesco Cubadda<sup>4</sup>, Federica Aureli<sup>4</sup>, Marilena D'Amato<sup>4</sup>, Andrea Raggi<sup>4</sup>, Cristina Lenardi<sup>1,3,5</sup>, Paolo Milani<sup>1,3,5</sup> and Eugenio Scanziani<sup>1,2</sup>

## Abstract

**Background:** Silver nanoparticles (AgNPs) are an important class of nanomaterials used as antimicrobial agents for a wide range of medical and industrial applications. However toxicity of AgNPs and impact of their physicochemical characteristics in *in vivo* models still need to be comprehensively characterized. The aim of this study was to investigate the effect of size and coating on tissue distribution and toxicity of AgNPs after intravenous administration in mice, and compare the results with those obtained after silver acetate administration.

**Methods:** Male CD-1(ICR) mice were intravenously injected with AgNPs of different sizes (10 nm, 40 nm, 100 nm), citrate- or polyvinylpyrrolidone-coated, at a single dose of 10 mg/kg bw. An equivalent dose of silver ions was administered as silver acetate. Mice were euthanized 24 h after the treatment, and silver quantification by ICP-MS and histopathology were performed on spleen, liver, lungs, kidneys, brain, and blood.

**Results:** For all particle sizes, regardless of their coating, the highest silver concentrations were found in the spleen and liver, followed by lung, kidney, and brain. Silver concentrations were significantly higher in the spleen, lung, kidney, brain, and blood of mice treated with 10 nm AgNPs than those treated with larger particles. Relevant toxic effects (midzonal hepatocellular necrosis, gall bladder hemorrhage) were found in mice treated with 10 nm AgNPs, while in mice treated with 40 nm and 100 nm AgNPs lesions were milder or negligible, respectively. In mice treated with silver acetate, silver concentrations were significantly lower in the spleen and lung, and higher in the kidney than in mice treated with 10 nm AgNPs, and a different target organ of toxicity was identified (kidney).

**Conclusions:** Administration of the smallest (10 nm) nanoparticles resulted in enhanced silver tissue distribution and overt hepatobiliary toxicity compared to larger ones (40 and 100 nm), while coating had no relevant impact. Distinct patterns of tissue distribution and toxicity were observed after silver acetate administration. It is concluded that if AgNPs become systemically available, they behave differently from ionic silver, exerting distinct and size-dependent effects, strictly related to the nanoparticulate form.

**Keywords:** Silver nanoparticles, Silver acetate, Dissolution, *In vivo* study, Mouse, Intravenous route, Tissue distribution, Toxicity, Hepatocellular necrosis, Hemorrhage

\* Correspondence: camilla.recordati@gmail.com

†Equal contributors

<sup>1</sup>Fondazione Filarete, 20139 Milan, Italy

Full list of author information is available at the end of the article



## Background

Silver nanoparticles (AgNPs) are an important class of nanomaterials characterized by sizes ranging approximately from 1 to 100 nm: these small dimensions result in a high surface area to volume ratio determining unique chemical, physical and biological properties different from those of bulk material with the same composition [1]. Nowadays, AgNPs are the most common nanomaterial found in consumer products (including cosmetics, textiles, food boxes, sprays), appliances (refrigerators, washing machines) and medical applications (wound dressings, medical devices, drug-delivery systems, bio-sensing and imaging methods) [2–5]. The widespread application of AgNPs is mainly related to the renowned antimicrobial activity of silver, whether ionic or nanoparticulate [6, 7]. However, extensive use of AgNPs may lead to environmental contamination and human exposure by inhalation, dermal and oral routes, raising concerns about their potential environmental impact and toxicity [4].

The majority of toxicity studies on AgNPs have been performed on bacteria, cell lines, and non-mammalian animal species, with still comparatively limited information available from *in vivo* studies [1, 8]. *In vitro* studies revealed distinct (but not necessarily mutually exclusive) mechanisms of toxicity of AgNPs, including 1) ROS generation, with subsequent oxidative stress; 2) interaction with cellular proteins and enzymes by binding to free thiol groups; and 3) mimicry of endogenous ions (e.g. calcium, sodium, or potassium) leading to ionoregulatory disturbances [1]. These mechanisms lead to cytokine production, cellular damage, and eventually apoptosis or necrosis. Numerous *in vitro* studies have demonstrated that the cytotoxic and genotoxic effects of AgNPs are size- and dose-dependent, as well as coating- and cell type-dependent [9–14].

*In vivo* studies in rodents (rats, mice, guinea pigs) and occasionally in non-rodents species (pigs) have been carried out, using different routes of exposure, in the attempt to characterize kinetics, tissue distribution and toxicity of AgNPs [15–26]. Compared to the general consensus of *in vitro* studies, the results of the *in vivo* studies are controversial regarding the onset of adverse effects after AgNPs administration. Some of these studies indicate that AgNPs may have toxic effects on liver, lung, intestine, nervous and immune systems, either after single or repeated administration, and following different routes of exposure [15–17, 22, 23, 26]. However, other studies found no relevant adverse effects [19–21, 24]. These contradictory results may depend on the high variability of the tested AgNPs, in terms of source (generated in the laboratory or commercially available materials), size, dispersion state, coating, and concentration (i.e. number of particles and silver mass). Also, the animal species, strain, sex, age, and the overall experimental design (dose, exposure time, end points for

sampling) may have an impact on the outcome of the study [21].

With the effort to standardize and compare *in vivo* experiments, as well as to properly correlate nanoparticles' properties with their *in vivo* effects, a prior and rigorous physicochemical characterization of AgNPs is required [27]. In particular, the assessment of size, monodispersity, and aggregation is fundamental for a comprehensive understanding of their biological effects. However such measurements, albeit fundamental, are not sufficient for fully predicting nanotoxicological effects, likely because of effects related to the still poorly understood behavior of nanoparticles in the biological milieu. Indeed, AgNPs after injection readily interact with blood components (proteins, lipids, etc.), forming on their surface a biomolecular corona that influences the biological interactions of nanoparticles and cellular uptake [28]. *In vivo* toxicological studies are thus considered critical for correlating the physicochemical properties of nanoparticles with their effects in living systems [29]. However, only very few *in vivo* studies have been performed so far to evaluate the role of size and coating of AgNPs, and based on these studies tissue distribution and toxicity appeared to be consistently size-dependent, whereas the effect of coating was less obvious and only observed in the lung [21, 30–33]. In addition to influencing the formation of the biomolecular corona, size and coating are critical factors affecting the release of silver ions from AgNPs. There has been much debate in the literature regarding whether the adverse effects caused by AgNPs are mediated by the release of silver ions [34]. Although it is generally accepted that dissolution of AgNPs does account for at least a degree of toxicity observed under AgNP exposure, it appears that effects cannot be fully attributed to the measured dissolved fraction of silver especially for the smaller particles ( $\leq 10$  nm), which proved to be more toxic than predicted on the basis of silver ion release [35, 36].

In view of the need to improve the understanding of the impact of physicochemical characteristics of AgNPs in *in vivo* models, the aim of this study was to investigate the effect of the size and coating on tissue distribution and toxicity of AgNPs and compare the results with those obtained after administration of silver ions, in the form of silver acetate. Since this study was not intended to mimic human exposure scenarios, to avoid limited systemic exposure due to the cellular barriers present in the skin, gastrointestinal tract and lungs, we used intravenous (IV) administration of AgNPs and ionic silver to evaluate their potential systemic toxicity. The study design included a thorough characterization of AgNPs suspensions before use, assessment of tissue distribution by measuring silver concentrations in blood and main organs, and histopathological examination to evaluate the presence of adverse effects and silver localization.

## Results and discussion

### Physicochemical characterization of silver nanoparticles

Commercial AgNPs with a nominal size of 10, 40 and 100 nm were tested in this study. Citrate (CT)- and polyvinylpyrrolidone (PVP)-coated AgNPs were investigated to probe the effect of surface stabilizing agents. Details provided by the manufacturer on the physico-chemical properties of the studied AgNPs are reported in Table 1. The particles were thoroughly characterized before the investigation of their toxicological effects *in vivo* and their accordance to manufacturer's specifications assessed. A rigorous characterization of the test dispersions is prerequisite to produce data that can help provide scientific answers to regulatory issues, which are impelling for a widely used nanomaterial type such as AgNPs.

Three different techniques were employed, namely Dynamic Light Scattering (DLS), UV-visible (UV-Vis) spectroscopy, and Transmission Electron Microscopy (TEM). First, the hydrodynamic diameter of the particles and their possible aggregation when suspended in the testing medium were evaluated by DLS. The results are summarized in Table 2. Monomodal distributions were observed for 40 nm and 100 nm AgNPs, coated with both CT and PVP. The 10 nm AgNP-CT and 10 nm AgNP-PVP suspensions showed multimodal distributions. In particular, the peaks at 18.1 and 19.6 nm were indicative of isolated nanoparticles in 10 nm AgNP-CT and 10 nm AgNP-PVP, respectively, while larger peaks in both samples suggested the possible presence of aggregates with variable dimensions. However, these large peaks were still detected by DLS even after filtration (0.22  $\mu\text{m}$  pore size), thus indicating their dynamic nature.

To further investigate the intrinsic features of the putative aggregates detected in 10 nm AgNPs, UV-Vis

spectroscopy measurements were performed. AgNPs exhibit a characteristic absorbance maximum in the visible range due to the surface plasmon resonance (SPR) effect [37]. Notably, optical properties of AgNPs are closely related to their morphology, therefore UV-Vis spectroscopy is able to detect any change in size/shape as well as the presence of aggregates. The UV-Vis results are shown in Table 2. The correspondence between the optical properties given by the manufacturer and those measured in our laboratory appeared satisfactory; in particular, no decrease in the maximum absorbance value ( $H_{\text{max}}$ ) was observed, indicating absence of aggregates. Then, full absorbance spectra of all samples were considered (Fig. 1). The optical density in the 600–800 nm range, which is typical for aggregate absorption, was not detected in 10 nm AgNP-CT and 10 nm AgNP-PVP, further demonstrating that the presence of stable aggregates in these samples could be excluded [38].

Eventually, TEM analysis was performed to assess the shape and primary size distribution of tested AgNPs. All the tested AgNPs were spherical in shape (Fig. 2), and their Feret diameter distributions were in good accordance with data reported by the manufacturer ( $p > 0.05$  in all cases) (Table 2).

According to these analyses, both the 10 nm AgNP-CT and the 10 nm AgNP-PVP gave questionable DLS results, since peaks by far larger than 10 nm were detected. Similar findings were recently reported for AgNPs with size lower than 20 nm and 15 nm [21]. Here, the absorbance spectra clearly confirmed the absence of any stable aggregate, since neither the  $H_{\text{max}}$  decrease nor the absorbance in the 600–800 nm range were visible. TEM analysis further confirmed the absence of aggregates. Therefore, the large peaks detected in the DLS analyses of 10 nm AgNPs were ascribed to

**Table 1** Main physicochemical properties of tested AgNPs provided by the manufacturer and reported in the datasheet

Biopure™ Silver nanoparticle	Lot N°	DLS Mean hydrodynamic diameter (nm)	UV-Vis		TEM		Mass concentration (mg/ml)	Particle concentration (n° of particles/ml)	Solvent	pH of solution
			$\lambda_{\text{max}}$ (nm)	$H_{\text{max}}$ (a.u.)	Diameter (mean $\pm$ SD) (nm)	Variation coefficient (%)				
10 nm AgNP-CT	DAG1542	na	388	164.9	8.8 $\pm$ 1.7	19.6	1.03	3.5*10 <sup>14</sup>	2.0 mM citrate	7.3
10 nm AgNP-PVP	DAG1823A	21.3	389	160.2	9.5 $\pm$ 1.9	7.5	1.1	2.2*10 <sup>14</sup>	MilliQ water	6.9
40 nm AgNP-CT	DAG1176	53.7	411	151.1	40.6 $\pm$ 3.0	7.0	1.12	2.7*10 <sup>12</sup>	2.0 mM citrate	7.6
40 nm AgNP-PVP	DAG1391	49.3	411	148.2	40.7 $\pm$ 4.1	20.2	1.1	2.7*10 <sup>12</sup>	MilliQ water	6.7
100 nm AgNP-CT	DAG1186	99.8	495	49.2	99.4 $\pm$ 7.0	10.0	1.0	1.9*10 <sup>11</sup>	2.0 mM citrate	7.3
100 nm AgNP-PVP	DAG1189	117.0	492	48.2	99.0 $\pm$ 5.7	5.8	1.07	1.9*10 <sup>11</sup>	MilliQ water	5.9

CT sodium citrate, PVP polyvinylpyrrolidone, na not available (not reported in the datasheet)

**Table 2** Physicochemical characterization of tested AgNPs. The main findings in AgNPs characterization are reported for each tested sample. For DLS analyses, the mean size of AgNPs is expressed in terms of hydrodynamic diameter, however this parameter is fully informative only for samples with monomodal distributions. Accordingly, the maximum intensity peaks were also reported to describe more comprehensively samples having multimodal distributions (i.e. 10 nm AgNP-CT and 10 nm AgNP-PVP). The pdl provides a measure of particles uniformity. For UV-Vis analyses, the maximum wavelength ( $\lambda_{\max}$ , i.e. the wavelength corresponding to the highest absorbance of AgNPs) and the maximum absorbance value ( $H_{\max}$ ) are reported. The  $\lambda_{\max}$  and  $H_{\max}$  values were expressed in nanometer (nm) and arbitrary units (a.u.), respectively. Finally, AgNPs size distributions expressed as Feret diameter (mean  $\pm$  SD, nm) and variation coefficient (%) were obtained from TEM analysis

Biopure™ Silver nanoparticle	Lot N°	DLS			UV-Vis		TEM	
		Mean hydrodynamic diameter (nm)	Max intensity peaks (nm)	pdl	$\lambda_{\max}$ (nm)	Hmax (a.u.)	Diameter (mean $\pm$ SD, nm)	Variation coefficient (%)
10 nm AgNP-CT	DAG1542	np	18.1– 4046	0.258	392	163.5	8.4 $\pm$ 1.5	25.4
10 nm AgNP-PVP	DAG1823A	np	19.6– 111– 4292	0.343	389	163.6	10.8 $\pm$ 2.6	24.0
40 nm AgNP-CT	DAG1176	40.1	49.8	0.213	412	152.6	39.3 $\pm$ 4.8	12.3
40 nm AgNP-PVP	DAG1391	51.8	67.6	0.251	410	145.7	40.3 $\pm$ 5.6	13.9
100 nm AgNP-CT	DAG1186	87.6	102.9	0.148	490	45.1	107.7 $\pm$ 10.5	9.8
100 nm AgNP-PVP	DAG1189	104.1	119.4	0.124	491	46.8	105.5 $\pm$ 10.9	10.4

np not provided for samples with multimodal distributions

dynamic aggregates, which are unstable and do not represent a problem for *in vivo* experiments. In conclusion, the characterization by DLS, UV-Vis spectroscopy, and TEM of stock AgNPs suspensions confirmed the particle size certified by the manufacturer and their suitability for *in vivo* administration.

#### Dissolution of silver nanoparticles in mouse serum

The presence of ionic silver in the stock suspensions of CT-coated AgNPs as well as AgNPs dissolution upon

interaction with mouse serum was investigated by filtration on membranes with a pore size allowing discrimination of ionic silver from AgNPs. The percentage of ionic silver in the original stock suspensions was found to be negligible (0.002 %, 0.001 %, 0.001 % of total silver for 10, 40 and 100 nm AgNPs, respectively). Time-dependent dissolution of AgNPs in simulated biological conditions is shown in Table 3. As expected, dissolution was greater for smaller particles and increased with time; however even for 10 nm-sized particles at 24 h, the

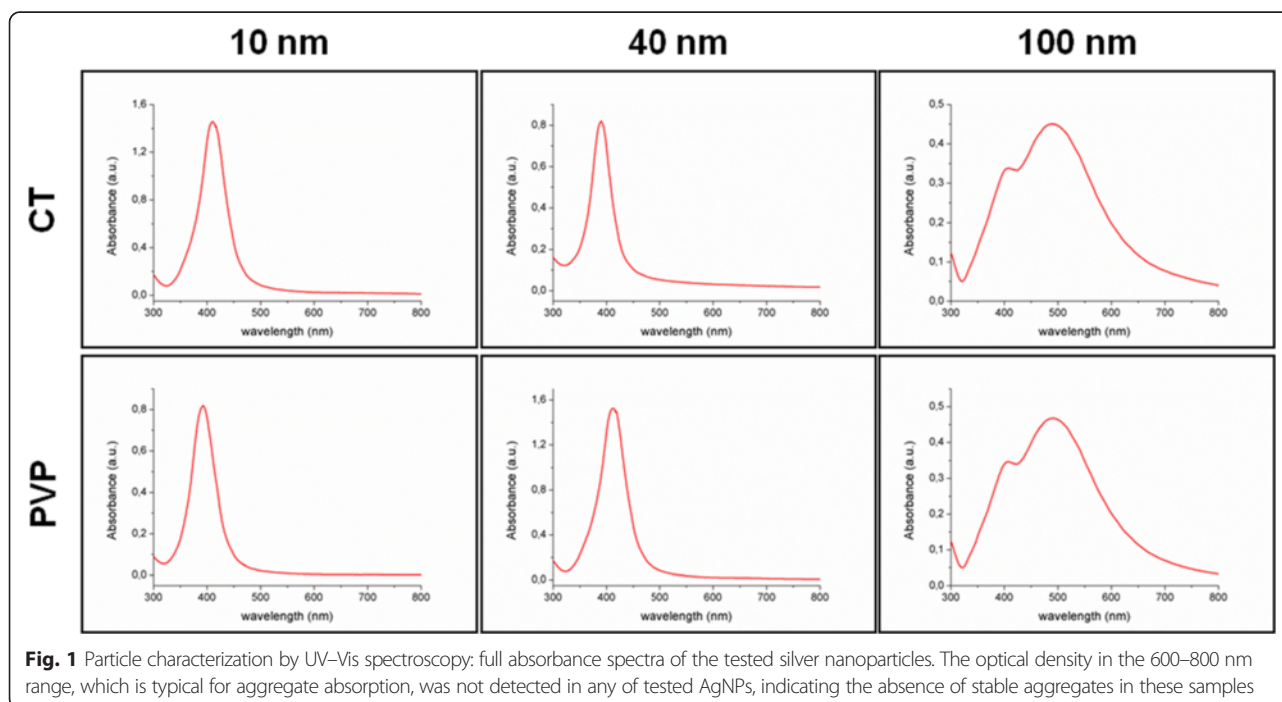
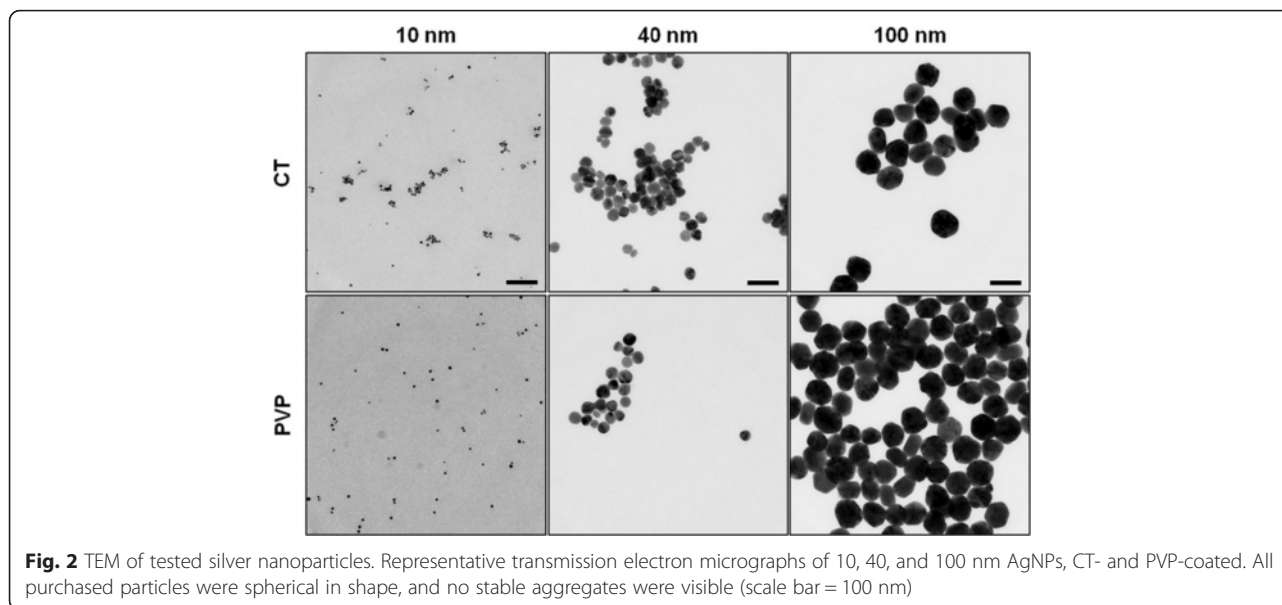


**Fig. 1** Particle characterization by UV-Vis spectroscopy: full absorbance spectra of the tested silver nanoparticles. The optical density in the 600–800 nm range, which is typical for aggregate absorption, was not detected in any of tested AgNPs, indicating the absence of stable aggregates in these samples



percentage of ionic silver was found to be exceedingly low (0.005 %).

The low dissolution of AgNPs when incubated in mouse serum is in accordance with other studies, which put forward that following introduction into a physiological environment the ability of AgNPs to release  $\text{Ag}^+$  is likely inhibited due to the formation of the protein corona [39]. Interaction of protein thiol groups with the charged surface of AgNPs in a medium with a high ionic strength is at the basis of the sulfidation process that leads to an extensive decrease of the dissolution rate *in vitro*, causing also the formation of nanobridges between particles, and has the potential to stabilize them *in vivo* [40]. Formation of the protein corona decreases the extracellular dissolution of AgNPs leading to cellular uptake of particles, which may lose the corona after internalization resulting in an exacerbated release of Ag ions and toxicity [39].

Dissolved silver ions are likely to immediately react with chlorine in serum to form  $\text{AgCl}$  [41]. On the other hand, it cannot be ruled out that a minor part of the released silver ions might have been complexed with high affinity S-containing proteins and thus been

excluded by the membrane used, leading to a possible underestimation of the level of released  $\text{Ag}^+$  [42]. However, even though the method used for studying particle dissolution may have not provided an entirely accurate measure of ionic silver formation in physiological conditions – all available methods have some limitations in this respect [43] – it clearly shows that extracellular dissolution of the AgNPs used in this study is very limited and animals dosed with AgNPs were internally exposed to particulate and not ionic silver.

#### *In vivo* study

Mice were intravenously (IV) injected with CT- or PVP-coated AgNPs of different sizes at a single dose of 10 mg/kg body weight (bw). For comparison, a group was treated with silver acetate (AgAc), used as source of silver ions, at a dose of 15.5 mg/kg bw, containing the equivalent dose of 10 mg Ag/kg bw. The body weight of each mouse was measured before treatment and at sacrifice. Mice were euthanized 24 h after the treatment, and blood and organs were collected for silver quantification and histological examination.

**Table 3** Time dependent dissolution of AgNPs in simulated biological conditions. Results for ionic silver are expressed as percentage of total silver measured in the stock suspensions

Biopure™ Silver nanoparticle	5 min	10 min	60 min	24 h
10 nm AgNP-CT	$0.377 \cdot 10^{-3}$	$0.510 \cdot 10^{-3}$	$0.937 \cdot 10^{-3}$	$5.010 \cdot 10^{-3}$
40 nm AgNP-CT	$0.049 \cdot 10^{-3}$	$0.075 \cdot 10^{-3}$	$0.176 \cdot 10^{-3}$	$1.235 \cdot 10^{-3}$
100 nm AgNP-CT	$0.005 \cdot 10^{-3}$	$0.016 \cdot 10^{-3}$	$0.038 \cdot 10^{-3}$	$0.366 \cdot 10^{-3}$

In this study, the IV route of administration was selected in order to avoid the variability in absorption from the different exposure sites and identify the potential target organs for distribution and toxicity of particles of different size and coating as well as of ionic silver. Although IV administration is not considered a relevant route of exposure to AgNPs for the consumer, this route of exposure can provide valuable information about the *in vivo* behavior of AgNPs crossing the primary barriers (skin, lung, gastrointestinal tract) and entering blood circulation, or administered for clinical purposes (e.g. intravascular medical devices, wound dressings, imaging, drug delivery) [44–47]. In many studies silver was detected in the main organs after exposure to AgNPs by different routes [15, 16, 21, 25, 48, 49], but only few studies investigated the presence of silver particles in tissues after oral exposure in rats [21, 48]. Loeschner et al. [48] found silver granules by using TEM in the same size range of administered AgNPs in the intestine (basal lamina, macrophages, connective tissue of submucosa), but not in the liver, after oral administration of 14 nm AgNPs and AgAc (9 mg/kg b.w. of silver. Another study [21], by using single particle ICP-MS, revealed the presence of NPs in the examined organs (gastrointestinal tract, liver, spleen, lungs) after oral administration of 15–20 nm AgNPs (90 mg/kg b.w) and AgNO<sub>3</sub> (9 mg/kg). In both studies, nanoparticles were found also in the group treated with Ag<sup>+</sup>, indicating that nanoparticles can be formed *in vivo* from soluble silver. Even though there is still little information on the ability of AgNPs to be absorbed, and distribute systemically after dermal application, inhalation, or ingestion, a definite conclusion about the complete dissolution of AgNPs before reaching the blood circulation or within the blood cannot be drawn as well, leaving open the question about the potential effects of AgNPs in case they enter (even partially) blood circulation.

A dose of 10 mg/kg bw was chosen since it was in the range of doses used in previous IV studies without eliciting relevant adverse effects in animals [22, 23, 30, 31, 50]. A dose of 10 mg/kg bw in mice is equivalent to a human dose of 0.81 mg/kg bw, corresponding to approximately 50 mg for a human of 60 kg, according

to guidelines for dose translation from animals to humans [51].

#### Animal behavior, body and organ weights

Immediately after administration of AgNPs and AgAc and during the following hours, all mice appeared healthy and no abnormal behavior was observed. However, 24 h after the treatment two mice (one mouse treated with 10 nm AgNP-CT and another one treated with 10 nm AgNP-PVP) were found dead. Complications related to the injection procedure or formation of large aggregates after administration were reasonably ruled out given the delayed onset of mortality and results of later histopathological evaluation (i.e. absence of thromboembolic lesions associated with silver aggregates). At sacrifice, no significant differences in body weight gain and organ weights were recorded between CT- and PVP-coated AgNPs of the same size (Additional file 1: Table S1). In mice treated with 10 nm AgNPs a significant difference in percentage of weight loss and relative spleen weight were observed compared to control and 40 and 100 nm AgNP-treated mice (Table 4). No other significant differences were observed in relative organ weights between treated and control mice.

#### Tissue distribution and localization of silver

Distribution and localization of silver in the different organs 24 h after IV exposure to CT- and PVP-coated AgNPs of three different sizes, and AgAc, were evaluated using two distinct but complementary approaches, i.e. inductively coupled plasma mass spectrometer (ICP-MS) and autometallography (AMG) staining. ICP-MS was used to quantitatively measure the total silver concentration in spleen, liver, lung, kidney, brain, and blood, while AMG was used to qualitatively assess silver localization within the sampled organs.

In the control group, silver was present at background levels as shown by ICP-MS data for the examined organs (Additional file 1: Table S2). In the treated animals, at 24 h after administration the silver concentration in blood was drastically reduced in all groups compared to the peak concentrations expected on the basis of the administered dose, in agreement with

**Table 4** Body weight gain and relative organ weight (%) after IV administration of 10 mg silver/kg. Data are expressed as means ± SD

Group	n	Body weight gain	Spleen	Liver	Lung	Kidney	Brain
Control	3	-3.3 ± 5	0.45 ± 0.1	6.61 ± 0.8	0.66 ± 0.0	1.80 ± 0.2	1.77 ± 0.1
10 nm AgNP	6	-12.1 ± 4.1*	0.67 ± 0.0*	7.23 ± 1.1	0.76 ± 0.1	1.75 ± 0.1	1.81 ± 0.2
40 nm AgNP	6	-1.3 ± 2.8 <sup>++</sup>	0.54 ± 0.1 <sup>++</sup>	6.87 ± 0.6	0.65 ± 0.1	1.79 ± 0.3	1.78 ± 0.1
100 nm AgNP	6	-0.1 ± 5.0 <sup>++</sup>	0.40 ± 0.1 <sup>++</sup>	6.97 ± 0.2	0.63 ± 0.1	1.80 ± 0.1	1.65 ± 0.1
AgAc	3	-6.3 ± 3.3	0.47 ± 0.0 <sup>+</sup>	6.99 ± 0.0	0.80 ± 0.1	1.92 ± 0.2	1.78 ± 0.2

\**p* < 0.05 vs Control; + *p* < 0.05 ++*p* < 0.01 vs 10 nm AgNP

previous studies of kinetics performed after one single IV administration of 120 mg/kg of 15 nm AgNPs [22] and 0.8 mg/kg of 20, 80, and 110 nm AgNPs [30]. In the blood of 10 nm AgNPs-treated mice silver was approximately 1.5 times and 3.5 times higher than in mice treated with 40 nm and 100 nm AgNPs, respectively (Additional file 1: Table S2). Since previous studies demonstrated a rapide decline (minutes to few hours) of silver blood levels after IV injection of AgNPs regardless of nanoparticle size [22, 30, 50], the greater silver concentration of 10 nm AgNPs-treated mice 24 h after exposure might indicate an increased and earlier redistribution of silver from organs to blood in the case of 10 nm AgNPs compared to larger ones. The results obtained for 10 nm AgNPs are in agreement with those of a IV study on CT-coated AgNPs having a similar size (8 nm), administered to rats at the same dose of the present study (10 mg/kg bw); after an initial decrease (up to 4 h post injection) blood silver levels increased again and did not decrease during the experimental period until 96 h [50].

For all particle sizes, regardless of their coating, the highest silver concentrations were found in the spleen and liver, followed by lung, kidney and brain (Fig. 3, and Additional file 1: Figure S1). These results are in line with previous studies that investigated tissue distribution of AgNPs 24 h after IV administration [22, 30, 50]. When considering the percentage of the administered silver dose recovered after administration, for all tested AgNPs approximately 40 % of the administered dose was found in the liver, which resulted to be the main target organ of silver distribution, followed by spleen, lung, kidney, and brain (Table 5). Most of the silver that reaches the blood is filtered by the liver and excreted into the bile [50], while the remaining circulating particles distributed to organs

containing large numbers of phagocytic cells, such as liver, spleen, and lung, which are devoted to clearing foreign body particles from the circulating blood. The role of macrophages in general, and Kupffer cells in particular, in clearance and accumulation of nanoparticles was the same observed after intravenous administration of other metallic nanoparticles (e.g. gold NPs) [52, 53].

With exception of the liver, where similar silver concentrations were identified regardless of the source of administered silver (AgNP or silver ions), in the other examined organs silver concentrations were higher in mice treated with 10 nm AgNPs (including both CT- and PVP-coated particles) than in mice treated with larger particles (40 nm, 100 nm), and concentrations decreased with increasing size of AgNPs. Since the silver concentrations found in the brain and kidney were comparable or lower than those found in the blood, silver contribution of residual blood contained in these organs cannot be completely ruled out.

As regards the role of coating on silver tissue distribution, no significant differences were found between CT- and PVP-coated AgNPs of the same size, in line with previous studies [21]. However, Principal Component Analysis (PCA) highlighted a trend of CT-coated 10 nm AgNPs to cluster separately from PVP-coated 10 nm AgNPs (right side of the first Principal Component, PC1) likely due to the higher silver concentrations of the 10 nm AgNP-CT in spleen, lungs, liver, and, to a lesser extent, in kidneys compared to 10 nm AgNP-PVP (Additional file 1: Figure S2). PCA thus revealed that the coating might have a potential effect of on tissue distribution at least for the smallest (10 nm) AgNPs.

Silver localization within organs was evaluated histologically. In H&E stained sections intracytoplasmic

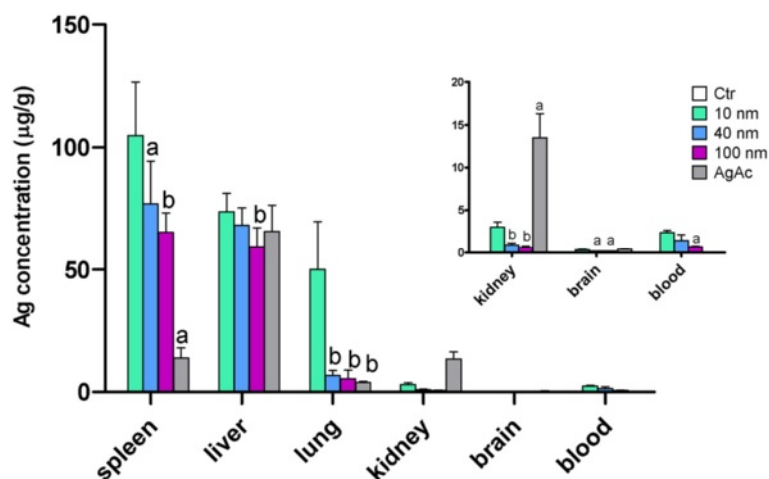


**Fig. 3** Silver tissue concentration after IV administration of AgNPs and AgAc in mice. Data are expressed as means  $\pm$  SD. Statistical significance: a =  $p < 0.05$ ; b =  $p < 0.01$  vs 10 nm



**Table 5** Percentage of recovered silver dose in mice after IV administration of 10 mg silver/kg. Data are expressed as means  $\pm$  SD

Group	n	Spleen	Liver	Lung	Kidney	Brain
10 nm AgNP-CT	3	6.6 $\pm$ 1.2	52.0 $\pm$ 4.7	4.2 $\pm$ 1.1	0.5 $\pm$ 0.1	0.056 $\pm$ 0.015
10 nm AgNP-PVP	3	5.3 $\pm$ 1.0	41.1 $\pm$ 2.3	1.5 $\pm$ 1.2	0.4 $\pm$ 0.1	0.049 $\pm$ 0.016
40 nm AgNP-CT	3	3.6 $\pm$ 1.1	46.1 $\pm$ 2.5	0.5 $\pm$ 0.1	0.1 $\pm$ 0.1	0.037 $\pm$ 0.007
40 nm AgNP-PVP	3	3.1 $\pm$ 1.1	45.5 $\pm$ 1.9	0.3 $\pm$ 0.1	0.2 $\pm$ 0.0	0.035 $\pm$ 0.009
100 nm AgNP-CT	3	2.7 $\pm$ 0.4	36.7 $\pm$ 0.3	0.5 $\pm$ 0.1	0.1 $\pm$ 0.0	0.029 $\pm$ 0.004
100 nm AgNP-PVP	3	2.5 $\pm$ 0.6	45.7 $\pm$ 1.1	0.2 $\pm$ 0.0	0.1 $\pm$ 0.0	0.028 $\pm$ 0.003
AgAc	3	0.6 $\pm$ 0.2	42.6 $\pm$ 4.5	0.3 $\pm$ 0.1	2.4 $\pm$ 0.6	0.064 $\pm$ 0.011

black granular pigment was multifocally (and often barely) visible in the liver (along the sinusoids), spleen (marginal zone and red pulp), and lungs (alveolar septa) of all AgNP-treated mice, but not in AgAc-treated mice (Additional file 1: Figure S3).

The tissue localization of silver was better detailed after AMG staining (Fig. 4), which enhances the silver present within the tissues, providing a rapid, cost-effective histochemical means of detecting the distribution of silver within organs [54]. In AgNP-treated mice,

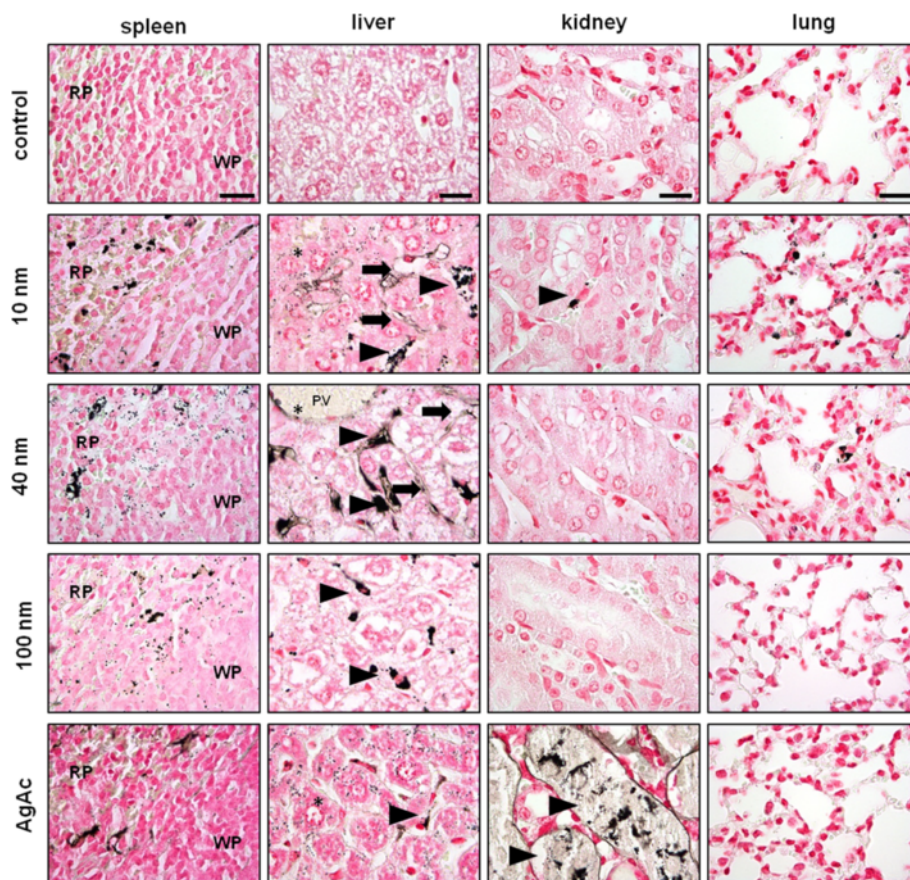


**Fig. 4** Histological evaluation of silver tissue localization by AMG. Representative images of spleen, liver, kidney, and lung (scale bar = 20  $\mu$ m), from vehicle- (control), AgNP (10 nm, 40 nm, 100 nm), and AgAc-treated mice. In the spleen, silver was localized within the cytoplasm of macrophages in the marginal zone of the white pulp (WP) and in the red pulp (RP). In the liver, the cellular localization of silver varied depending on the size of the AgNPs. In 10 nm AgNP-treated mice, silver was present in the cytoplasm of Kupffer cells (arrowhead), sinusoidal endothelial cells (arrow) and hepatocytes (\*). In 40 nm AgNPs-treated mice, silver was localized in the cytoplasm of portal endothelial cells (\*), sinusoidal endothelial cells (arrow) and Kupffer cells (arrowhead). In 100 nm AgNPs-treated mice, most of silver was concentrated in the cytoplasm of Kupffer cells (arrowhead). In AgAc-treated mice, silver was present in the cytoplasm of hepatocytes (\*), and Kupffer cells (arrowhead). In the kidney, occasional silver-containing cells were observed in the renal interstitium of 10 nm AgNP treated-mice (arrowhead), and large amounts of silver were identified in necrotic tubules of AgAc-treated mice (arrowhead). In the lung, scattered silver-containing cells were found in the alveolar septa of 10 nm and 40 nm AgNP-treated mice

regardless of the particle size and coating, the organs showing the greatest silver accumulation were the spleen and liver in agreement with the results of total silver quantification obtained by ICP-MS. Occasionally, enhanced silver clusters were found in the lung and occasionally in the kidney (mainly in 10 nm AgNPs-treated mice), and none in the brain. In the spleen, silver was localized within the cytoplasm of macrophages in the marginal zone of the white pulp and in the red pulp, and occasionally within splenic endothelial cells. In the liver most of the silver was found in the cytoplasm of Kupffer cells along the sinusoids, and occasionally within sinusoidal and portal endothelial cells, and more rarely within hepatocytes, in accordance with previous studies [23, 31, 55]. A sort of size-dependent pattern of silver distribution in the liver was observed, suggesting that silver uptake by Kupffer cells is almost exclusive after administration of 100 nm AgNPs, while administration of 10 nm and 40 nm AgNPs resulted in silver uptake also by endothelial cells, and hepatocytes, in addition to Kupffer cells. Only occasionally, the silver was identified in the gall bladder of 10 nm AgNP-treated mice (within gall bladder epithelial cells and endothelial cells of blood vessels). In the lung, scattered silver containing cells were found in the alveolar septa, either within the capillaries or the interstitium. In the kidney, only in mice treated with 10 nm AgNPs there were occasional silver-containing cells in the glomerular tufts, and renal interstitium, morphologically consistent with circulating leukocytes (monocytes) that were also occasionally observed in the other examined organs. No enhanced silver clusters were identified in the brain sections of treated mice. This lack of histological identification of silver in the brain is consistent with the very small concentrations of silver detected in this organ by ICP-MS.

In mice treated with AgAc silver concentrations determined by ICP-MS were similar in the liver and brain, but significantly lower in the spleen and lung, and higher in the kidney compared to mice treated with 10 nm AgNPs (Fig. 3). Differently from AgNP-treated mice, no black granular deposits (reminiscent of silver) were found throughout the examined tissues stained with H&E. In AMG stained sections, silver enhanced clusters were identified in the liver (within Kupffer cells and hepatocytes), spleen (marginal zone and red pulp), and kidney (at level of degenerated/necrotic tubules) (Fig. 4). No silver was identified in the lung and brain. Organs from AgAc-treated mice showed higher values than those from the control and AgNP-treated mice on PC2, due to the higher silver concentration in the kidney (Additional file 1: Figure S2). Overall these results suggest that silver ions have a different biodistribution pattern, and likely also of cell uptake, and excretion (i.e. enhanced role of renal excretion in addition to biliary

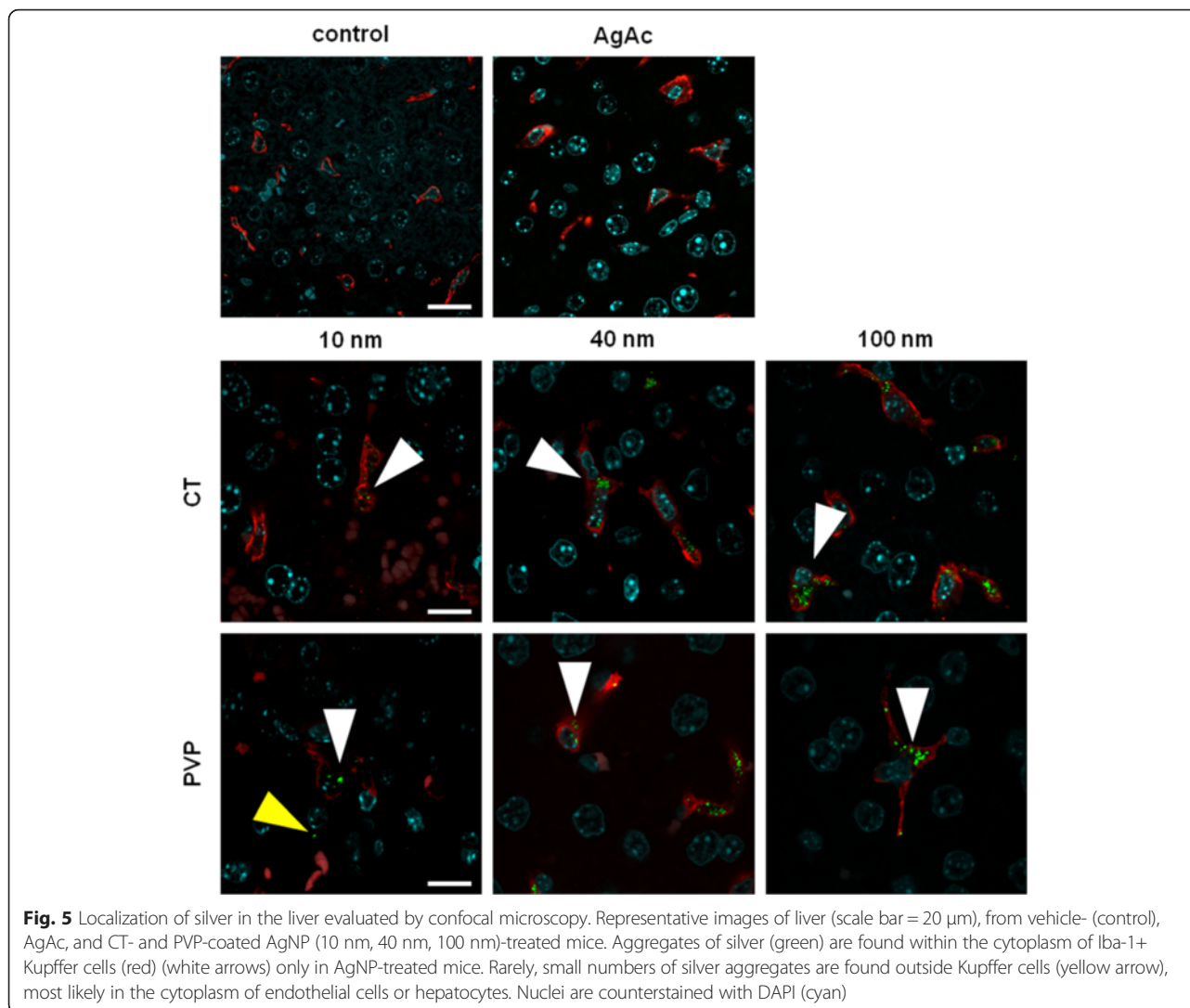
excretion) compared to nanoparticles. This difference in kinetics was reflected also by the identification of distinct target organ of toxicity for silver ions and AgNPs, as discussed below.

Immunostaining of sections with IBA1 (a pan-macrophage marker) further confirmed that most of silver-containing aggregates were present within the cytoplasm of Kupffer cells in the liver, in all AgNP-treated groups (Fig. 5). The amount and size of silver-containing aggregates within macrophages decreased with decreasing size of AgNPs. In 10 nm AgNPs-treated mice only scattered and very small aggregates were found throughout the liver, while no visible silver-containing aggregates were found in the liver of AgAc treated mice, despite the identification of silver by AMG staining within Kupffer cells and hepatocytes. This result may suggest a different intracellular behavior of silver depending on its form and size.

Since ICP-MS does not provide information about the soluble or particulate form of silver detected within the tissue, it is not possible to know whether the silver-containing aggregates identified histologically in this study were composed of silver nanoparticles or silver salts formed upon interaction of silver ions with sulphur and selenium, as previously described in the intestine of rats following oral administration of AgNPs and AgAc [48], or in the skin of patients with argyria [56, 57]. Additional analyses, e.g. employing TEM with energy dispersive x-ray spectroscopy (EDX), and Single Particle ICP-MS (not for the 10 nm AgNPs, which are below the size detection limit of the technique) should be taken into consideration in future studies, to assess the composition and subcellular localization of silver within tissues, allowing to better understand the intracellular fate of AgNPs and/or silver ions.

### Toxicity

Two mice out of six were found dead 24 h after treatment with 10 nm AgNPs. No relevant gross changes were observed in the examined mice, except for a moderate splenomegaly in mice treated with 10 nm AgNPs. Histological AgNP-related lesions were observed in the spleen, liver, and gall bladder of AgNP-treated mice (Fig. 6). No relevant differences were found between CT- and PVP-coated particles of the same size. Overall the prevalence and severity of lesions (in particular those involving liver and gall bladder) were size-dependent, with mice treated with 10 nm AgNPs most frequently and severely affected compared to 40 nm and 100 nm AgNP-treated mice that had milder or negligible lesions, respectively (Tables 6 and 7). Splenic hyperemia was present in all mice treated with AgNPs, but only in mice treated with 10 nm-sized particles it was particularly pronounced, and thus likely responsible for inducing



splenomegaly, as well as the increased relative spleen weight observed in this group. Mice treated with 10 nm AgNPs were affected by diffuse and severe midzonal hepatocellular necrosis and hemorrhage, multifocal peri-biliary microhemorrhages, occasional portal vein endothelial damage (i.e. endothelial sloughing, subendothelial hemorrhages, intraluminal fibrin thrombi) (Additional file 1: Figure S4), and diffuse mural and intraluminal hemorrhage of the gall bladder. Among mice treated with 40 nm AgNPs only one out of six had early periportal coagulative necrosis, scattered hepatic single cell necrosis, and gall bladder severe mural and intraluminal hemorrhage. In the other mice treated with 40 nm AgNPs, the hepatic lesions were not observed and gall bladder lesions were milder, usually consistent with mural hyperemia and/or edema. Mice treated with 100 nm AgNPs had only occasional and mild gall bladder mural hyperemia and/or edema. No relevant

pathological changes were observed in the lung, kidney and brain of AgNP-treated mice, and in all the examined organs of control mice.

A completely different pathological scenario was observed after administration of AgAc. Hepatobiliary lesions were not observed, whereas a marked acute renal tubular necrosis and apoptosis with intraluminal accumulation of hyaline casts was found in all treated mice. Presence of renal lesions, associated with identification of silver in the affected renal tubules and relevant silver concentrations in the kidney of AgAc-treated mice indicates that dissolved silver ions resulted in an increased renal silver distribution compared to AgNPs, and that renal lesions were likely secondary to the renal excretion of silver.

Although liver is considered one of the most important target organs for AgNPs, given its capacity of AgNP accumulation and its role in biliary excretion of AgNPs [49], so

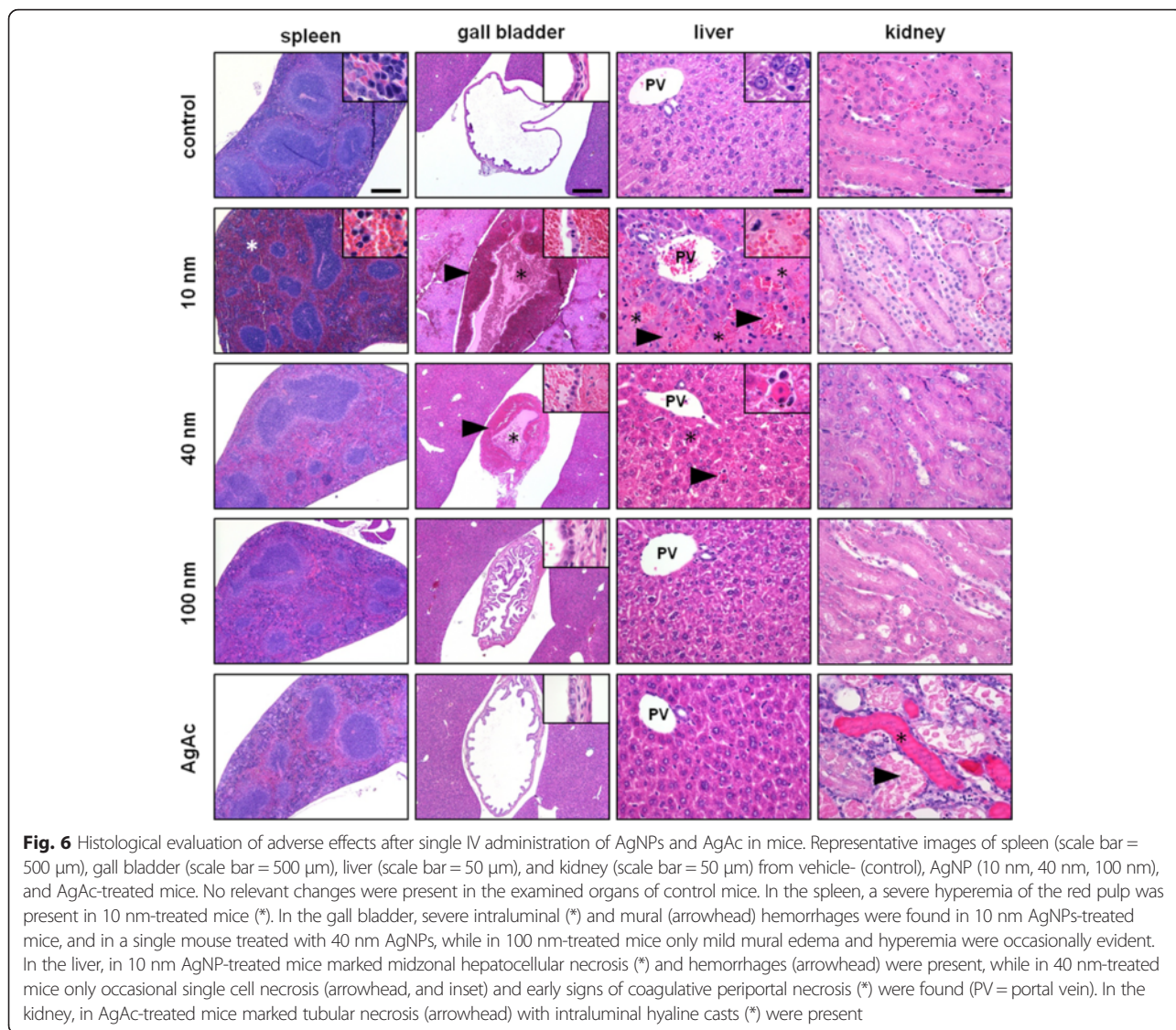


**Table 6** Prevalence of histopathological lesions in mice following IV exposure to 10 mg silver/kg. Data are expressed as number of mice with lesions/total number of examined mice per group (%)

Group	Spleen	Liver	Gall bladder	Lung	Kidney	Brain
Control	1/3 (33 %)	0/3 (0 %)	0/3 (0 %)	0/3 (0 %)	0/3 (0 %)	0/3 (0 %)
10 nm AgNP-CT	3/3 (100 %)	3/3 (100 %)	3/3 (100 %)	0/3 (0 %)	0/3 (0 %)	0/3 (0 %)
10 nm AgNP-PVP	3/3 (100 %)	3/3 (100 %)	3/3 (100 %)	0/3 (0 %)	0/3 (0 %)	0/3 (0 %)
40 nm AgNP-CT	3/3 (100 %)	1/3 (33 %)	2/3 (67 %)	0/3 (0 %)	0/3 (0 %)	0/3 (0 %)
40 nm AgNP-PVP	2/3 (67 %)	0/3 (0 %)	1/3 (33 %)	0/3 (0 %)	0/3 (0 %)	0/3 (0 %)
100 nm AgNP-CT	1/3 (33 %)	0/3 (0 %)	2/3 (67 %)	0/3 (0 %)	0/3 (0 %)	0/3 (0 %)
100 nm AgNP-PVP	1/3 (33 %)	0/3 (0 %)	0/3 (0 %)	0/3 (0 %)	0/3 (0 %)	0/3 (0 %)
AgAc	0/3 (0 %)	0/3 (0 %)	0/3 (0 %)	0/3 (0 %)	3/3 (100 %)	0/3 (0 %)

**Table 7** Grading of most relevant histopathological lesions in mice after IV administration of 10 mg silver/kg. Results are expressed as median score per group (range) ( $n = 3$ )

Group	Hepatobiliary tract				Spleen	Kidney
	Hepatocellular necrosis and hemorrhage	Peribiliary hemorrhage	Portal vein endothelial damage	Gall bladder hemorrhage	Red pulp hyperemia	Tubular necrosis
Control	0 (0–0)	0 (0–0)	0 (0–0)	0 (0–0)	1 (0–2)	0 (0–0)
10 nm AgNP-CT	4 (3–4)	2 (1–4)	1 (0–4)	2 (2–4)	2 (2–3)	0 (0–0)
10 nm AgNP-PVP	4 (2–4)	2 (1–4)	2 (0–4)	2 (1–4)	3 (3–4)	0 (0–0)
40 nm AgNP-CT	0 (0–1)	0 (0–1)	0 (0–0)	1 (1–4)	2 (2–3)	0 (0–0)
40 nm AgNP-PVP	0 (0–0)	0 (0–0)	0 (0–0)	0 (0–1)	2 (1–2)	0 (0–0)
100 nm AgNP-CT	0 (0–0)	0 (0–0)	0 (0–0)	1 (0–1)	0 (0–1)	0 (0–0)
100 nm AgNP-PVP	0 (0–0)	0 (0–0)	0 (0–0)	0 (0–0)	1 (0–2)	0 (0–0)
AgAc	0 (0–0)	0 (0–0)	0 (0–0)	0 (0–0)	0 (0–0)	4 (3–4)

far hepatotoxic effects of AgNPs have been inconstantly demonstrated in *in vivo* studies, either after IV, oral, or inhalation exposure to AgNPs. In particular, hepatotoxicity was generally recognized through changes in the blood biochemical parameters of liver function (such as ALT, AST, ALP, and cholesterol) [16, 17, 23, 58], while only occasionally mild histopathological changes were reported, such as biliary hyperplasia, fibrosis, hepatocellular vacuolar degeneration, and rarely necrosis [15, 16, 22]. The lack of overt hepatic histopathological lesions in previous studies that used small-sized particles could be related to a poor dispersion of AgNPs in the administered suspensions [22], since agglomeration of particles can affect bioavailability by reducing the rate of degradation or cell uptake [8]. According to our characterization of AgNPs, we administered well-dispersed 10 nm-sized particles. Another aspect is that most of earlier *in vivo* studies of distribution and toxicity of AgNPs have been performed in rats and not in mice. Further investigation should be performed in order to assess whether there is a different sensitivity between these two species.

In addition to the severity of the hepatic lesions found in mice treated with 10 nm AgNPs, also the pattern of hepatocellular necrosis observed is very unusual. Midzonal necrosis is the least common histologic pattern of hepatocellular necrosis following exposure to hepatotoxicants [59]. Because hepatocytes are extremely variable in their metabolic capacity and oxygen tension, midzonal necrosis of hepatocytes is presumably dictated by a unique susceptibility of these hepatocytes based on their location within the hepatic lobule [60]. The hemorrhage observed in the gall bladder of mice treated with 10 nm AgNPs and occasionally in mice treated with 40 nm AgNPs is another very unusual finding. We can speculate that gall bladder

mural hemorrhage, as well as portal peribiliary hemorrhages, could be the result of endothelial damage secondary to a massive elimination of AgNPs in the bile, which is considered the main route of silver excretion following IV administration of AgNPs [31, 50]. The hypothesis of particle-induced endothelial damage is further corroborated by the presence of endothelial damage found in the intrahepatic branches of portal veins that may have occurred after intestinal re-absorption of AgNPs excreted in the bile. Another concurrent factor in the pathogenesis of gall bladder hemorrhage could be the anti-platelet properties of AgNPs that may have impaired a prompt clotting response [61].

In this study relevant size-dependent adverse effects were observed 24 h after IV administration of AgNPs in mice. First of all, and differently from previous studies where AgNPs were administered IV (up to a dose of 120 mg/kg bw) [22, 23, 30, 31, 50], mortality was observed in 2 out of 6 mice treated with the smallest particles (10 nm AgNPs), regardless of the coating. The most striking finding was the marked hepatotoxicity demonstrated by 10 nm AgNPs (both CT and PVP-coated), associated with a massive hemorrhage of the gall bladder. These lesions (in particular the hemorrhage) were especially severe in the two mice found dead, and can thus be regarded as the most likely cause of death. Of note, administration of AgNPs of different sizes and silver acetate resulted in similar liver content of total silver (as determined by ICP-MS), indicating that hepatobiliary toxicity induced by 10 nm AgNPs was not related to the mass of silver contained in the liver, but rather it was imputable to their small size. Size-dependent toxicity of AgNP was previously demonstrated in *in vitro* [11, 13, 14, 36], as well as in *in vivo* studies using the respiratory route of

administration [32, 33]. Our results further support the importance of nanoparticle size for AgNP toxicity *in vivo*. Release of silver ions following oxidation of particle surface after administration of AgNPs is believed to constitute the major mechanism contributing to AgNP toxicity and since dissolution increases with decreasing size of AgNPs [33], this appears to be the determinant of the enhanced toxicity of smaller AgNPs compared to larger ones. The most obvious explanation for increased dissolution of smaller particles, compared to an equivalent mass concentrations of larger particles, is their higher number (in this study, the number of administered 10 nm AgNPs was about 100 fold greater compared to 40 nm AgNPs) and consequent larger surface area per unit mass. The results of our study however demonstrated that systemic availability of silver ions is not responsible for the *in vivo* hepatobiliary toxicity observed in mice treated with 10 nm AgNPs, because dissolution of 10 nm AgNPs in mouse serum was very low (0.005 %) and administration of AgAc resulted in a distinct target organ of toxicity (kidney instead of hepatobiliary system). Cell-type-dependent toxicity of silver ions and AgNPs was previously demonstrated in *in vitro* studies. Furthermore, recent *in vitro* studies demonstrated that toxicity of AgNPs rather than being caused by silver ions liberated in the culture medium is actually dependent on their intracellular release [35, 62, 63]. According to the recently proposed general mechanism for toxicity of metal-containing nanoparticles, the so-called “Lysosome-Enhanced Trojan Horse effect”, toxicity of these particles occurs after cellular uptake by endocytosis and it is mediated by enhanced intracellular release of ions secondary to the acidic corrosion within lysosomes [62]. Increased toxicity of smaller AgNPs is then explained by their increased number and reactive surface area, resulting in increased intracellular release of silver ions. The fact that the entry of AgNPs into cells is size-dependent contribute to further enhance the toxic potential of small particles, owing to their higher bioavailability to cells [11, 13, 14, 35].

In our study, coating of AgNPs with CT and PVP did not have a detectable effect on toxicity indicating that particle size is more important than coating to predict potential adverse effects of silver nanoparticles, at least for the coatings tested herein. Coating-dependent toxic effects were demonstrated *in vitro* [9, 10], and only in the lungs *in vivo* [32, 33]. It can be speculated that in *in vivo* studies, including ours, coating has a minor effect, if any, as a consequence of the formation of a corona after the adsorption of proteins (and other biomolecules) on the surface of particles once they enter in contact with biological fluids [28]. The protein corona might mask the effect of the different particle coatings that is evident in *in vitro* studies. This is in agreement with the

recent view that to predict the biological behavior of nanoparticles the fingerprinting of the protein corona is more accurate than the sole characterization of their physicochemical properties, since the protein corona confers to nanoparticles a ‘biological identity’ that is strongly dependent but distinct from its ‘synthetic identity’ [64, 65].

## Conclusions

With this study, the influence of two distinct nanoparticle properties, size and coating, was comprehensively investigated in an *in vivo* model. We observed that tissue distribution and toxic effects of AgNPs in mice after IV administration are strongly size-dependent, while coating (CT or PVP) did not have a sizeable impact on tissue distribution and toxicity. Overall, the smallest (10 nm) particles resulted in higher silver tissue distribution and caused overt acute adverse effects (centered on the hepatobiliary tract) compared to the larger ones (40 and 100 nm). Overall, these results suggest that in the safety assessment of silver particles the effect of size has to be carefully considered, with a focus on small particles ( $\leq 10$  nm). Comparison with AgAc revealed a distinct pattern of tissue distribution and toxicity between AgNP and silver ions, indicating that the *in vivo* effects of AgNPs are not attributable merely to the *in vivo* release of silver ions in circulating blood but are strictly related to the nanoparticulate form.

## Methods

### Characterization of silver nanoparticles

Suspensions of BioPure™ Silver Nanoparticles (AgNPs) of 10, 40 and 100 nm in size, coated with either citrate (CT) or polyvinylpyrrolidone (PVP), were purchased from NanoComposix (San Diego, USA). All the suspensions were supplied at a concentration of about 1.0 mg/ml. BioPure™ AgNPs were chosen because they were guaranteed to be sterile and with an endotoxin level lower or equal to 2.5 EU/ml. The suspending solvents of CT- and PVP-coated AgNPs were 2.0 mM sodium citrate and Milli-Q water (Millipore), respectively. For particle characterization, the CT and PVP-coated AgNPs were diluted with 2.0 mM sodium citrate (cod. W302600, Sigma-Aldrich) buffer and Milli-Q water, respectively. When necessary, samples were sonicated (Elmasonic S 30 H) for up to 30 s, in accordance with the manufacturer’s instructions. In order to prevent contamination, measurements were run using disposable plastic cuvettes. The AgNPs were tested immediately after their delivery and *in vivo* experiments were run in the following week. In the meanwhile, the AgNPs were stored at +4 °C, according to manufacturer’s instructions.

### **Dynamic Light Scattering (DLS)**

The actual size of AgNPs in dispersion was measured by DLS. Measurements were performed with a Malvern Zetasizer Nano ZS90 instrument operating with a light source wavelength of 532 nm and a fixed scattering angle of 90°. All the nanoparticles were diluted 1:100 with the exception of 10 nm-sized AgNPs. Indeed, due to their small size, the 10 nm AgNPs presented increased absorption and lower scattering intensity compared to 40 nm and 100 nm AgNPs. Accordingly, the 10 nm AgNPs were diluted 1:50. All measurements were run at room temperature for at least three times.

### **UV-Visible (UV-Vis) Spectrophotometry**

The UV-Vis spectra were acquired in the 300–800 nm range using a DU730 Beckman Coulter Spectrophotometer. All the nanoparticles were diluted 1:100 with the exception of 10 nm AgNPs, which were diluted 1:200 because of their increased UV-Vis absorbance with respect to larger nanoparticles. All measurements were run at room temperature for at least three times.

### **Transmission Electron Microscopy (TEM)**

Formvar coated copper TEM grids (cod. PE1GC300, Pelco) were pre-treated with 20 µl of poly-L-lysine 0.01 % (w/v) (Sigma Aldrich) for 15 min. After washing twice with MilliQ water, 3 µl of AgNPs suspensions were deposited onto the grid for 5 min and then rinsed with 3 µl of 2-propanol (Sigma Aldrich). According to the manufacturer's advice, 100 and 40 nm AgNPs were used at the concentration of 1.0 mg/ml, while 10 nm AgNPs were diluted up to 0.1 mg/ml before use. The grids were allowed to dry overnight at room temperature in a covered crystallizing dish. TEM (FEI Tecnai G2, Eindhoven) images were analyzed with the ImageJ software (<http://imagej.nih.gov/ij/>) to obtain the nanoparticles dimensional distribution. In particular, small objects due to background and overlapping nanoparticles were omitted by using proper cut-off filters and Feret diameter (intended as the larger diameter of the NP projection) was used to evaluate the size of the particles. For each sample, a minimum of about 250 nanoparticles was considered.

### **Dissolution study**

CT-coated particles were selected for this investigation given the higher stability and lower dissolution generally showed by PVP-coated AgNPs [66, 67]. Dissolution of CT-coated AgNPs of 10, 40 and 100 nm was ascertained by ultrafiltration, using a PES spin filter membrane (Vivaspin 500, 3 kDa MWCO, Sartorius, Göttingen, Germany) and centrifugation at 15000 g for 20 min, followed by quantification of silver in the filtrates. The concentration of ionic silver was measured both in the

AgNPs stock suspensions and in conditions simulating AgNPs interaction with biological fluids. For the latter purpose, each stock suspension was spiked to mouse serum (Euroclone, Milan, Italy) in order to provide the mass concentration of AgNPs of a single dose of 10 mg/kg bw, which approximately corresponded to a 1:5 dilution (v/v) of the original AgNPs suspension. Spiked samples and serum blank were prepared in triplicate and incubated at 37 °C under agitation for 5, 10, 60 min and 24 h. Ionic silver was assessed for each timepoint. For ICP-MS determination of ionic silver, filtrates (prepared in triplicate) were vigorously shaken before further dilution and analysis as described in the section "Determination of silver". In addition to ionic silver, each stock suspension of CT-coated AgNPs was characterized in terms of total silver concentration and the results for ionic silver were expressed as percentages of total silver (AgNPs + Ag<sup>+</sup>). Samples for total silver determinations were prepared in triplicate by dilution with acidified (HNO<sub>3</sub>) water as necessary. In order to establish possible sources of bias from the filtration membrane, procedural blanks were run in parallel and the recovery of ionic silver (10 µg/L) from the filtration unit was assessed. No silver was detected in the procedural blanks and the average recovery of ionic silver was found to be 102.6 ± 3.8 %, showing absence of silver release/adsorption during filtration.

### **Animals**

Male CD-1(ICR) mice of 4–5 weeks were purchased from Charles River (Calco, Italy). They were acclimated to the environment for a week prior to the initiation of the study, with free access to water and a standard pellet diet *ad libitum*. The environmental conditions were set at a temperature of 22 ± 2 °C, relative humidity of 55 ± 10 % and a 12 h light/dark cycle.

### **Experimental design**

Mice were randomly assigned to groups of treatments. The mice were intravenously (IV) injected into the lateral tail vein with AgNPs of different sizes (10 nm, 40 nm, 100 nm), either CT- or PVP-coated, at a single dose of 10 mg/kg body weight (bw), and with AgAc at a single dose of 15.5 mg/kg, corresponding to 10 mg Ag/kg bw (3 mice per group). The AgNPs suspensions were administered to animals without any dilution. The control group was treated with sterile water for injection. Immediately after the treatment and the following hours, the general health and behavior of mice were monitored. The body weight of each mouse was measured before treatment and at sacrifice. Mice were euthanized 24 h after the treatment. The experiment was approved by an independent Ethical Committee on Animal Experimentation (Ethical Committee of the University of Milan, Opinion no. 81/14)

and was performed in accordance with the Italian Laws (D.L.vo 116/92 and following additions), which enforce EU 86/609 Directive.

### Sampling

At 24 h after IV administration mice were euthanized by carbon dioxide inhalation. After drawing blood from the heart, mice underwent complete necropsy. Blood, liver, spleen, kidneys, lungs, and brain were collected for silver quantification and histopathological examination. The organ weight was measured and relative organ weights (%) were calculated as wet organ weight/total body weight. For quantification of silver, blood and a portion of the collected organs were stored at -80 °C for later analysis.

### Determination of silver

#### Chemicals

Ultrapure deionized water obtained by a Milli-Q Element System (Millipore, Molsheim, France), ultrapure grade nitric acid (67–69 % v/v) (Carlo Erba Reagenti, Rodano, Italy), ultrapure grade hydrochloric acid (32–35 % v/v) (Romil Ltd, Cambridge, UK) and ultrapure grade hydrogen peroxide (30 % v/v) (Merck, Darmstadt, Germany) were used throughout. For ICP-MS measurements, silver calibrants and rhodium solutions used were obtained from standard certified solutions of 1 mg/ml (High Purity Standard, Charleston, SC) by dilution with acidified (HNO<sub>3</sub> and HCl) water, as necessary.

#### Determination of total silver content

Total silver concentrations were determined in organs and whole blood by means of a triple quadrupole inductively coupled plasma mass spectrometer (ICP-MS). A 8800 ICP-QQQ spectrometer (Agilent Technologies, Japan, Tokio) equipped with an autosampler, a peristaltic pump, a Micro-Mist glass concentric nebuliser, and operated at a RF power of 1550 W, was used. All sample manipulations were carried out in clean room conditions under a laminar flow box (Spetec GmbH, Erding, Germany). Before ICP-MS measurements, whole organs and blood were placed in Falcon tubes and pre-digested for 5 h at room temperature with 2–4 ml HNO<sub>3</sub>, depending on the organ weight. After adding 1 ml H<sub>2</sub>O<sub>2</sub>, samples were digested in a microwave system (Milestone Ethos E microwave labstation, FKV, Bergamo, Italy) at 90 °C for 8 h, maximum power 800 W. After cooling, the digests were diluted by adding HCl (final concentration 3.0 M) to promote the formation of soluble silver complexes and prevent the precipitation of insoluble Ag<sup>+</sup> salts. Prior to analysis the digests were highly diluted with 0.1 % HNO<sub>3</sub> and the appropriate amount of HCl so as to maintain the silver in complexed form. Measurements were carried out on <sup>107</sup>Ag and <sup>103</sup>Rh, as internal standard, by the method of external calibration. The method

detection limit ranged from 0.4 to 0.7 µg/kg, depending on the tissue, and was 0.09 µg/l for blood.

#### Analytical quality control

Trueness of ICP-MS measurements was assessed by analysing the certified reference material SRM 1577c Bovine Liver (NIST, Gaithersburg, MD, USA), with a certified value for silver of 5.9 ± 1.6 µg/kg and the control material Seronorm™ Trace Elements Whole Blood L-1 (SERO AS, Billingstad, Norway) with a indicative value for silver of 185 ± 10 ng/l, both included in every analytical batch. The average determined silver concentrations were 6.0 ± 0.5 µg/kg (*n* = 6) and 179 ± 2 ng/l (*n* = 6) for the liver-based and the blood-based materials, respectively, in good agreement with the reference values. The trueness of determinations was also assessed through spikes of known amounts of silver in tissues and blood before sample dissolution, giving recoveries within the range of 90–100 % with no appreciable differences between sample types.

#### Histopathological examination

For histological examination, liver (median lobe including the gall bladder), spleen (apical portion), kidney (half of the right kidney), lung (left lobe), brain (half brain, cut along the sagittal plane) were fixed in 10 % neutral buffered formalin for at least 48 h at room temperature, routinely processed for paraffin embedding, sectioned at 4 µm thickness, stained with hematoxylin-eosin (H&E), and evaluated under a light microscope. Grading of histopathological lesions in the examined organs was performed as follows: 0 = absence of lesions; 1 = minimal lesions; 2 = mild lesions; 3 = moderate lesions; 4 = severe lesions.

To analyze the tissue distribution and localization of silver, autometallography (AMG) [42] and immunofluorescence were performed on serial sections. After AMG staining, sections were counterstained with safranin O and evaluated under a light microscope for the identification of tissue and cellular localization of silver, visible as black granular pigment. For immunofluorescence, liver sections were immunostained with rabbit monoclonal anti-IBA1 antibody (Wako Chemicals Richmond, VA, USA, cat. No. 019-19741), a pan-macrophage marker [68]. Secondary antibody, Alexa Fluor® 555 F(ab')<sub>2</sub> Fragment of Goat Anti-Rabbit IgG (H + L) (Life Technologies Europe BV, Monza, Italy, cat. No. A-21430) was then added. Immunofluorescently labeled sections were acquired with the Leica TCS SP5 confocal microscope (Leica Microsystems GmbH, Wetzlar, Germany). The Alexa555 fluorophore was excited with the 561 nm laser line and the emitted fluorescence (570–700 nm) acquired with a 63x/1.4 oil immersion objective (Leica Microsystems GmbH). Nuclei were visualized by DAPI staining (405 nm laser line



excitation, 415–500 nm acquisition window). Silver aggregates were visualized by reflection of light at 561 nm [24].

### Statistical analysis

Data were analyzed using Graph Pad Prism version 5.0 (GraphPad Software, San Diego, CA). For TEM, paired samples *t*-test was performed. Since the number of data (weights and silver concentrations) obtained from *in vivo* experiments was small, nonparametric tests (Kruskal-Wallis and Mann–Whitney *U* test) were used to detect differences between groups. The *P*-values <0.05 were considered statistically significant. Data were additionally explored by Principal Component Analysis, in order to understand the relationships among variables and their effect on data distribution.

### Additional file

**Additional file 1: Table S1.** Body weight gain and relative organ weight (%) after IV administration of differently coated AgNPs. **Table S2.** Silver tissue concentration determined by ICP-MS after IV administration of AgNPs and AgAc. **Figure S1.** Silver tissue concentration after IV administration of differently coated AgNPs and AgAc. **Figure S2.** Principal component analysis of silver tissue concentration data. **Figure S3.** Histology of spleen and liver after IV administration of 10 mg Ag/Kg in mice. **Figure S4.** Histology of liver from mice treated with 10 nm AgNPs. (PDF 728 kb)

### Abbreviations

AgAc: silver acetate; AgNP: silver nanoparticle; AMG: autometallography; bw: body weight; CT: sodium citrate; DLS: dynamic light scattering; H&E: hematoxylin and eosin; ICP-MS: inductively coupled plasma mass spectroscopy; PVP: polyvinylpyrrolidone; TEM: transmission electron microscopy; UV-Vis: UV-visible.

### Competing interests

The authors declare that they have no competing interests.

### Authors' contributions

CR conceived and designed the study, performed the histopathological analysis, analyzed and interpreted the data, and drafted the manuscript. MDM participated in the design of the study, conducted the animal exposures, performed the histochemical stainings, participated in the data analysis, and drafted the manuscript. SB conducted the animal exposures. SA and CC carried out the particle characterization, data analysis, and drafted the manuscript. SM performed the statistical analysis. FA, MDA, AR conducted the dissolution study, the ICP-MS measurements, and related data analysis. FC planned and supervised the dissolution study and ICP-MS characterization of tissue distribution, and critically revised the manuscript. CL was the project leader, and critically revised the manuscript. PM critically revised the manuscript. ES participated in the planning of the study, supervised the histopathological analysis, and critically revised the manuscript. All authors read and approved the final manuscript.

### Acknowledgements

This research was supported by Fondazione Cariplo for the project "Toxicology of chronic exposure to engineered silver nanoparticles", under the 2011 call "Nanoparticles, nanotechnologies and ultrafine particles". We are grateful to S. Rodighiero for assistance in the analysis at confocal microscope, D. Marchesi for assistance in TEM imaging, and M. Losa for technical histological support.

### Author details

<sup>1</sup>Fondazione Filarete, 20139 Milan, Italy. <sup>2</sup>Dipartimento di Scienze Veterinarie e Sanità Pubblica (DIVET), Università degli Studi di Milano, 20133 Milan, Italy. <sup>3</sup>Dipartimento di Fisica, Università degli Studi di Milano, 20133 Milan, Italy.

<sup>4</sup>Department of Food Safety and Veterinary Public Health, Istituto Superiore di Sanità - National Health Institute, 00161 Rome, Italy. <sup>5</sup>Centro Interdisciplinare Materiali e Interfacce Nanostrutturate (CIMAINA), Università degli Studi di Milano, 20133 Milan, Italy.

Received: 29 June 2015 Accepted: 22 February 2016

Published online: 29 February 2016

### References

- Völker C, Oetken M, Oehlmann J. The biological effects and possible modes of action of nanosilver. *Rev Environ Contam Toxicol.* 2013;223:81–106.
- Ahamed M, Alsalhi MS, Siddiqui MK. Silver nanoparticle applications and human health. *Clin Chim Acta.* 2010;411:1841–8.
- The Project on Emerging Nanotechnologies. Consumer Products Inventory. 2015. <http://www.nanotechproject.org/cpi>. Accessed 15 April 2015.
- Schäfer B, Brocke JV, Epp A, Götz M, Herzberg F, Kneuer C, et al. State of the art in human risk assessment of silver compounds in consumer products: a conference report on silver and nanosilver held at the BfR in 2012. *Arch Toxicol.* 2013;87:2249–62.
- Schluesener JK, Schluesener HJ. Nanosilver: application and novel aspects of toxicology. *Arch Toxicol.* 2013;87:569–76.
- Mijnendonckx K, Leys N, Mahillon J, Silver S, Vanhoudt R. Antimicrobial silver: uses, toxicity and potential for resistance. *Biomaterials.* 2013;26:609–21.
- Morones JR, Elechiguerra JL, Camacho A, Holt K, Kouri JB, Ramirez JT, et al. The bactericidal effect of silver nanoparticles. *Nanotechnology.* 2005;16:2346–53.
- Stensberg MC, Wei Q, McLamore ES, Porterfield DM, Wei A, Sepúlveda MS. Toxicological studies on silver nanoparticles: challenges and opportunities in assessment, monitoring and imaging. *Nanomedicine.* 2011;6:879–98.
- El Badawy AM, Silva RG, Morris B, Scheckel KG, Suidan MT, Tolaymat TM. Surface charge-dependent toxicity of silver nanoparticles. *Environ Sci Technol.* 2011;45:283–7.
- Nguyen KC, Seligy VL, Massarsky A, Moon TW, Rippstein P, Tan J, et al. Comparison of toxicity of uncoated and coated silver nanoparticles. *J Phys Conf Ser.* 2013;429:012025.
- Carlson C, Hussain SM, Schrand AM, Braydich-Stolle LK, Hess KL, Jones RL, et al. Unique cellular interaction of silver nanoparticles: size-dependent generation of reactive oxygen species. *J Phys Chem B.* 2008;112:13608–19.
- Hsin YH, Chen CF, Huang S, Shih TS, Lai PS, Chueh PJ. The apoptotic effect of nanosilver is mediated by a ROS- and JNK-dependent mechanism involving the mitochondrial pathway in NIH3T3 cells. *Toxicol Lett.* 2008;179:130–9.
- Kim TH, Kim M, Park HS, Shin US, Gong MS, Kim HW. Size-dependent cellular toxicity of silver nanoparticles. *J Biomed Mater Res A.* 2012;100:1033–43.
- Park MV, Neigh AM, Vermeulen JP, de la Fonteyne LJ, Verharen HW, Briedé JJ, et al. The effect of particle size on the cytotoxicity, inflammation, developmental toxicity and genotoxicity of silver nanoparticles. *Biomaterials.* 2011;32:9810–7.
- Sung JH, Ji JH, Park JD, Yoon JU, Kim DS, Jeon KS, et al. Subchronic inhalation toxicity of silver nanoparticles. *Toxicol Sci.* 2009;108:452–61.
- Kim YS, Song MY, Park JD, Song KS, Ryu HR, Chung YH, et al. Subchronic oral toxicity of silver nanoparticles. *Part Fibre Toxicol.* 2010;7:20.
- Park EJ, Bae E, Yi J, Kim Y, Choi K, Lee SH, et al. Repeated-dose toxicity and inflammatory responses in mice by oral administration of silver nanoparticles. *Environ Toxicol Pharmacol.* 2010;30:162–8.
- Samberg ME, Oldenburg SJ, Monteiro-Riviere NA. Evaluation of silver nanoparticle toxicity in skin *in vivo* and keratinocytes *in vitro*. *Environ Health Perspect.* 2010;118:407–13.
- Stebounova LV, Adamcakova-Dodd A, Kim JS, Park H, O'Shaughnessy PT, Grassian VH, et al. Nanosilver induces minimal lung toxicity or inflammation in a subacute murine inhalation model. *Part Fibre Toxicol.* 2011;8:5.
- Hadrup N, Loeschner K, Bergström A, Wilks A, Gao X, Vogel U, et al. Subacute oral toxicity investigation of nanoparticulate and ionic silver in rats. *Arch Toxicol.* 2012;86:543–51.
- van der Zande M, Vandebriel RJ, Van Doren E, Kramer E, Herrera Rivera Z, Serrano-Rojero CS, et al. Distribution, elimination, and toxicity of silver nanoparticles and silver ions in rats after 28-day oral exposure. *ACS Nano.* 2012;6:7427–42.
- Xue Y, Zhang S, Huang Y, Zhang T, Liu X, Hu Y, et al. Acute toxic effects and gender-related biokinetics of silver nanoparticles following an intravenous injection in mice. *J Appl Toxicol.* 2012;32:890–9.

23. De Jong WH, Van Der Ven LT, Sleijffers A, Park MV, Jansen EH, Van Loveren H, et al. Systemic and immunotoxicity of silver nanoparticles in an intravenous 28 days repeated dose toxicity study in rats. *Biomaterials*. 2013;34:8333–43.
24. Gaiser BK, Fernandes TF, Jepson MA, Lead JR, Tyler CR, Baalousha M, et al. Interspecies comparisons on the uptake and toxicity of silver and cerium dioxide nanoparticles. *Environ Toxicol Chem*. 2012;31:144–54.
25. Korani M, Rezaayat SM, Arbabi BS. Sub-chronic dermal toxicity of silver nanoparticles in guinea pig: special emphasis to heart, bone and kidney toxicities. *Iran J Pharm Res*. 2013;12:511–9.
26. Shahare B, Yashpal M. Toxic effects of repeated oral exposure of silver nanoparticles on small intestine mucosa of mice. *Toxicol Mech Methods*. 2013;23:161–7.
27. Reidy B, Haase A, Luch A, Dawson KA, Lynch I. Mechanisms of silver nanoparticle release, transformation and toxicity: a critical review of current knowledge and recommendations for future studies and applications. *Materials*. 2013;6:2295–350.
28. Monopoli MP, Aberg C, Salvati A, Dawson KA. Biomolecular coronas provide the biological identity of nanosized materials. *Nat Nanotechnol*. 2012;7:779–86.
29. Warheit DB. Debunking some misconceptions about nanotoxicology. *Nano Lett*. 2010;10:4777–82.
30. Lankveld DP, Oomen AG, Krystek P, Neigh A, Troost-de Jong A, Noorlander CW, et al. The kinetics of the tissue distribution of silver nanoparticles of different sizes. *Biomaterials*. 2010;31:8350–61.
31. Dziendzikowska K, Gromadzka-Ostrowska J, Lankoff A, Oczkowski M, Krawczyńska A, Chwastowska J, et al. Time-dependent biodistribution and excretion of silver nanoparticles in male Wistar rats. *J Appl Toxicol*. 2012;32:920–8.
32. Wang X, Ji Z, Chang CH, Zhang H, Wang M, Liao YP, et al. Use of coated silver nanoparticles to understand the relationship of particle dissolution and bioavailability to cell and lung toxicological potential. *Small*. 2014;10:385–98.
33. Seiffert J, Hussain F, Wiegman C, Li F, Bey L, Baker W, et al. Pulmonary toxicity of instilled silver nanoparticles: influence of size, coating and rat strain. *PLoS One*. 2015;10:e0119726.
34. SCENIHR (Scientific Committee on Emerging and Newly Identified Health Risks). Nanosilver: safety, health and environmental effects and role in antimicrobial resistance. 2014. [http://ec.europa.eu/health/scientific\\_committees/consultations/public\\_consultations/scenihhr\\_consultation\\_17\\_en.htm](http://ec.europa.eu/health/scientific_committees/consultations/public_consultations/scenihhr_consultation_17_en.htm). Accessed 15 April 2015.
35. Gliga AR, Skoglund S, Wallinder IO, Fadeel B, Karlsson HL. Size-dependent cytotoxicity of silver nanoparticles in human lung cells: the role of cellular uptake, agglomeration and Ag release. *Part Fibre Toxicol*. 2014;11:11.
36. Ivask A, Kurvet I, Kasemets K, Blinova I, Aruoja V, Suppi S, et al. Size-dependent toxicity of silver nanoparticles to bacteria, yeast, algae, crustaceans and mammalian cells *in vitro*. *PLoS One*. 2014;9:e102108.
37. Noguez C. Surface plasmons on metal nanoparticles: the influence of shape and physical environment. *J Phys Chem C*. 2007;111:3806–19.
38. Izquierdo-Lorenzo I, Kubackova J, Manchon D, Mosset A, Cottancin E, Sanchez-Cortes S. Linking Ag nanoparticles by aliphatic  $\alpha$ ,  $\omega$ -dithiols: a study of the aggregation and formation of interparticle hot spots. *J Phys Chem C*. 2013;117:16203–12.
39. Shannahan JH, Podila R, Brown JM. A hyperspectral and toxicological analysis of protein corona impact on silver nanoparticle properties, intracellular modifications, and macrophage activation. *Int J Nanomedicine*. 2015;10:6509–21.
40. Bachler G, von Goetz N, Hungerbühler K. A physiologically based pharmacokinetic model for ionic silver and silver nanoparticles. *Int J Nanomedicine*. 2013;8:3365–82.
41. Loza K, Diendorf J, Sengstock C, Ruiz-Gonzalez L, Gonzalez-Calbet JM, Vallet-Regi M, et al. The dissolution and biological effects of silver nanoparticles in biological media. *J Mater Chem B*. 2014;2:1634–43.
42. Su C, Sun Y. Considerations of inductively coupled plasma mass spectrometry techniques for characterizing the dissolution of metal-based nanomaterials in biological tissues. *J Anal At Spectrom*. 2015;30:1689–705.
43. Utembe W, Potgieter K, Stefaniak AB, Gulumian M. Dissolution and biodegradability: Important parameters needed for risk assessment of nanomaterials. *Part Fibre Toxicol*. 2015;12:11.
44. Roe D, Karandikar B, Bonn-Savage N, Gibbins B, Roullet JB. Antimicrobial surface functionalization of plastic catheters by silver nanoparticles. *J Antimicrob Chemother*. 2008;61:869–76.
45. Rigo C, Ferroni L, Tocco I, Roman M, Munivrana I, Gardin C, et al. Active silver nanoparticles for wound healing. *Int J Mol Sci*. 2013;14:4817–40.
46. Schrand AM, Braydich-Stolle LK, Schlager JJ, Dai L, Hussain SM. Can silver nanoparticles be useful as potential biological labels? *Nanotechnology*. 2008;19:235104.
47. Wei L, Lu J, Xu H, Patel A, Chen ZS, Chen G. Silver nanoparticles: synthesis, properties, and therapeutic applications. *Drug Discov Today*. 2015;20:595–601.
48. Loeschner K, Hadrup N, Qvortrup K, Larsen A, Gao X, Vogel U, et al. Distribution of silver in rats following 28 days of repeated oral exposure to silver nanoparticles or silver acetate. *Part Fibre Toxicol*. 2011;8:18.
49. Kwon JT, Minai-Tehrani A, Hwang SK, Kim JE, Shin JY, Yu KN, et al. Acute pulmonary toxicity and body distribution of inhaled metallic silver nanoparticles. *Toxicol Res*. 2012;28:25–31.
50. Park K, Park EJ, Chun IK, Choi K, Lee SH, Yoon J, et al. Bioavailability and toxicokinetics of citrate-coated silver nanoparticles in rats. *Arch Pharm Res*. 2011;34:153–8.
51. Reagan-Shaw S, Nihal M, Ahmad N. Dose translation from animal to human studies revisited. *FASEB J*. 2008;22:659–61.
52. Sadauskas E, Wallin H, Stoltenberg M, Vogel U, Doering P, Larsen A, et al. Kupffer cells are central in the removal of nanoparticles from the organism. *Part Fibre Toxicol*. 2007;4:10.
53. Sadauskas E, Danscher G, Stoltenberg M, Vogel U, Larsen A, Wallin H. Protracted elimination of gold nanoparticles from mouse liver. *Nanomedicine*. 2009;5:162–9.
54. Danscher G, Stoltenberg M. Silver enhancement of quantum dots resulting from (1) metabolism of toxic metals in animals and humans, (2) *in vivo*, *in vitro* and immersion created zinc-sulphur/zinc-selenium nanocrystals, (3) metal ions liberated from metal implants and particles. *Prog Histochem Cytochem*. 2006;41:57–139.
55. Danscher G. Light and electron microscopic localization of silver in biological tissue. *Histochemistry*. 1981;71:177–86.
56. Matsumura T, Kumakiri M, Ohkawara A, Himeno H, Numata T, Adachi R. Detection of selenium in generalized and localized argyria: report of four cases with X-ray microanalysis. *J Dermatol*. 1992;19:87–93.
57. Massi D, Santucci M. Human generalized argyria: a submicroscopic and X-ray spectroscopic study. *Ultrastruct Pathol*. 1998;22:47–53.
58. Lee JH, Kim YS, Song KS, Ryu HR, Sung JH, Park JD, et al. Biopersistence of silver nanoparticles in tissues from Sprague-Dawley rats. *Part Fibre Toxicol*. 2013;10:36.
59. Thoolen B, Maronpot RR, Harada T, Nyska A, Rousseaux C, Nolte T, et al. Proliferative and nonproliferative lesions of the rat and mouse hepatobiliary system. *Toxicol Pathol*. 2010;38:55–81S.
60. Haschek WM, Wallig MA, Rousseaux CG. The liver. In: *Fundamentals of Toxicologic Pathology*. London: Academic; 2010. p. 197–235.
61. Shrivastava S, Bera T, Singh SK, Singh G, Ramachandrarao P, Dash D. Characterization of antiplatelet properties of silver nanoparticles. *ACS Nano*. 2009;3:1357–64.
62. Sabella S, Carney RP, Brunetti V, Malvindi MA, Al-Juffali N, Vecchio G, et al. A general mechanism for intracellular toxicity of metal-containing nanoparticles. *Nanoscale*. 2014;6:7052–61.
63. De Matteis V, Malvindi MA, Galeone A, Brunetti V, De Luca E, Kote S, et al. Negligible particle-specific toxicity mechanism of silver nanoparticles: The role of Ag(+) ion release in the cytosol. *Nanomedicine*. 2015;11:731–9.
64. Walkey CD, Chan WCW. Understanding and controlling the interaction of nanomaterials with proteins in a physiological environment. *Chem Soc Rev*. 2012;41:2780–99.
65. Walkey CD, Olsen JB, Song F, Liu R, Guo H, Olsen W, et al. Protein corona fingerprinting predicts the cell association of gold nanoparticles. *ACS Nano*. 2014;8:2439–55.
66. Tejamaya M, Römer I, Merrifield RC, Lead JR. Stability of citrate, PVP, and PEG coated silver nanoparticles in ecotoxicology media. *Environ Sci Technol*. 2012;46:7011–7.
67. An Huynh K, Chen KL. Aggregation kinetics of citrate and polyvinylpyrrolidone coated silver nanoparticles in monovalent and divalent electrolyte solutions. *Environ Sci Technol*. 2011;45:5564–71.
68. Reh G, Bush D, Ward JM. The utility of immunohistochemistry for the identification of hematopoietic and lymphoid cells in normal tissues and interpretation of proliferative and inflammatory lesions of mice and rats. *Toxicol Pathol*. 2012;40:345–74.

# New synthesis and biodistribution of the D-amino acid oxidase-magnetic nanoparticle system

**Background:** Application of nanoenzymes, based on D-amino acid oxidase (DAAO) conjugated to magnetic nanoparticles (NPs), as anticancer system requires improvement of the synthesis protocol and *in vivo* distribution evaluation. **Results:** A new and more efficient synthesis via EDC-NHS produced an Fe<sub>3</sub>O<sub>4</sub>NP-APTES-DAAO system with a specific activity of 7 U/mg NPs. IR spectroscopy showed that all Fe<sub>3</sub>O<sub>4</sub> NP sites are saturated with APTES and all available NH<sub>2</sub> sites with DAAO. The acute cytotoxicity of the new system does not differ from that of the previous one. *In vivo* experiments showed that the system did not cause adverse effects, cross the brain–blood barrier and accumulate in the heart. **Conclusions:** Our results support the possibility to use enzymes conjugated to magnetic NPs for cancer treatment. Besides, we think that enzymes and other biological molecules efficiently conjugated to magnetic NPs might constitute a category of ‘bionanoparticles’ to be exploited, not only in medical, but also in industrial biotechnology.

**Lay abstract:** We have linked magnetic nanoparticles to D-amino acid oxidase, an enzyme capable of producing, in the presence of its substrate, reactive oxygen species. The scope is to use the magnetic properties of the enzyme-nanoparticle system to direct it to a desired area where its cytotoxicity can be controlled by the addition of exogenous substrate. Besides the possible applications in cancer therapy, we think that enzymes and other biological molecules linked to magnetic nanoparticles might also be exploited in industrial biotechnology.

First draft submitted: 24 April 2015; Accepted for publication: 15 July 2015;  
Published online: 11 September 2015

**Keywords:** anticancer system • bionanoparticles • *in vivo* analysis • iron • IR spectroscopy  
• nanoenzyme • nanoparticles

Nanoparticles (NPs) and other nanomaterials permeate several areas of our everyday life. In industrial applications, they have become indispensable components of catalysts [1], sensors [2] and photovoltaic devices [3]. Unfortunately, the same peculiar properties that make nanomaterials so attractive may create potentially new and largely undefined risks for human health. NPs, in effect, are capable to cross biological barriers [4–6] and are readily taken up by cells [7] where they can exert their toxicity. However, NPs have

also found widespread use in the biomedical field, as nanovaccines, nanodrugs and diagnostic imaging tools [8]. The increasing number of nanotechnology patents related to healthcare reflects the rapid expansion of this pioneering industry [9].

The impact of nanobiotechnology on oncology is huge and includes fields ranging from discovery of tumor biomarkers to development of devices for cancer surgery [10,11]. In particular, drug-delivery, the most explored field, aims to design carriers that deliver

Francesca Cappellini<sup>1</sup>,  
Camilla Recordati<sup>2</sup>, Marcella  
De Maglie<sup>2,3</sup>, Loredano  
Pollegioni<sup>1,4</sup>, Federica Rossi<sup>1</sup>,  
Marco Daturi<sup>5</sup>, Rosalba  
Gornati<sup>1,4</sup> & Giovanni  
Bernardini<sup>\*1,4</sup>

<sup>1</sup>Dipartimento di Biotecnologie e Scienze della Vita, Università degli Studi dell’Insubria, Via Dunant 3, Varese, Italy

<sup>2</sup>Mouse & Animal Pathology Laboratory, Fondazione Filarete, Viale Ortles, Milano, Italy

<sup>3</sup>Dipartimento di Scienze Veterinarie e Sanità Pubblica, Università degli Studi di Milano, Via Celoria, Milano, Italy

<sup>4</sup>The Protein Factory, Politecnico di Milano and Università degli Studi dell’Insubria, Via Mancinelli 7, Milano, Italy

<sup>5</sup>Laboratoire Catalyse et Spectrochimie, ENSICAEN, Université de Caen, CNRS, 6 Bd Maréchal Juin, F-14050 Caen, France

\*Author for correspondence:  
[giovanni.bernardini@uninsubria.it](mailto:giovanni.bernardini@uninsubria.it)

drugs more precisely to tumor cells and maintain them at therapeutic concentrations over a long period [12]. Besides considerable progress in cancer therapy and the many anticancer drugs available, the treatment of cancer has still a lot of side effects [13] and NPs could be an efficient alternative to conventional therapies, serving as carrier systems capable of enhancing efficacy, while simultaneously reducing side effects. Magnetic NPs can be functionalized with anticancer drugs and guided along an externally placed magnet into the tumor [14]. Moreover, magnetic NPs can produce heat through various energy losses under an external alternating magnetic field, causing cancer destruction by hyperthermia [15–20].

In a previous work [21], we set up the synthesis of an NP-enzyme system for cancer therapy via glutaraldehyde. The system ( $\text{Fe}_3\text{O}_4$ -APTES-DAAO) was based on iron oxide magnetic NPs conjugated to the ROS-producing enzyme D-amino acid oxidase from *Rhodotorula gracilis* (RgDAAO, EC 1.4.3.3).  $\text{Fe}_3\text{O}_4$ -APTES-DAAO aims to combine the advantages of magnetic NPs (low acute toxicity, specific target by a magnetic field, ability to cross biological barriers) with those of RgDAAO (no acute toxicity, easy modulation of the activity, hence of ROS generation). The system can be intravenously injected and addressed by an external magnetic field in the tumor area, where D-amino acids (naturally present or externally injected) act as substrate for the enzyme, causing  $\text{H}_2\text{O}_2$  production and tumor cell death by apoptosis.

This work is on continuing the research of using magnetic NPs conjugated to DAAO for the potential treatment of cancer, a step forward in the possible realization of this clinical technique. To this aim, we present a new and more efficient synthesis of this system via EDC-NHS and the characterization by infra red (IR) spectroscopy of the two systems resulting from the old and the new methods of synthesis. Moreover, we have analyzed the *in vivo* distribution as well as the acute toxicity of the new system after single intravenous administration in mice. We have also realized that enzymes conjugated to magnetic NPs could be of interest also for industrial purposes [22].

## Materials & methods

### Coating of magnetic NPs with APTES

$\text{Fe}_3\text{O}_4$  NPs were functionalized according to the protocol of Bava *et al.* [21]. Briefly, 150 mg of  $\text{Fe}_3\text{O}_4$  NPs (Sigma, cat. number 637,106) were ultrasonicated in 10 ml of  $\text{H}_2\text{O}$  MilliQ for 15 min. A solution of 5 ml APTES (2% v/v, Sigma cat. number A3648) in  $\text{H}_2\text{O}$  MilliQ was then added and the reaction was maintained under mechanical stirring for 5 h at 50°C.  $\text{Fe}_3\text{O}_4$ -APTES were then separated from unbound

APTES by a commercial parallelepiped neodymium magnet (Webcraft GmbH, Uster, Switzerland; Ni-Cu-Ni plated; magnetization: N45; size: 30 × 30 × 15 mm), washed several times with water and anhydri-ficated with ethanol overnight.  $\text{Fe}_3\text{O}_4$ -APTES were suspended again in water, ultrasonicated for 30 min and left at room temperature for 1 h, isolated and dried at 50°C overnight.

### Synthesis of $\text{Fe}_3\text{O}_4$ NP-APTES-DAAO

Four milligrams of  $\text{Fe}_3\text{O}_4$ NP-APTES were suspended by sonication for 15 min with 1-ethyl-3-(3-dimethylaminopropyl)carbodiimide (EDC, Sigma cat. number 03450) and N-hydroxysuccinimide (NHS, Sigma, cat. number 130,672) in 3:2 (w/w) ratio in 5 mM sodium pyrophosphate (NaPPi) buffer, pH 8.5. Two hundred and fifty micrograms of recombinant RgDAAO [19] were added and the reaction was carried out for 4 h at 4°C using a rotating plate tube stirrer. Subsequently,  $\text{Fe}_3\text{O}_4$ -APTES-DAAO were collected by a magnet and washed twice with 1 ml of 5 mM NaPPi pH 8.5. The supernatant was stored for further analysis.

### DAAO activity assay

The activity of  $\text{Fe}_3\text{O}_4$ -APTES-DAAO was determined by measuring the absorbance increase accompanying the  $\text{H}_2\text{O}_2$ -induced oxidation of *o*-dianisidine [20]. One DAAO unit corresponds to the amount of enzyme that converts 1  $\mu\text{mol}$  of substrate per min at 25°C and at 0.253 mM oxygen concentration [23,24]. The standard assay mixture contained 890  $\mu\text{l}$  of 100 mM D-alanine in 100 mM NaPPi buffer, pH 8.5 buffer, 100  $\mu\text{l}$  of 3.2 mg/ml *o*-dianisidine in water, 10  $\mu\text{l}$  of 0.4 mg/ml horseradish peroxidase in 100 mM NaPPi buffer, pH 8.5 buffer and 10  $\mu\text{l}$  of 0.4 mg/ml  $\text{Fe}_3\text{O}_4$ NP-APTES-DAAO in the same buffer. The reaction was initiated by the addition of the enzyme and the absorbance increase was monitored at 440 nm for 1 min using an UV-Vis Jasco V-560 spectrophotometer.

### IR analysis

$\text{Fe}_3\text{O}_4$ NP-APTES-DAAO were characterized by IR analysis in different conditions. Samples (disks of 2  $\text{cm}^2$  area) were placed in a quartz cell equipped with KBr windows. A movable quartz sample holder allows to adjust the pellet in the infrared beam for spectra recording and to displace it into a furnace at the top of the cell for thermal treatment. The cell was connected to a vacuum line for evacuation ( $P_{\text{residual}} = \sim 10^{-6}$  torr) and for the introduction of gases into the infrared cell. Spectra were recorded at room temperature. The addition of well-known doses of gas in the cell was possible via a pressure gauge for the control of the gas pressure. A Nicolet Nexus spectrometer equipped with

a Mercury Cadmium Telluride (MCT) cryodetector and an extended KBr beam splitter was used for the acquisition of spectra in the 600–5500  $\text{cm}^{-1}$  range. IR spectra are absorption spectra and the notation used is a.u. for absorption units. The resolution of the spectra was 4  $\text{cm}^{-1}$ , and 256 scans were accumulated for each spectrum.

Three kinds of experiments have been performed: first the samples have been dispersed in the KBr, then on the surface of a silica pellet; finally on a silicon disk. In details: a wafer containing 98 mg of KBr has been pressed at 4 tons/ $\text{cm}^2$ , together with ~2 mg of the targeted sample; a wafer of 20 mg silica has been casted mixing in its center ~6–7 mg of sample, then pressed to 2 tons / $\text{cm}^2$  and ~2 mg of powder have been dispersed on the surface of a 2  $\text{cm}^2$  silicon disk by the help of a spot of ethanol.

### Dynamic light scattering (DLS) analysis

$\text{Fe}_3\text{O}_4$ ,  $\text{Fe}_3\text{O}_4$ -APTES and  $\text{Fe}_3\text{O}_4$ -APTES-DAAO NPs were analyzed at concentrations of 250, 25 and 2.5  $\mu\text{g}/\text{ml}$  in water. Sample dilutions were done in order to analyze the effect of concentration on NP aggregation. Each measurement was preceded by an equilibration time of 90 s. Analyzes were performed with Zetasizer Nano ZS90 (Malvern, UK) instrument. Measures were reported as scattering intensity in function to diameter.

### Cell viability

SKOV-3 cell lines were maintained as adherent cells in RPMI1640 medium (supplemented with 10% fetal bovine serum, 1% L-glutamine and 1% penicillin/streptomycin solution) at 37°C in a humidified 5%  $\text{CO}_2$  atmosphere. Cells were passaged as needed using 0.25% trypsin-EDTA.

Cell viability was determined as ATP content by using the CellTiter-Glo Luminescent Cell Viability Assay according to the manufacturer's instruction. In details,  $1 \times 10^4$  cells were seeded into 96-well assay plates and cultivated for 24 h at 37°C in 5%  $\text{CO}_2$  to equilibrate and become attached prior to the treatment. Cells were then exposed to increasing amounts of  $\text{Fe}_3\text{O}_4$ -APTES-DAAO, in presence or not of its substrate, for 24 h in a final volume of 100  $\mu\text{l}$ . Following the treatment, plates were equilibrated for 30 min at room temperature and 100  $\mu\text{l}$  of CellTiter-Glo Reagent was then added to each well. Plates were shaken for 2 min and left at room temperature for 10 min prior to the recording of luminescent signals using the Infinite F200 plate reader (Tecan Group, Männedorf, Switzerland). The experiments were performed in triplicate. Cell viability, expressed as ATP content, was normalized against control values.

### In vivo studies

To evaluate the biodistribution and acute toxicity of NPs, two *in vivo* studies were performed. In both experiments, male CD-1(ICR) mice of 4–5 weeks were purchased from Charles River (Calco, Italy). They were acclimated to the environment for a week prior to the initiation of the study, with free access to water and a standard pellet diet *ad libitum*. The environmental conditions were set at a temperature of  $22 \pm 2^\circ\text{C}$ , relative humidity of  $55 \pm 10\%$  and a 12 h light:dark cycle. The mice ( $n = 3$ ) were intravenously injected with a single dose of  $\text{Fe}_3\text{O}_4$ -APTES-DAAO (in the first experiment 100 mg/kg bodyweight (bw) of NPs in NaCl 0.9%, and in the second experiment 20 mg/kg bw of NPs in NaPPI buffer at pH 7.4) and sacrificed 24 h after the treatment. The control groups were treated with the corresponding vehicle (NaCl 0.9% or NaPPI buffer). Immediately after the treatment and the following hours, the general health and behavior of mice were monitored. The bodyweight of each mouse was measured before treatment and at sacrifice. The experiment was performed in accordance with the Italian Laws (D.L. 116/92 and following additions), which enforce EU 86/609 Directive (Council Directive 86/609/EEC of 24 November 1986, on the approximation of laws, regulations and administrative provisions of the member states regarding the protection of animals used for experimental and other scientific purposes).

### Sacrifice, sampling & pathological examination procedures

Mice were euthanized at 24-h post-treatment according to standard procedures and in compliance with local regulations, and underwent complete necropsy. Liver, spleen and kidney were weighed and the relative organ weight (wet organ/total bodyweight) was calculated.

Liver, kidney, spleen, lung, heart, testis and brain were fixed in 10% neutral-buffered formalin, and routinely processed for paraffin embedding. Four micrometer sections from each tissue were stained with hematoxylin and eosin (HE) and Perls iron stain [25], and evaluated under a light microscope. Quantitative evaluation of iron deposits in Perls iron stained sections was performed by digital image analysis: area of Perls staining was measured in three 200 $\times$  microscopic fields using the ImageJ analysis program [26], and the percentage of Perls positive area per field was then calculated.

For immunofluorescence, liver sections were immunostained with rabbit monoclonal anti-Iba1 antibody (Wako Chemicals, VA, USA, cat. number 019–19741), a pan-macrophage marker [27]. Secondary antibody, Alexa Fluor<sup>®</sup> 555 F(ab')<sub>2</sub> Fragment of Goat Anti-Rabbit IgG (H+L; Life Technologies Europe BV, Monza,

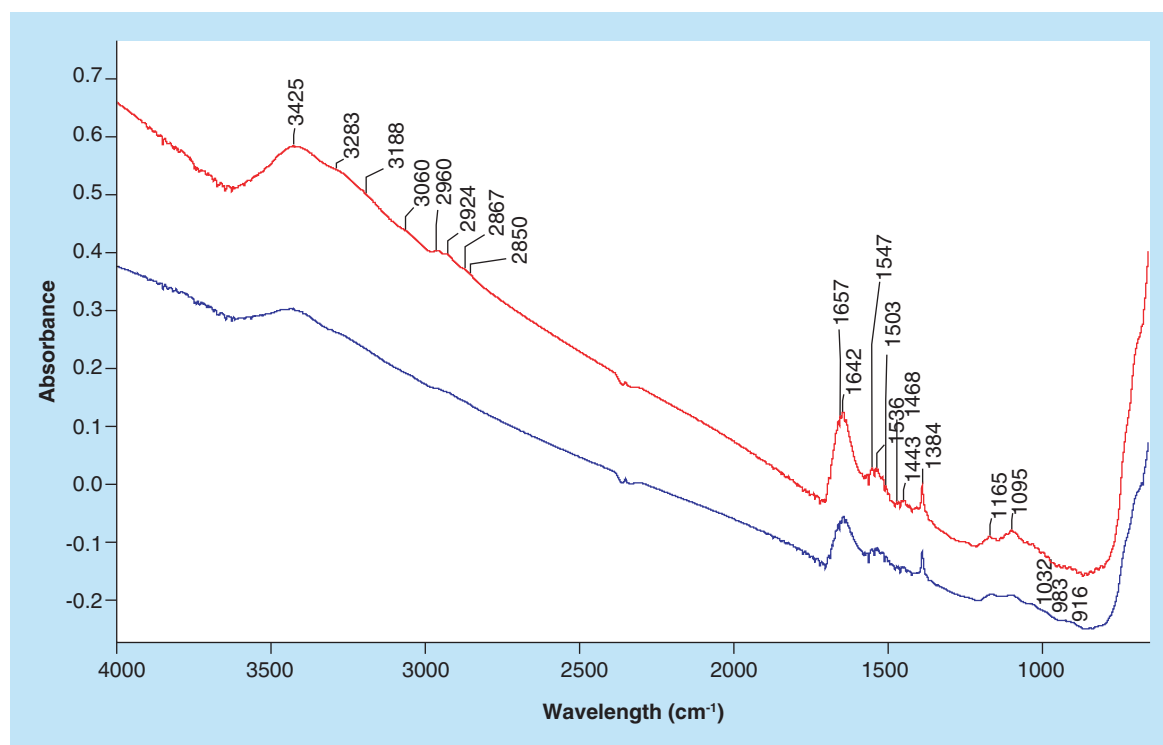


**Figure 1.** IR spectra of Fe<sub>3</sub>O<sub>4</sub>-APTES-DAAO prepared via glutaraldehyde (red) and via EDC/NHS (blue). Samples were dispersed in KBr (2% w/w).

Italy, cat. number A-21430) was then added. Immunofluorescently labeled sections were acquired with the Leica TCS SP5 confocal microscope (Leica Microsystems GmbH, Wetzlar, Germany). The Alexa555 fluo-

rophore was excited with the 561 nm laser line and the emitted fluorescence (570–700 nm) acquired with a 63×/1.4 oil immersion objective (Leica Microsystems, GmbH). Nuclei were visualized by DAPI staining

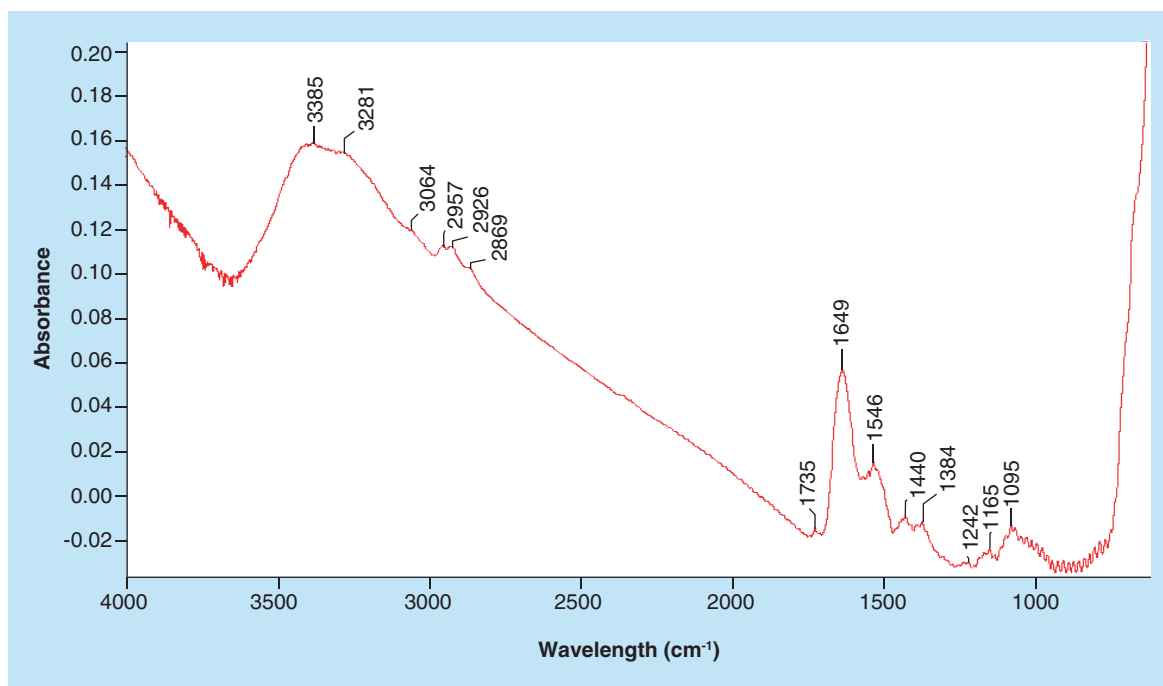


**Figure 2.** IR spectral subtraction. Spectrum of Fe<sub>3</sub>O<sub>4</sub>-APTES-DAAO prepared with the first method minus those prepared with the second method.

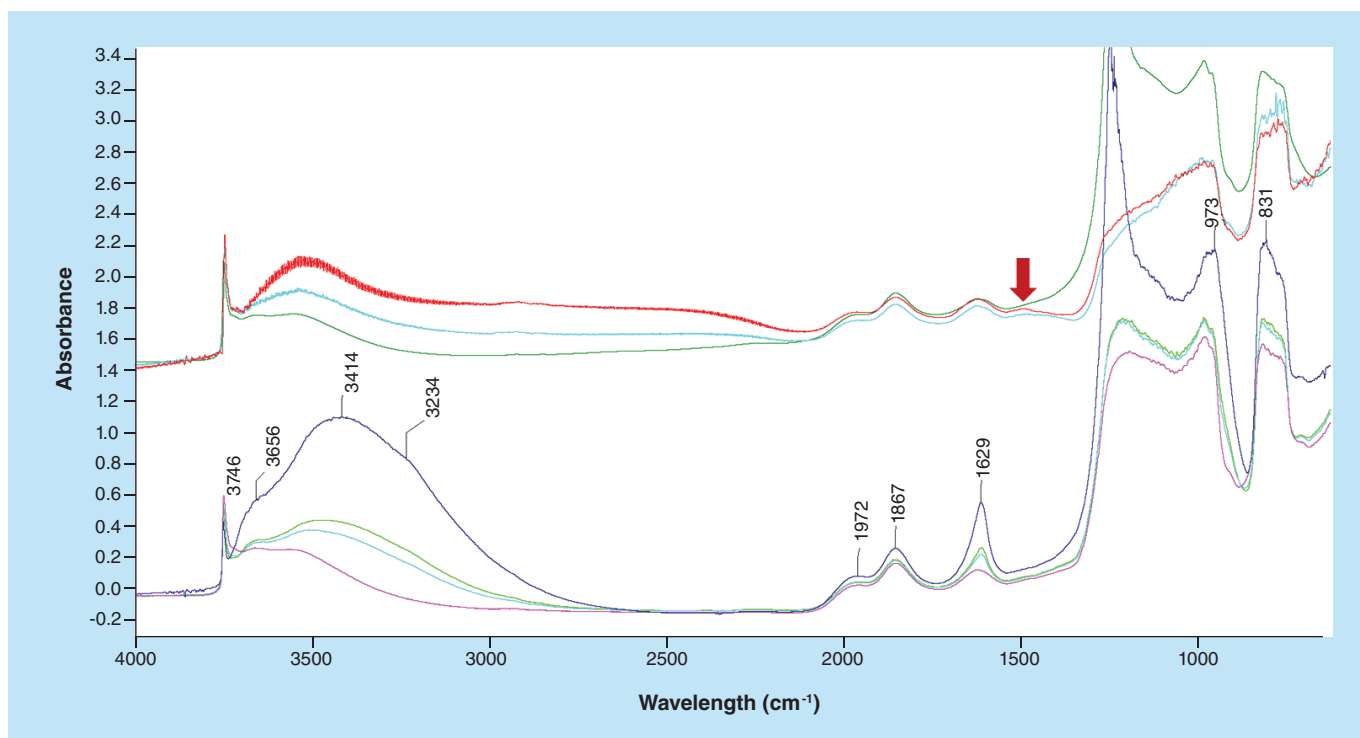


**Figure 3.** IR spectra of samples dispersed in silica. Bottom: in blue, subtraction of glutaraldehyde and EDC/NHS samples, in cyan, magenta and green spectra of glutaraldehyde samples after NO and CO adsorption. Top: EDC/NHS samples spectra after CO adsorption. Arrow indicates peak at 1508  $\text{cm}^{-1}$ .

(405 nm laser line excitation, 415–500 nm acquisition window). Iron aggregates were visualized by reflection of light at 561 nm.

#### Statistical analysis

Data were analyzed using GraphPad Prism version 5.0 (GraphPad Software, CA, USA). Statistical analyses

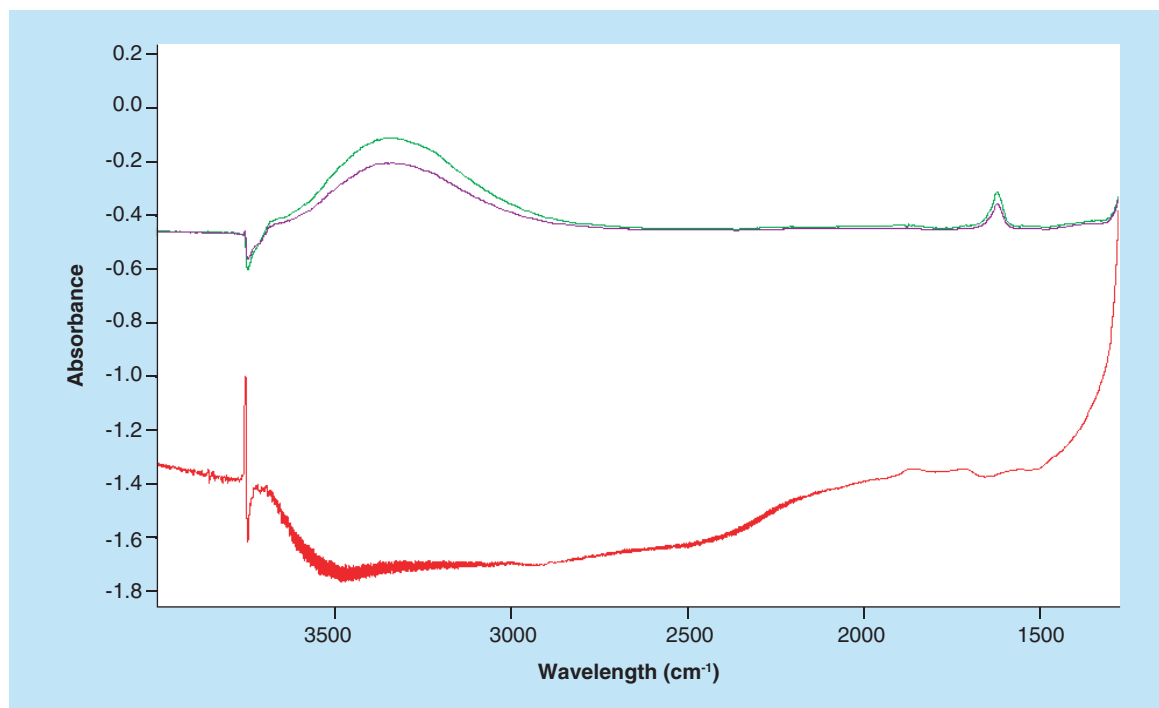


**Figure 4.** Spectra in the top refer to NO adsorption (10 and 18 torr at the equilibrium) on the glutaraldehyde sample. Spectrum in the bottom is the difference before and after the adsorption of CO on the EDC/NHS sample.

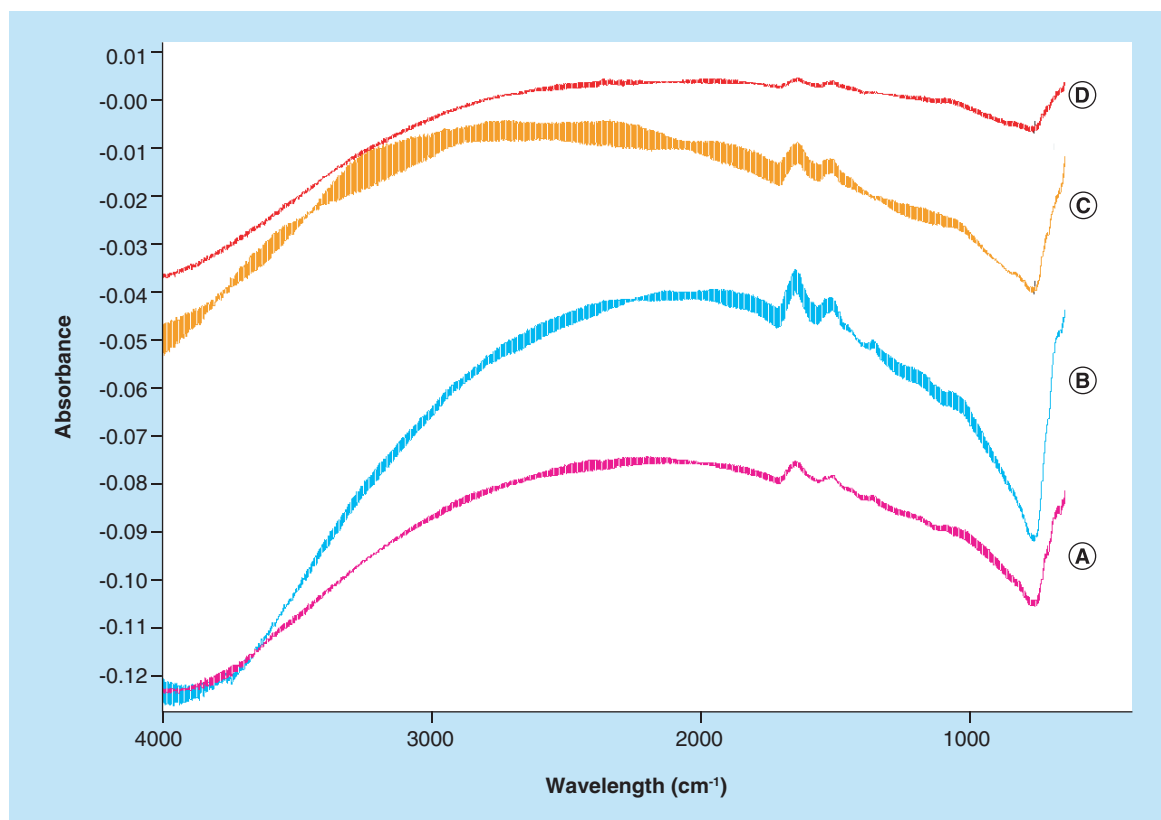


**Figure 5.** Spectra of samples collected on a silicon wafer. A and B refer to glutaraldehyde samples while C and D refers to EDC/NHS samples.

of the results were performed using Mann–Whitney U test to compare the experimental conditions with controls. *p*-values <0.05 were considered statistically significant.

## Results

### Activity analysis

RgDAAO was conjugated to Fe<sub>3</sub>O<sub>4</sub>-APTES by means of EDC and NHS. Under best experimental conditions, the amount of enzyme bound to NPs, determined as the difference between the protein amount added and that recovered in the supernatant, is close to 100%, with an enzymatic activity of approximately 7 U/mg NP.

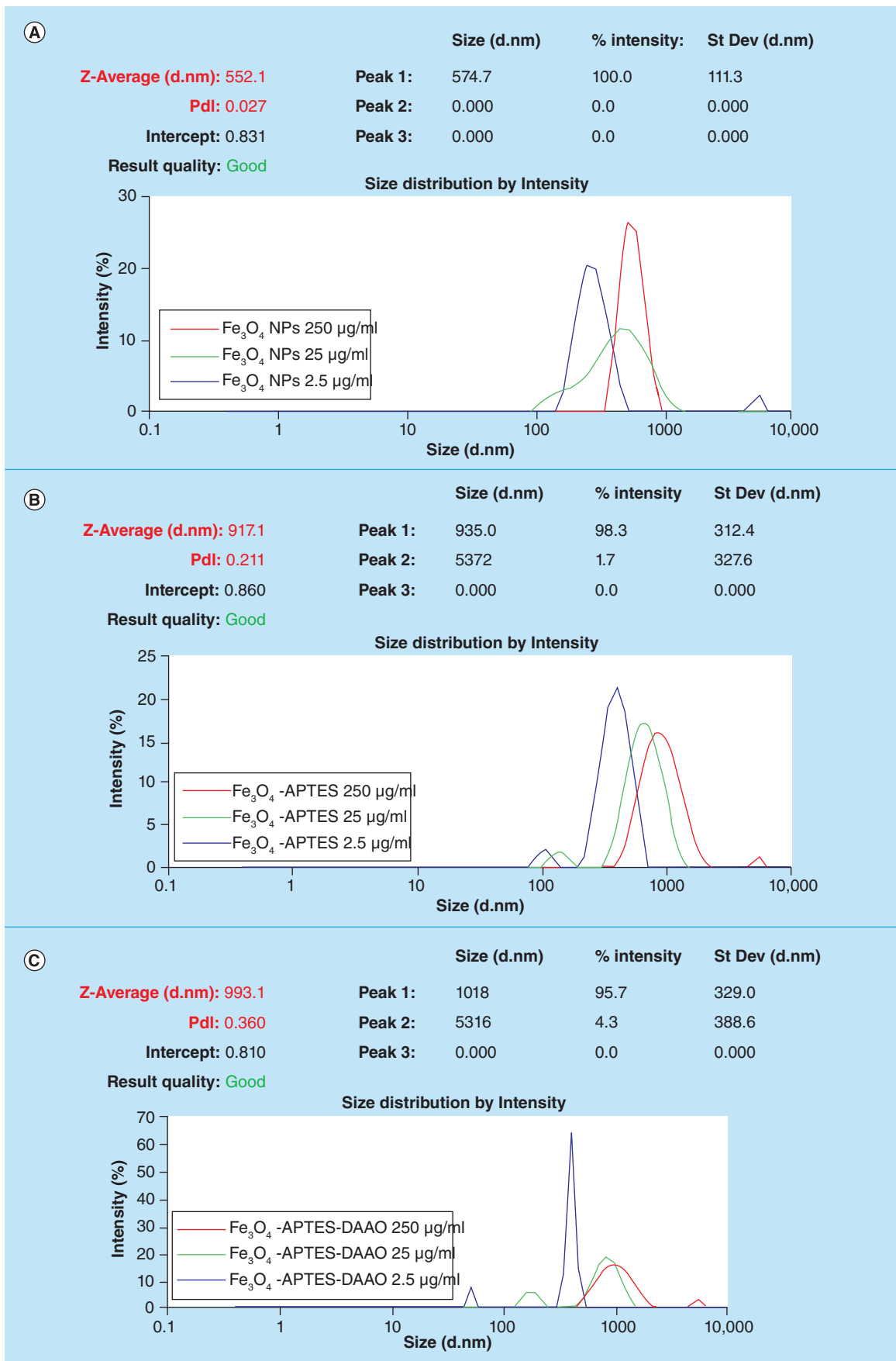
### IR characterization

The spectra of Fe<sub>3</sub>O<sub>4</sub>-APTES-DAAO prepared with the two methods (the old one *via* glutaraldehyde and the new one presented here), dispersed in the KBr (to identify the structural components), are reported in Figure 1. The two spectra are similar. At the highest wavenumbers, we can observe the stretching of the OH groups of water adsorbed on KBr, likely 3425 cm<sup>-1</sup>. In

the 3300–3000 cm<sup>-1</sup> region, the ν(NH) vibrations are observed; they correspond to the NH<sub>2</sub> moieties present in the organic ligand. The corresponding bending mode is at 1650–1640 cm<sup>-1</sup> and 1546 cm<sup>-1</sup>, partially overlapped with the δ(HOH) of water at ~1630 cm<sup>-1</sup>. Below 800 cm<sup>-1</sup>, only structural (saturated) bands are visible, containing bending, twisting and rocking modes, together with the stretches of M–O bonds. The other bands (in the 1600–1000 cm<sup>-1</sup> region) are due to C–C and C–O bonds, while those in the 3000–2800 cm<sup>-1</sup> interval to C–H stretches, difficult to be discriminated at this step. Interestingly, no bands at ~1745 cm<sup>-1</sup>, typical of the C=O bonds of the aldehydes, can be distinguished. Performing a spectral subtraction (Figure 2) we can better scrutinize the differences in the two compounds: the vibrations associated to the NH<sub>2</sub> species almost disappear in the compound prepared via EDC/NHS, as indicated by the bands in positive in the difference spectrum (3400–3000 cm<sup>-1</sup> region, plus 1649 and 1546 cm<sup>-1</sup> peaks) and by the absence of the corresponding bands in the blue spectrum in Figure 1. A very weak feature appears at 1735 cm<sup>-1</sup>, accounting for aldehyde typical vibration.

**Figure 6 (see facing page).** DLS analysis on Fe<sub>3</sub>O<sub>4</sub> NPs (A), Fe<sub>3</sub>O<sub>4</sub>-APTES (B) and Fe<sub>3</sub>O<sub>4</sub>-APTES-DAAO (C) at different concentrations.





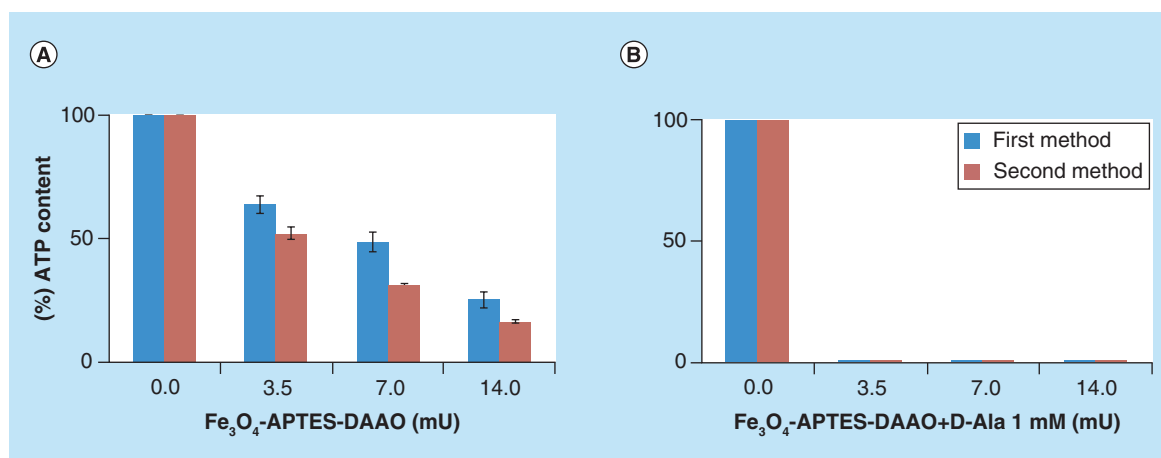


**Figure 7.** Comparison of cytotoxicity, on SKOV-3, of Fe<sub>3</sub>O<sub>4</sub>-APTES-DAAO prepared with the two methods, without and with 1 mM D-Ala.

When dispersing the samples on silica as a support (Figure 3), the observed bands essentially deal with OH groups on silica (3746 cm<sup>-1</sup>) and adsorbed water (~3450 and 1630 cm<sup>-1</sup>). The features at 1972 and 1867 cm<sup>-1</sup> are overtones and combination bands of the silica framework (massif below 1300 cm<sup>-1</sup>) (spectrum blue, Figure 3). The sample has been probed by adsorption of CO and NO, two molecules adapted to reveal (and quantify) the presence of coordinatively unsaturated iron cations [28]. After CO or NO adsorptions, no remarkable differences can be distinguished especially on the glutaraldehyde sample (Figure 3, spectra cyan, magenta and green). In the case of the EDC/NHS sample, a weak component appears at 1508 cm<sup>-1</sup> (Figure 3, spectrum red, red arrow), which cannot be related directly with the probe molecules. Eventually, it could be ascribed to CO interactions with some accessible ligand in the organic part, inducing a shift in a C–C or C–O vibration. Subtraction spectra (Figure 4) confirm that no effect of probe molecule adsorption can be detected, so suggesting the absence of unsaturated iron moieties.

Spectra of the samples characterized after deposition on a silicon wafer (to discard any potential interaction with a support) are reported in Figure 5. Besides the interference fringes due to the specular surfaces of the Si disks, we can observe only bands due to the

organic ligands, already mentioned above. Comparing the spectra during the adsorption of CO as probe molecule and after evacuation (B and A for glutaraldehyde, respectively, and C and D for EDC/NHS), we cannot observe any difference, if we exclude the changes in the baseline, irrelevant for the present study. Even, this latter approach for the sample analysis seems less appropriate, providing spectra of relatively low quality.

#### DLS analysis

In all samples, production of NP aggregates of 300 nm or more is evident. The size of the aggregates varies with the dilution: at increased dilution the diameter decreases. Aggregation of metal NPs in aqueous environment has been demonstrated to depend on several factors, concentration included [29]. Moreover, the polydispersity index (pdi) increases from Fe<sub>3</sub>O<sub>4</sub> NPs to Fe<sub>3</sub>O<sub>4</sub>-APTES-DAAO (Figure 6).

#### Cytotoxicity

The cytotoxicity of the two systems was tested on SKOV-3 cells with and without the substrate D-alanine (1 mM). As reported in Figure 7, no significant differences were evident: both systems in the presence of the substrate fully depleted the ATP content at 3.5 mU of DAAO.

**Table 1.** Mean bodyweight gain (%) and relative organ weight (%) following intravenous administration of vehicle, 100 and 20 mg/kg bodyweight of nanoparticles in mice.

EXP	Group	Bodyweight gain	Liver	Spleen	Kidney
1	Vehicle (0.9% NaCl)	-1.6 ± 1.9	6.6 ± 1.2	0.5 ± 0.1	1.9 ± 0.0
	Fe <sub>3</sub> O <sub>4</sub> -DAAO 100 mg/kg	-3.5 ± 2.2	7.8 ± 0.3	0.6 ± 0.1	1.6 ± 0.1
2	Vehicle (NaPPI)	-2.9 ± 0.4	6.7 ± 0.1	0.5 ± 0.1	1.8 ± 0.1
	Fe <sub>3</sub> O <sub>4</sub> -DAAO 20 mg/kg	-3.5 ± 2.8	6.9 ± 0.2	0.5 ± 0.1	1.6 ± 0.2

Results are expressed as means ± SD.

**In vivo study****Mice treated with 100 mg NP/kg**

Immediately after the administration of NPs, and during the following hours, all mice appeared healthy and no relevant behavioral alterations were observed. At necropsy, the liver of three out of three treated mice had a diffuse mild black-brown discoloration compared with control mice. No significant differences in

bodyweight gain and relative organ weights of liver, spleen and kidney were observed between control and  $\text{Fe}_3\text{O}_4$ -APTES-DAAO treated group (Table 1). Histologically, in three out of three treated mice, intracytoplasmic brown granular material (consistent with iron pigment, as confirmed by Perls iron stain) was found in HE stained sections of the liver, spleen and lung, and only occasionally in the kidney (at level of blood vessels)

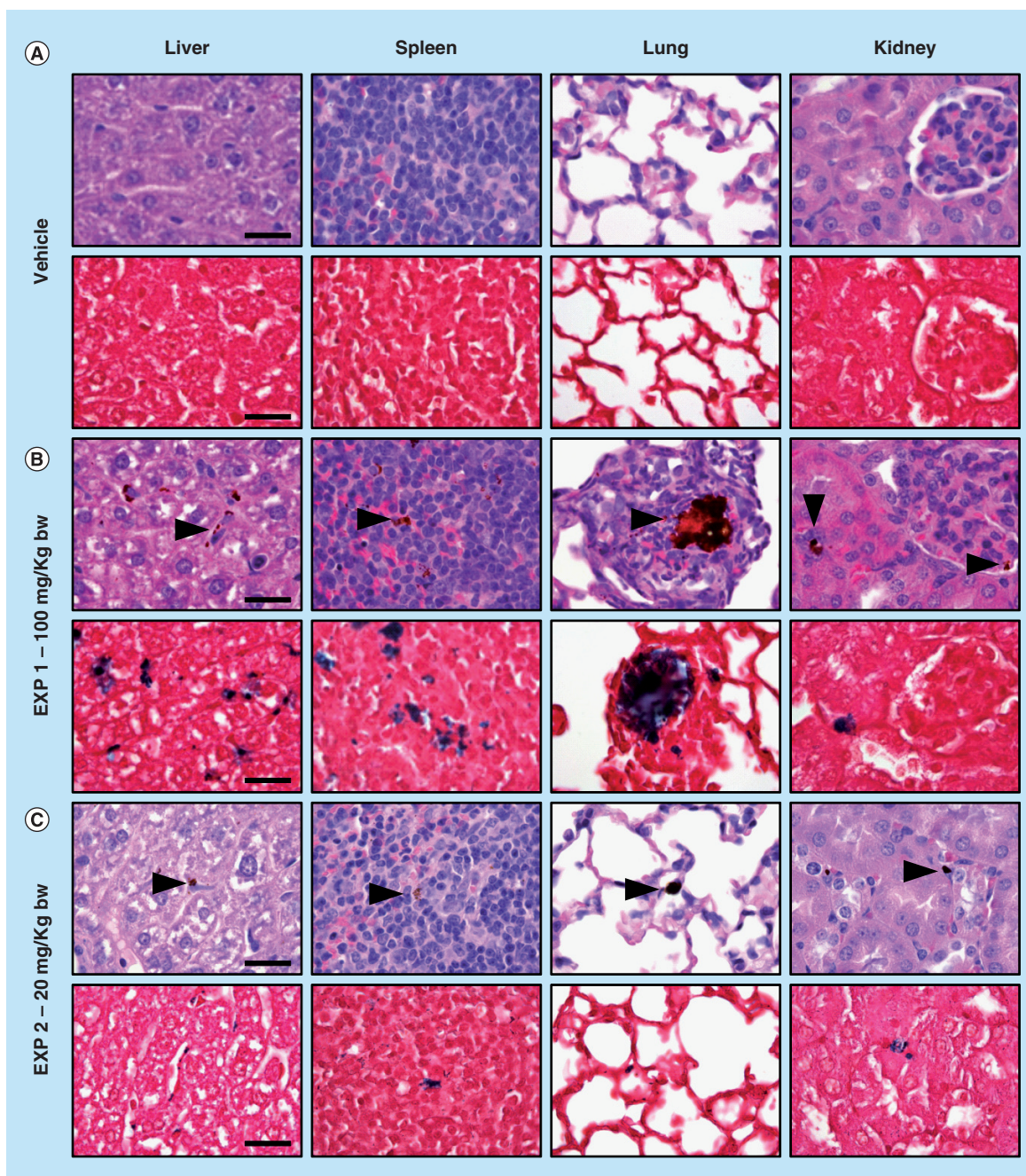


**Figure 8.** Histology of liver, spleen, lung, and kidney of mice treated with vehicle (A), 100 mg/kg (B; EXP 1), and 20 mg/kg (C; EXP 2) of NPs (upper panel: HE; lower panel: Perls stain; scale bar = 25  $\mu\text{m}$ ). Brown granular material is evident in HE stained sections (arrowheads) of NP treated mice, consistent with iron aggregates, as confirmed by Perls stain (blue).

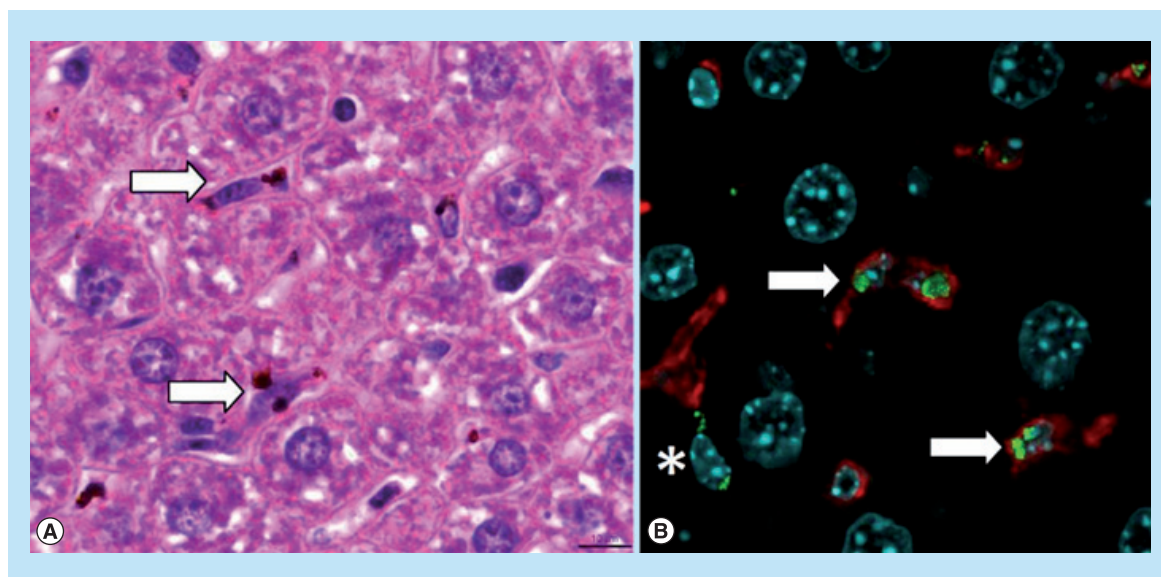


**Figure 9.** Histological examination of mouse liver. (A) Brown aggregates of iron-containing NPs within the cytoplasm of Kupffer cells lining hepatic sinusoids (HE staining). (B) Iron-containing NPs (green) are mainly found in the cytoplasm of Iba1+ Kupffer cells (red, arrows) and occasionally in spindled cells (\*). Nuclei stained with DAPI (cyan).

(Figure 8). The results of the quantitative evaluation of the iron deposits detected in Perls iron stained sections of examined organs is reported in Table 2. In the liver the iron pigment was found mainly in the cytoplasm of Kupffer cells (immunostained with Iba1), but occasionally also within spindle-shaped cells, likely consistent with hepatic sinusoidal endothelial cells (Figure 9). In the lung, there were moderate numbers of cells (monocytes/macrophages) with intracytoplasmic iron pigment infiltrating the alveolar septa, throughout the pulmonary parenchyma. Multifocally, intravascular up to 100  $\mu\text{m}$  in diameter iron aggregates (emboli) surrounded by granulocytes, were found in association with interstitial infiltrates of histiocytes expanding the alveolar septa (Figure 8). In the spleen, large numbers of histiocytes with intracytoplasmic iron pigment were found in the red pulp, marginal zone, and PALS/germinal center. The white pulp was affected by mild-to-moderate follicular reactive hyperplasia. No iron deposits were observed in the heart, and brain of treated mice.

#### Mice treated with 20 mg NP/kg

No relevant behavioral alterations and no significant differences of bodyweight gain, and relative organ

weights of liver, spleen and kidney were observed between control and  $\text{Fe}_3\text{O}_4$ -APTES-DAAO-treated group (Table 1). Grossly, a moderate splenomegaly was observed only in one out of three treated mice. Histologically, in three out of three treated mice, small-to-moderate amount of iron pigment was found in the liver (Kupffer cells), spleen (macrophages/histiocytes in the marginal zone, red pulp and PALS/germinal center) and rarely in the kidney (interstitial capillaries). In one out of three treated mice, only rare and small intracytoplasmic iron aggregates (monocytes/macrophages) were found in the lung alveolar septa (Figure 8). No iron deposits were observed in the heart, testis and brain. Reduced amount of iron-containing deposits were detected in liver and spleen compared with those found in mice treated with 100 mg NP/kg (Table 2).

#### Discussion

In our previous work, we designed a protocol for the immobilization of RgDAAO on magnetic iron oxide NPs for antitumor therapy ( $\text{Fe}_3\text{O}_4$ -APTES-DAAO) [21]. The conjugation was performed via glutaraldehyde obtaining a system with an activity of 4 U/mg NP. In this work, we improved the protocol for

**Table 2.** Quantitative evaluation of iron deposits detected in Perls iron stained sections.

Group	Liver	Spleen	Lung	Kidney	Brain	Heart
Vehicle	0.02 $\pm$ 0.02	0.02 $\pm$ 0.00	0.05 $\pm$ 0.02	0.04 $\pm$ 0.01	0.00 $\pm$ 0.00	0.00 $\pm$ 0.00
$\text{Fe}_3\text{O}_4$ -DAAO 100 mg/kg	2.98 $\pm$ 1.11	1.40 $\pm$ 0.55	0.51 $\pm$ 0.13	0.09 $\pm$ 0.05	0.00 $\pm$ 0.00	0.00 $\pm$ 0.00
$\text{Fe}_3\text{O}_4$ -DAAO 20 mg/kg	0.23 $\pm$ 0.07	0.17 $\pm$ 0.06	0.13 $\pm$ 0.08	0.04 $\pm$ 0.01	0.00 $\pm$ 0.00	0.00 $\pm$ 0.00

Results are expressed as means  $\pm$  SD.

the synthesis of  $\text{Fe}_3\text{O}_4$ -APTES-DAAO, enhancing the yield by 40%, reaching 100% of conjugated enzyme in term of activity and quantity. The conjugation of RgDAAO occurs by means of EDC and NHS and the reaction times are reduced by 2 h. The new system has an activity of 7 U/mg NP, 1.5-fold more than the old one (characterized by 4.5 U/mg NP). A schematic representation of the two protocols of conjugation is reported in **Figure 10**.

The comparison of the two systems by IR analysis demonstrates that all the ligands are functionalized in the EDC-NHS sample, whereas a small portion of them present free coordination ends in the glutaraldehyde compound (**Figures 1 & 2**). In light of this, we can say that the EDC-NHS sample higher activity in respect with the glutaraldehyde sample is due to a higher efficiency of bound. In fact, apparently all available  $\text{NH}_2$  sites are saturated with DAAO, while glutaraldehyde

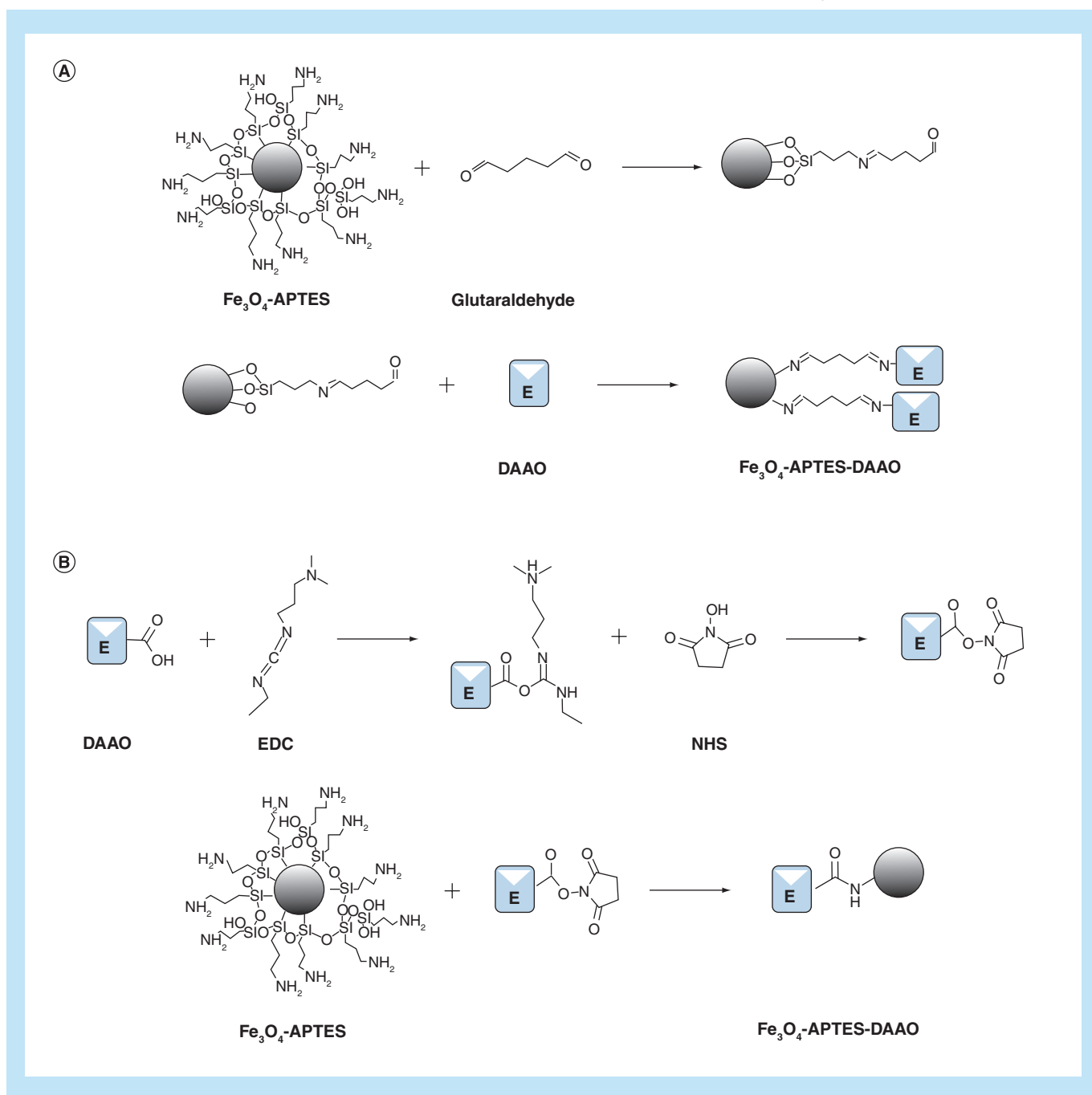


**Figure 10.** Schematic representation of the two DAAO conjugation methods on  $\text{Fe}_3\text{O}_4$ -APTES: **(A)** Conjugation via glutaraldehyde; **(B)** Conjugation via EDC and NHS.

sample shows some free  $\text{NH}_2$  and aldehyde sites. Moreover all conjugation sites of  $\text{Fe}_3\text{O}_4$  NPs are saturated, signifying that APTES functionalization is absolute.

DLS analysis shows that the population of  $\text{Fe}_3\text{O}_4$ -APTES-DAAO is stable around a dimension of 1  $\mu\text{m}$  indicating that the enzyme conjugation process induces aggregation of NPs. However, more information on the hydrodynamic diameter of the iron core, the magnetization capabilities and the iron content would allow to better compare these newly created particles to others.

The cytotoxicity analysis does not highlight any difference between the two systems; indeed, both completely deplete the ATP content at 3.5  $\mu\text{M}$  in the presence of the DAAO substrate D-alanine. Worthy of note is that the second system employs a lower amount of  $\text{Fe}_3\text{O}_4$  NPs, because of the higher enzymatic activity.

In the present paper, we have also evaluated the *in vivo* safety of the  $\text{Fe}_3\text{O}_4$ -APTES-DAAO system produced with the EDC-NHS procedure. In the first experiment, after intravenous injection in mice of 100 mg NP/kg diluted in 0.9% NaCl no significant alterations of behavior, bodyweight gain and relative organ weight of liver, spleen and kidney were observed. Histologically, iron deposits were detected in the liver, spleen, lungs and kidneys, while none was found in the heart and brain. Mainly, iron deposits were found in the cytoplasm of monocytes/macrophages/histiocytes, indicating that most of injected particles were removed from blood circulation by phagocytic cells, as previously reported for other nanoparticles [30]. However, presence of intravascular iron deposits associated with interstitial inflammation were found in the lung, indicating that pulmonary embolization occurred after intravenous administration of aggregated NPs, as confirmed by the results of DLS analysis. In the spleen of mice treated with 100 mg/kg, reactive follicular hyperplasia was observed. This finding may be interpreted as an antigenic response, likely directed against the enzymatic portion of the NP system. In general, no overt adverse effects have been observed 24 h after intravenous administration of 100 mg  $\text{Fe}_3\text{O}_4$ -APTES-DAAO/kg, however, the presence of pulmonary embolization of iron aggregates prompted us to perform a second experiment using a lower dose (20 mg NP/kg), and a different vehicle (NaPPi buffer instead of 0.9% NaCl) in order to prevent particle aggregation. No clinicopathological adverse effects were observed after intravenous administration of 20 mg NP/kg, and histologically, a dose-dependent decrease of iron deposits was found in the liver and spleen. In addition, absence of detectable iron deposits in the brain and testis (examined only for 20 mg  $\text{Fe}_3\text{O}_4$ -DAAO/kg) suggests that our system is not able to cross biological barriers, or, at least, not in

the absence of an external magnetic field and under tested conditions.

We also think that biological molecules, such as enzymes, polysaccharides [31,32], antibiotics, antibodies and nucleic acids [33], efficiently conjugated to magnetic NPs might constitute a category of 'bionanoparticles' to be exploited in medical as well as industrial biotechnology.

## Conclusion

We have improved the synthesis protocol of  $\text{Fe}_3\text{O}_4$ -APTES-DAAO, reaching the highest activity allowed by the system. The acute cytotoxicity of the newly synthesized nanoenzyme does not differ from the previously synthesized one. Moreover, no relevant adverse effects were observed after *in vivo* intravenous administration in mice of a single dose of 20 mg NP/kg bw.

## Future perspective

Future aim will be the investigation of the biodistribution of NPs under application of an external magnetic field. The ability of an external magnetic field to accumulate NPs in a determined area as well as that to make NPs crossing biological barriers will be investigated. The ability of the system to destroy tumors will also be tested *in vivo*.

Moreover, we are convinced that flavoenzymes efficiently conjugated to magnetic NPs could be exploited also in industrial biotechnology [34].

## Author contributions

F Cappellini performed the synthesis and the *in vitro* experiments, analyzed the data and drafted the manuscript; C Recordati and M De Maglie performed the *in vivo* experiments and are responsible of the histology; M Daturi supervised the infrared spectroscopy experiments, analyzed and interpreted the data; L Pollegioni produced the enzyme; F Rossi, R Gornati and G Bernardini supervised the study; G Bernardini wrote the paper.

## Financial & competing interests disclosure

This work was partially supported by a CARIPO grant number 2013–1052. Some of these data arise from a collaboration started in the context of the COST action MODENA TD1204. The authors have no other relevant affiliations or financial involvement with any organization or entity with a financial interest in or financial conflict with the subject matter or materials discussed in the manuscript apart from those disclosed.

No writing assistance was utilized in the production of this manuscript.

## Open access

This work is licensed under the Creative Commons Attribution-NonCommercial 4.0 Unported License. To view a copy of this license, visit <http://creativecommons.org/licenses/by-nc-nd/4.0/>

**Executive summary****Improvement of the synthesis protocol of the system Fe<sub>3</sub>O<sub>4</sub>-APTES-DAAO**

- The protocol reached the highest possible efficiency in terms of enzyme immobilization yield and activity and the time of production was reduced by 2 h.

**Characterization of the old & the new system & analysis of *in vivo* biodistribution**

- IR analysis confirmed the absolute saturation of all binding sites. Fe<sub>3</sub>O<sub>4</sub>-APTES-DAAO cannot cross biological barrier without a magnetic field. The intravenous injection of 20 mg Fe<sub>3</sub>O<sub>4</sub>-APTES-DAAO/kg does not cause adverse effects.

**Future perspective**

- The capability of the system to cross biological barriers, to be targeted in a specific area and to destroy a tumor will be investigated. Moreover, a possible exploitation of nanoenzymes in industrial biotechnology will be considered.

**References**

Papers of special note have been highlighted as: • of interest;

•• of considerable interest

- 1 Astruc D. Transition metal nanoparticles in catalysis: from historical background to the state of the art. In: *Nanoparticles and Catalysis (Chapter 1)*. Astruc D (Ed.). Wiley-VCH Verlag GmbH & Co. KGaA Publisher, Weinheim, Germany, 1–48 (2008).
- 2 Saha K, Agasti SS, Kim C, Li XN, Rotello VM. Gold nanoparticles in chemical and biological sensing. *Chem. Rev.* 112, 2739–2779 (2012).
- 3 Stratakis E, Kymakis E. Nanoparticle-based plasmonic organic photovoltaic devices. *Mater. Today* 16, 133–146 (2013).
- 4 Barua S, Mitragotri S. Challenges associated with penetration of nanoparticles across cell and tissue barriers: a review of current status and future prospects. *Nano Today* 9, 223–243 (2014).
- Deals with nanoparticle (NP) penetration across biological barriers.
- 5 Castellini C, Ruggeri S, Mattioli S *et al.* Long-term effects of silver nanoparticles on reproductive activity of rabbit buck. *Syst. Biol. Reprod. Med.* 60, 143–150 (2014).
- Deals with blood–testis barrier permeability to silver NPs.
- 6 Coccini T, Gornati R, Rossi F *et al.* Gene expression changes in rat liver and testes after lung instillation of a low dose of silver nanoparticles. *J. Nanomed. Nanotechnol.* 5, 227 (2014).
- Deals with blood–lung barrier permeability to silver NPs.
- 7 Papis E, Rossi F, Raspanti M, *et al.* Engineered cobalt oxide nanoparticles readily enter cells. *Toxicol. Lett.* 189, 253–259 (2009).
- 8 Cattaneo AG, Gornati R, Sabbioni E *et al.* Nanotechnology and human health: risks and benefits. *J. Appl. Toxicol.* 30, 730–744 (2010).
- 9 Antunes AMD, Alencar MSD, da Silva CH, Nunes J, Mendes FML. Trends in nanotechnology patents applied to the health sector. *Recent Pat. Nanotechnol.* 6, 29–43 (2012).
- 10 Jain KK. Advances in the field of nanooncology. *BMC Med.* 8, 83–94 (2010).
- 11 Salmasi S, Kalaskar DM, Yoon W-W, Blunn GW, Seifalian AM. Role of nanotopography in the development of tissue engineered 3D organs and tissues using mesenchymal stem cells. *World J. Stem Cells* 7, 266–280 (2015).
- 12 Ediriwickrema A, Saltzman WM. Nanotherapy for cancer: targeting and multifunctionality in the future of cancer therapies. *ACS Biomater. Sci. Eng.* 1, 64–78 (2015).
- 13 Kanwar JR. Nanotechnological based system for cancer. In: *Nanomedicine and Cancer Therapies (Volume 2)* Sebastian M, Ninan N, Elias E (Eds). Apple Academic Press, Oakville, Canada, 1–18 (2013).
- 14 Liberatore M, Barteri M, Megna V *et al.* Effect of external magnetic field on IV <sup>99m</sup>Tc-labeled aminosilane-coated iron oxide nanoparticles: demonstration in a rat model: special report. *Clin. Nucl. Med.* 40, e104–e110 (2015).
- Demonstrates that an external magnetic field can direct circulating NPs to selected areas of the body.
- 15 Lim EK, Jang E, Lee K, Haam S, Huh YM. Delivery of cancer therapeutics using nanotechnology. *Pharmaceutics* 5, 294–317 (2013).
- 16 Gang J, Park SB, Hyung W *et al.* Magnetic poly-ε-caprolactone nanoparticles containing Fe<sub>3</sub>O<sub>4</sub> and gemcitabine enhance anti-tumor effect in pancreatic cancer xenograft mouse model. *J. Drug Target.* 15, 445–453 (2007).
- 17 Lee JH, Chen KJ, Noh SH *et al.* On-demand drug release systems for *in vivo* cancer treatment through self-assembled magnetic nanoparticles. *Angew. Chem. Int. Ed.* 52, 1–6 (2013).
- 18 Cho MH, Lee EJ, Son M *et al.* A magnetic switch for the control of cell death signaling in *in vitro* and *in vivo* systems. *Nat. Mat.* 11, 1038–1043 (2012).
- 19 Thomas CR, Ferris DP, Lee JH *et al.* Noninvasive remote-controlled release of drug molecules *in vitro* using magnetic actuation of mechanized nanoparticles. *J. Am. Chem. Soc.* 132, 10623–10625 (2010).
- 20 Katagiri K, Imai Y, Kounoto K, Kaiden T, Kono K, Aoshima S. Magneto-responsive on-demand release of hybrid liposomes formed from Fe<sub>3</sub>O<sub>4</sub> nanoparticles and thermosensitive block copolymer. *Small* 7, 1683–1689 (2011).
- 21 Bava A, Gornati R, Cappellini F, Caldinelli L, Pollegioni L, Bernardini G. D-amino acid oxidase-nanoparticle system: a potential novel approach for cancer enzymatic therapy. *Nanomedicine (London)* 8, 1797–806 (2013).
- 22 Netto C, Toma HE, Andrade LH. Superparamagnetic nanoparticles as versatile carriers and supporting materials for enzymes. *J. Mol. Catalysis B Enz.* 85–86, 71–92 (2013).

- 23 Fantinato S, Pollegioni L, Pilone MS. Engineering, expression and purification of a His-tagged chimeric D-amino acid oxidase from *Rhodotorula gracilis*. *Enzyme Microb. Technol.* 29, 407–412 (2001).
- 24 Harris CM, Pollegioni L, Ghisla S. pH and kinetic isotope effects in d-amino acid oxidase catalysis. *Eur. J. Biochem.* 268, 5504–5520 (2001).
- 25 Peophet EB. Armed Forces Institute of Pathology Staf. In: *AFIP Laboratory Methods in Histotechnology*. Prophet EB, Mills B, Arrington JB, Sobin LH (Eds). American Registry of Pathology Publisher, Washington, DC, USA, 1–279 (1994).
- 26 ImageJ.  
<http://rsb.info.nih.gov/ij/>
- 27 Rehg JE, Bush D, Ward JM. The utility of immunohistochemistry for the identification of hematopoietic and lymphoid cells in normal tissues and interpretation of proliferative and inflammatory lesions of mice and rats. *Toxicol. Pathol.* 40, 345–374 (2012).
- 28 Wuttke S, Bazin P, Vimont A *et al.* Discovering the active sites for C3 separation in MIL-100(Fe) by using operando IR spectroscopy. *Chem. Eur. J.* 18, 11959–11967 (2012).
- 29 Keller AA, Wang H, Zhou D *et al.* Stability and aggregation of metal oxide nanoparticles in natural aqueous matrices. *Environ. Sci. Technol.* 44, 1962–1967 (2010).
- 30 Fujihara J, Tongu M, Hashimoto H *et al.* Distribution and toxicity evaluation of ZnO dispersion nanoparticles in single intravenously exposed mice. *J. Med. Invest.* 62, 45–50 (2015).
- 31 Bava A, Cappellini F, Pedretti E *et al.* Heparin and carboxymethylchitosan metal nanoparticles: an evaluation of their cytotoxicity. *Biomed. Res. Int.* 2013, 314091 (2013).
- 32 Vismara E, Valerio A, Coletti A, *et al.* Non-covalent synthesis of metal oxide nanoparticle–heparin hybrid systems: a new approach to bioactive nanoparticles. *Int. J. Mol. Sci.* 14, 13463–13481 (2013).
- 33 Fratila RM, Mitchell SG, del Pino P, Grazu V, de la Fuente JM. Strategies for the biofunctionalization of gold and iron oxide nanoparticles. *Langmuir* 30, 15057–15071 (2014).
- 34 Pollegioni L, Molla G. New biotech applications from evolved D-amino acid oxidases. *Trends Biotechnol.* 29, 276–283 (2011).